2023

MICROFLUIDIC DEVICES FOR MICROPLASTICS SEPARATION AND IDENTIFICATION

Pedro Mesquita
University of Rhode Island, pedro_mesquita@uri.edu

MICROFLUIDIC DEVICES FOR MICROPLASTICS SEPARATION AND IDENTIFICATION

BY

PEDRO HENRIQUE MORENO MESQUITA

A THESIS SUBMITTED IN PARTIAL FULFILLMENT OF THE

REQUIREMENTS FOR THE DEGREE OF

MASTER OF SCIENCE

IN

MECHANICAL ENGINEERING AND APPLIED MECHANICS

UNIVERSITY OF RHODE ISLAND

2023

MASTER OF SCIENCE THESIS

OF

PEDRO HENRIQUE MORENO MESQUITA

APPROVED:

Thesis Committee:

Major Professor Yang Lin

Chengzhi Yuan

Jie Shen

Brenton DeBoef
DEAN OF THE GRADUATE SCHOOL

UNIVERSITY OF RHODE ISLAND
2023

ABSTRACT

Considering its ubiquitous use, plastic pollution has been a worldwide concern for a long time. Recently, microplastics have been found both in water and animal samples (including humans), raising the necessity for novel analytical methods dedicated to the detection of these particles. This thesis explored the application of microfluidic devices in the separation and identification of microplastics. Firstly, the field of low-cost microfluidic devices for environmental applications was reviewed, obtaining an exhaustive perspective. The second chapter explores the development of a device used for microplastics identification using a staining method. The device was made from PDMS casting using a 3D printed mould. It was possible to continuously stain microplastic particles diluted in water samples. The staining quality depended on the device flow rate and operational temperature. The third chapter demonstrates the separation of microplastics from blood samples using acoustic waves. The device was fabricated using a combination of photolithography and lift-off techniques. The interaction between acoustic waves and submerged particles was modelled considering different microplastic types and sizes. The separation was demonstrated, and the effects of power and flow rate were analyzed.

ACKNOWLEDGMENTS

This thesis would not have been possible without the support and encouragement of Dr. Yang Lin. It has been an honor to be his student and to have learnt from him throughout this process. His motivation and patience were fundamental for the success of the experiments and to spark my curiosity to develop novel ideas. Moreover, I would like to thank Dr. Jie Shen and Dr. Chengzhi Yuan for being part of this committee and Dr. Ryan Poling-Skutvik for being the chair. In addition, I am thankful for working with Dr. Giri as a teaching assistant, which has also helped to shape myself professionally. Regarding microfabrication, I acknowledge Mr. Michael Jibistky for all his instructions in the cleanroom, his knowledge about photolithography and e-beam deposition were fundamental for the third chapter. I am thankful for my lab mate, Liyuan Gong, who has proofread and provided relevant feedback and discussions. In addition, I am grateful for all the members of the Microfluidics and Microsystems Lab, they have all been important. I extend my appreciation to the following people in the mechanical engineering department at URI, they were always positive and welcoming: Jim Byrnes, Rob D'Ambrosca, Nancy Santucci, Maria Fan. I appreciate the financial support of URI Graduate School and the Grants from RI Foundation. The support of my family was of utmost importance, I dedicate all my achievements to them.

PREFACE

This thesis is submitted as partial fulfillment of the requirements for the degree of Master of Science in Mechanical Engineering and Applied Mechanics at the University of Rhode Island. The experiments and research were conducted in the Microfluidics and Microsystems Lab at URI under the supervision of Dr. Yang Lin. The work is presented in form of a thesis consisting of three chapters. Two chapters have been published and the last one shall be submitted after the completion of this thesis.

The first chapter is a review about the field of low-cost microfluidic devices applied to environmental analysis. The second chapter studies the development of a microfluidic device used for microplastics identification. The third chapter studies the development of a microfluidic device used for the separation of microplastics from blood samples. Despite specific, the conclusions and experiments may be applied in other industries such as pharmaceutical and chemical. Manuscript format was used in this thesis.

Pedro Mesquita

March 2023

TABLE OF CONTENTS

APPENDICES

LIST OF TABLES

CHAPTER 1

CHAPTER 3

LIST OF FIGURES

CHAPTER 1

CHAPTER 2

CHAPTER 3

CHAPTER 1. Low-cost microfluidics: towards affordable environmental monitoring and assessment

by

Pedro Mesquita, Liyuan Gong, Yang Lin

Department of Mechanical, Industrial and Systems Engineering, University of Rhode Island, Kingston, Rhode Island, USA

Published in Frontiers in Lab on a Chip Technologies

Mesquita, P., Gong, L. and Lin, Y., Low-cost microfluidics: towards affordable environmental monitoring and assessment. Frontiers in Lab on a Chip Technologies, p.4. https://doi.org/10.3389/frlct.2022.1074009

ABSTRACT

Effective environmental monitoring has become a worldwide concern, requiring the development of novel tools to deal with pollution risks and manage natural resources. However, a majority of current assessment methods are still costly and labor-intensive. Thanks to the rapid advancements in microfluidic technology over the past few decades, great efforts have been made to develop miniaturized tools for rapid and efficient environmental monitoring. Compared to traditional large-scale devices, microfluidic approaches provide several advantages such as low sample and energy consumption, shortened analysis time and adaptabilities to onsite applications. More importantly, it provides a low-cost solution for onsite environmental assessment leveraging the ubiquitous materials such as paper and plastics, and cost-effective fabrication methods such as inkjet printing and drawing. At present, devices that are disposable, reproducible, and capable of mass production have been developed and manufactured for a wide spectrum of applications related to environmental monitoring. This review summarizes the recent advances of low-cost microfluidics in the field of environmental monitoring. Initially, common low-cost materials and fabrication technologies are introduced, providing a perspective on the currently available low-cost microfluidic manufacturing techniques. The latest applications towards effective environmental monitoring and assessment in water quality, air quality, soil nutrients, microorganisms, and other applications are then reviewed. Finally, current challenges on materials and fabrication technologies and research opportunities are discussed to inspire future innovations.

1. Introduction

Environmental pollution has continuously been a major threat due to fast-growing anthropogenic activities resulting from civilization and industrialization [1–4]. Associated burden of diseases and death arising from global air and water pollution poses a great challenge on public health, especially in underdeveloped regions and countries [5–7]. For instance, more than four millions of deaths related with gastrointestinal diseases may be attributed to water contamination in the United States [8]. The contaminated water, if used for irrigation, can also induce food safety issues involving bacterial contamination [9]. The pollution of oxides of nitrogen (NOx) was also found to play an important role in respiratory problems among children and adults in Nigeria [10]. Other pollutants such as waterborne pathogens, heavy metals, and toxic gases from industrial disposal effluents are also major contributors to global water pollution [11]. The existing evidence clearly speaks out the necessity of accurate pollution risk assessment for tracking pollution sources, determining long-term trends of pollution, and developing effective treatment methods. In particular, it is essential to conduct quantitative assessment on potential pollutants of various types of pollution (*e.g.*, air, water and land pollution) [12].

Conventionally, the assessment of pollutants is carried out in centralized laboratories following the collection of samples [13]. Indeed, these measurements could provide accurate and critical information about the pollutants. However, the use of bulky equipment makes them not adaptable to in situ and real-time assessment, thus hindering a universal and rapid environmental monitoring [14]. One promising solution to address this

downside is the development of miniaturized and potentially field-deployable analytical tools using microfluidic technologies [15]. Thanks to the miniaturization of the fluid domain, microfluidics offers several unique advantages such as low sample consumption, high surface-to-volume ratio, and powerful fluid/particle manipulation abilities [16–18]. However, as a technology benefiting from microelectromechanical systems (MEMS) microfabrication techniques, traditional microfluidic devices built on glass or silicon require complicated fabrication processes involving costly chemicals, materials, equipment, and trained personnel [19–23]. Moreover, a majority of microfluidic devices still do not bypass the requirements of external equipment and/or components (*e.g.,* syringe pumps, heaters, valves, and others) to realize various functions [24]. As a result, the use of microfluidics, to a large extent, is limited in research and laboratories. In order to reduce the cost and minimize the dependency on external instrumentations, low-cost microfluidic devices made from cheap and ubiquitous materials received extensive attentions for various applications in the past decade [25,26].

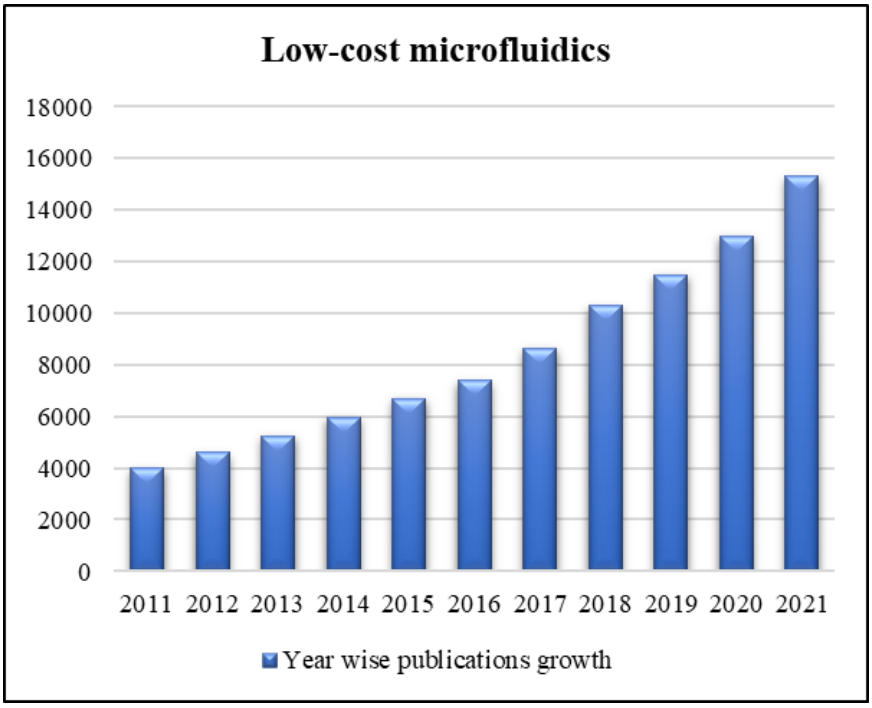

Figure 1.1. Year wise publications growth in regard to low-cost microfluidics from 2011 to 2021. Data were collected using Google Scholar.

Recent research publications have indicated a constant growth in the field of low-cost microfluidics [26], as evidenced by the increasing number of relevant articles found on Google Scholar (Figure 1.1) using the keyword “low-cost microfluidics”. In particular, great efforts have been made to develop novel low-cost microfluidic devices by exploring various low-cost materials and fabrication techniques. For example, wax printing was applied on filter papers to create paper devices [27]. Cloth was also applied because of the potentials to develop wearable sensors [28]. With advancements in 3D printing technologies, multi-layered microfluidic channels with complicated designs became achievable, which also opened new opportunities in various applications including environmental monitoring and assessment [29,30].

Note that the low-cost feature highlighted here is indeed not a rigorous description. It is largely dependent on how engineers, researchers and scientists define it. In this review, we refer the low-cost microfluidics to devices

and systems manufactured outside of cleanroom with all associated fabrication tools and materials readily accessible to most research laboratories. This definition was used by previous researchers when discussing upon low-cost microfluidics in review articles [25,26]. Although these devices and systems may not provide similar performance compared to the cleanroom-based counterparts at current stages, they hold promise in the global dissemination of the state-of-the-art environmental monitoring achievements when accuracy is not as significant as the accessibility to the analytical analysis tools [31]. For example, the availability of clean water in developing countries remains a challenge; the low-cost monitoring of contaminants in water such as heavy metals and infectious microorganisms provide direct benefits towards improving local public health. To achieve this goal, cellulose paper, a porous and ubiquitous material has been employed to build sensors to monitor the water quality [30]. The porous structure of this material enables passive capillary actions without external driving mechanisms [32], while its portable nature also benefits in situ measurements. Therefore, besides environmental monitoring, these devices are also useful for many other applications such as the point-of-care (POC) diagnostics [15,33–36].

In this review, we will start with the primary advances in the underlying materials and fabrication methods of low-cost microfluidic devices. Indeed, several good review papers have been published previously discussing the fabrication technologies for low-cost microfluidics and other major topics [25,26,36–38], however, as a promising tool for ongoing and future onsite environmental monitoring and assessment, a comprehensive review with this specific focus is still beneficial. Finally, latest applications on water, air, soil

quality and many others were introduced, along with conclusions, insights, and future perspectives.

2. Low-cost materials and fabrication methods

Over the past decades, a variety of low-cost materials have been explored to create microfluidic devices beyond glass and silicon [31,37,39]. In 2007, the Whitesides group developed the first modern microfluidic paper-based analytical device (μPAD) [40], by which glucose and protein assays were performed on a cellulose paper. The COVID-19 pandemic also necessitated the development and applications of low-cost analytical analysis tools [41,42]. For example, the Flowflex COVID-19 Antigen Home Test is built on top of a lateral flow chromatographic immunoassay, in which samples can be directly placed on the test device and the results are displayed on control and test lines in a few minutes [43]. Besides paper, plastics are important materials used in low-cost microfluidics and have been used as substrates or housing that protects major components. Polyethylene terephthalate (PET), a common thermoplastic polymer used to make bottles and packages, was used as a flexible substrate for various applications such as the single-cell trapping reported by our group [24]. Indeed, other materials such as cloth, elastomers and biomaterials are also good candidates [28,44,45] and will be discussed below.

Besides low-cost materials, selection of the most appropriate fabrication method is fundamental to reduce the overall cost of the final devices. So far, many fabrication technologies have been explored and developed in the field of microfluidics [46,47]. Conventional fabrication methods such as

photolithography, reactive-ion etching, electron-beam lithography, and LIGA (lithography, electroplating, and molding) often rely on sophisticated equipment and expensive materials, therefore not suitable for low-cost microfluidics [48]. On the other hand, fabrication methods such as wax printing, 3D printing and even drawing only require minimal investment on the equipment and materials, which attracted a lot of attention nowadays [26,37]. In this section, low-cost microfluidic materials and fabrication methods (Figure 2.1) are summarized and discussed.

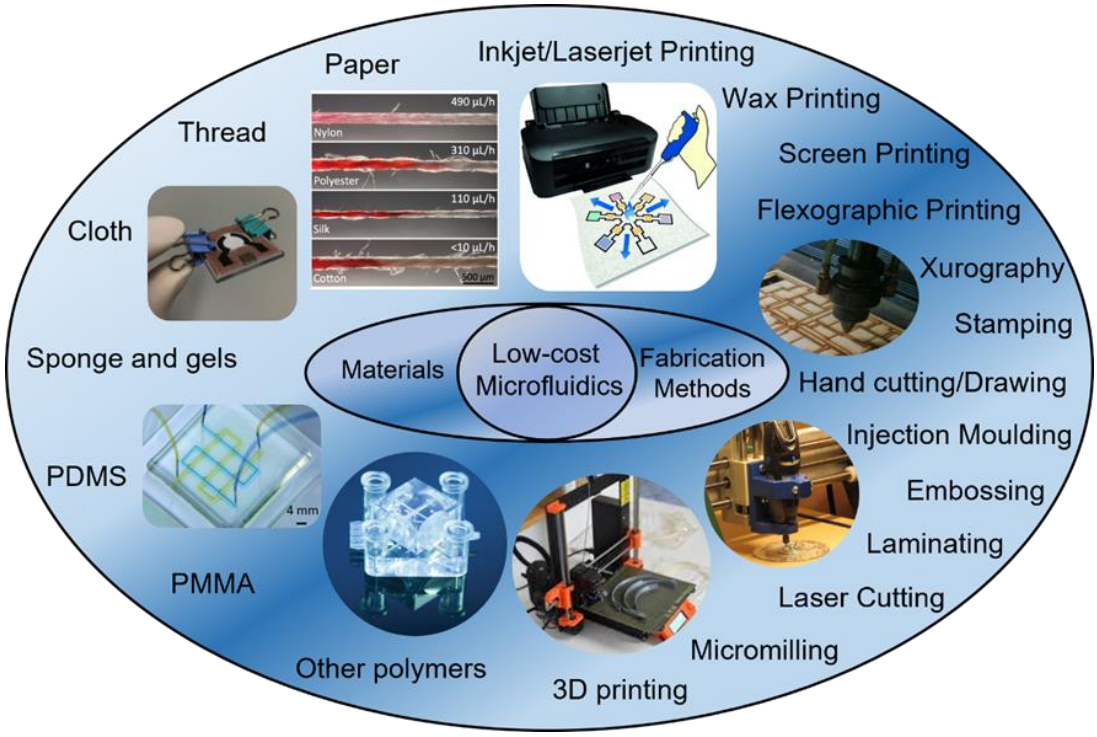

Figure 1.2. Summary of low-cost microfluidic materials and fabrication methods. Materials are showed in the left while fabrication methods are in the right. Commonly used low-cost materials are paper, thread, cloth, PDMS, and PMMA. Oftentimes used low-cost fabrication methods are 3D printing, micromilling, laser cutting, inkjet/laserjet printing, and xurography [28,49–52].

2.1. Low-cost materials

At present, many low-cost materials have been explored to develop tools for environmental monitoring, including cellulose paper, thread, cloth and

polymers [28,53–56]. In fact, devices made from the first three materials have caught intensive attention and are often called paper-based analytical devices (μPADs), thread-based analytical devices (μTADs), and cloth-based analytical devices (μCADs), respectively. Polymeric materials such as polydimethylsiloxane (PDMS), polymethyl methacrylate (PMMA) and PET are also major players thanks to advantages in their mechanical properties, optical and thermal stabilities, as well as the versatility to different environmental applications [57,58].

2.1.1. Paper-based analytical devices (μPADs)

Paper is an inexpensive and ubiquitous resource that has been used in various applications for a long time [59,60]. Its properties (*e.g.,* porosity, chemical composition, and wetting performance) are readily adjustable for different purposes [61–63]. Like other porous materials, the porous nature and high surface-to-volume ratio of the paper promote passive fluid driving and control. The fiber chemical composition (*e.g.,* degree of polarity) can also be modified to enhance sample-paper interactions and plays a key role in device design and operation [64–67]. Owing to a wide variety of paper types commercially available in the market, the correct property selection also saves time and labor for material treatments [37,68]. For example, nitrocellulose paper serves as a good substrate for covalent immobilization of the biomolecules due to the strong binding capability to proteins originated from the nitrate groups on their surfaces. Filter paper and chromatography paper can outperform other paper types in terms of uniform thickness and pore size [69].

Note that the paper material per se only provides the backbone of the devices, while analytical analysis taking place on papers is realized through

incorporation of various sensing or detection methods [70,71]. Existing detection methods can be categorized into several types including colorimetric, fluorescent, chemiluminescent, electrochemical, electro chemiluminescent and Raman sensing [72–75]. Review articles for in-depth discussions on advances in μPADs can be found in the following references: [64,65,74,76].

2.1.2. Thread-based analytic devices (μTADs)

The μTADs are another successful application of porous materials for environmental monitoring and general analytical analysis [77,78]. Similar to μPADs, these devices are good candidates for low-cost applications. The existing industry worldwide also promotes the applications without complex material modifications [79,80]. Currently, a variety of threads are available for different applications, including natural (*e.g.,* silk, wool, linen, *etc.*) and synthetic (*e.g.,* polyester, polyether-polyurea, acrylic, *etc.*) threads [81]. The flow characteristics and the detection methods employed in threads are similar to those employed in paper, since both are porous [77,82]. However, compared to paper devices, thread-based devices are more suitable for wearable applications since threads can be used to create clothing either by directly sewing, or having walls patterned onto cloth [77,83,84].

The detection methods used in μTADs are similar to those used in μPADs. Conventional detection methods (*e.g.,* fluorescence, electrochemical, Raman, *etc.*) are applicable to thread-based devices as well [80,85]. Moreover, distance and barcode-based detection are another two possible low-cost detection strategies [77]. Distance-based detection relies on the fact that disparate wetting performances can be induced by different analytes for identification [86–88]. Moreover, barcode detection can provide results of multiple analyte

reactions (*e.g.,* blood typing) that otherwise are difficult to achieve [89]. For a comprehensive review on thread devices, the readers are encouraged to read the suggested references: [77,79,80,84].

2.1.3. Other porous materials

Similar to paper and thread, cloth also has a porous structure, thus most fabrication and analytical approaches used in the aforementioned porous materials can also be extended and exploited [90,91]. Colorimetric method is the most popular method used in μCADs due to its simplicity and independence on external analysis tools [92–95]. Electrochemical and chemiluminescence methods and their combination were explored as well [91,96–98]. Readers are encouraged to read more detailed review papers that summarizes fabrication, detection methods and performances of μCADs [28,85,99]. In addition, other low-cost materials have also been reported. For example, sponge was used for the detection of heavy metal ions in environmental samples [100], leveraging the strength of sponge structure and the coupling with other materials for better mechanical properties [101,102]. A few examples of the applications of low-cost porous materials are shown in Figure 3.1.

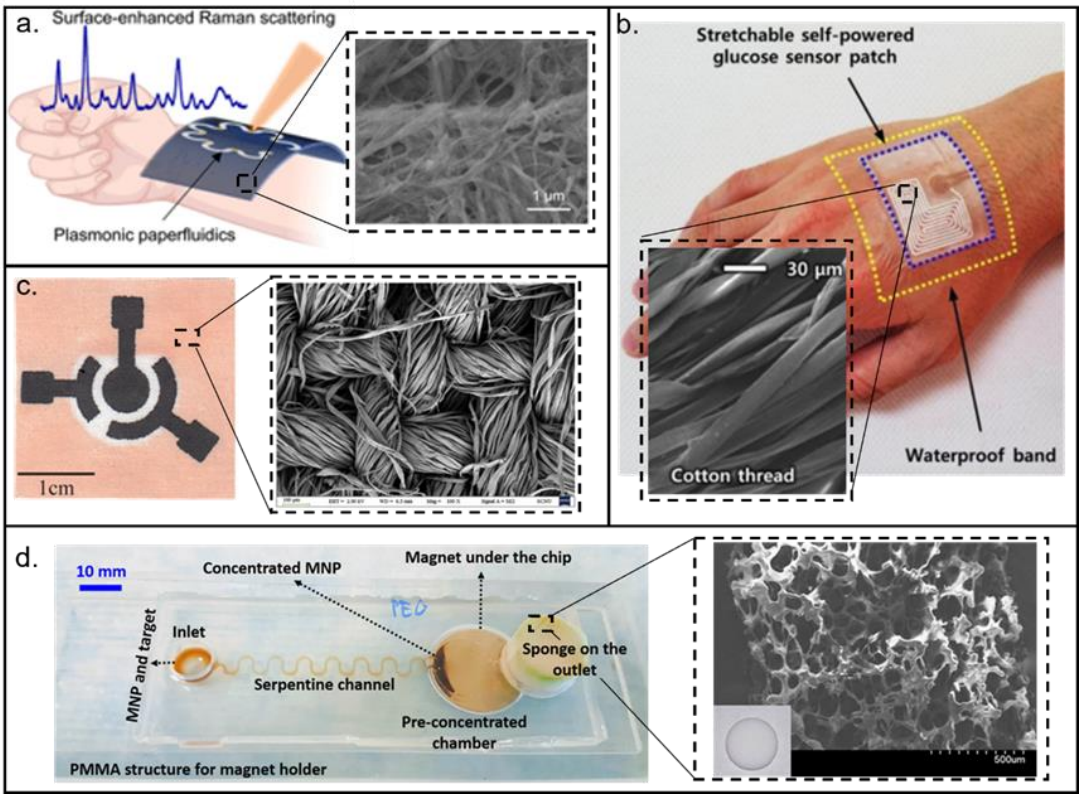

Figure 1.3. Materials used for the fabrication of low-cost porous (paper, thread, cloth, and sponge) microfluidic devices. A. Paper-based device [103]. B. Thread based device [104]. C. Cloth based device [105]. D. PMMA device using sponge in the outlet for sample collection [106]. The images show the structural differences between the porous materials. Cotton and cloth have more organized structures than paper and sponge.

2.1.4. Polymers and other materials

Polymer is a type of material that consists of large molecules called repeating units (or mer) arranged in a periodic manner within the structure [107,108]. Nature has generously provided us many polymeric materials such as wood and rubber [109,110]. The paper cellulose described above is indeed a type of polymer composed of glucose units [111,112]. Moreover, many synthetic polymers have been recently invented for various purposes [113]. For example, plastic is a large family of polymers, including polycarbonate (PC), polyethylene (PE), polypropylene (PP), polyethylene terephthalate (PETE or PET), polyvinyl chloride (PVC), acrylonitrile-butadiene-styrene (ABS) and many

others [107,113,114]. Oftentimes, to create microfluidic devices, the associated cost does not come from the materials themselves since they are cheap, instead, the fabrication methods such as photolithography that creates polymeric structures are responsible for the high cost [25,115]. In particular, PDMS is a popular polymeric material used in microfluidics [31,116,117]. It offers several advantages over other materials such as cost-effectiveness, good biocompatibility and transparency, favorable elasticity and flexibility, inertness to chemicals and permeability to gases [31,118]. To create PDMS based devices, soft lithography has been considered as a gold standard. Specifically, a mold with desired pattern is created first, and then the PDMS mixture is poured onto the mold allowing the curing over time to create PDMS replicas with identical patterns. Though the method itself is low-cost, the molds are made from complex conventional photolithography, for which a cleanroom is indispensable [37,119]. To reduce the cost and eliminate the needs of a cleanroom, other fabrication methods such as 3D printing and milling have been explored for mold manufacturing [48,120].

PMMA is another popular polymeric material used in microfluidics [121–123]. As a thermoplastic, PMMA becomes pliable when heated up above the glass transition temperature. Therefore, similar to PDMS, PMMA devices can be made by molding, thus holding promise for mass production [122,124]. In addition, PMMA can be used as an UV-sensitive material on which the structures are created by the UV radiation [125]. Thin plastic films such as the double-sided tapes, PET films are also explored to create lab-on-a-foil devices [126,127]. Unlike the porous materials described above, the devices made on thin films are much similar to regular PDMS devices, on which microchannels

can be created and active fluid and particle manipulation technologies can be integrated [48]. Another important polymer that has been widely used nowadays are the photosensitive resins used in 3D printing techniques. Note that although traditional 3D printing resins possess good mechanical and physical properties, limitations still exist in terms of the molding performance if used as the molds and the biocompatibility for biology and medical purposes [128]. Other issues such as flow control issues, channel dimensional accuracy, solvent compatibility, surface roughness and low wettability are still the major concerns for broader applications [48,129], though several studies have reported novel photopolymer formulations (resins) capable of potentially addressing these issues [129,130]. More comprehensive reviews of 3D printing materials for microfluidic devices can also help the readers understand the current status and future perspectives for this hot field [48,131].

2.2. Low-cost fabrication methods

The cost associated with the development of microfluidic devices is not completely related with the material selection, the processing methodology used as fabrication method can modify the price dramatically. For instance, a PDMS microfluidic device fabricated under conventional photolithography shall have a different price than the same device fabricated using 3D printing [31,51,121]. In this section, we will summarize the low-cost fabrication methods and provide a perspective of their advantages and limitations. Figure 4.1 shows examples of materials used for low-cost devices and their associated fabrication methods.

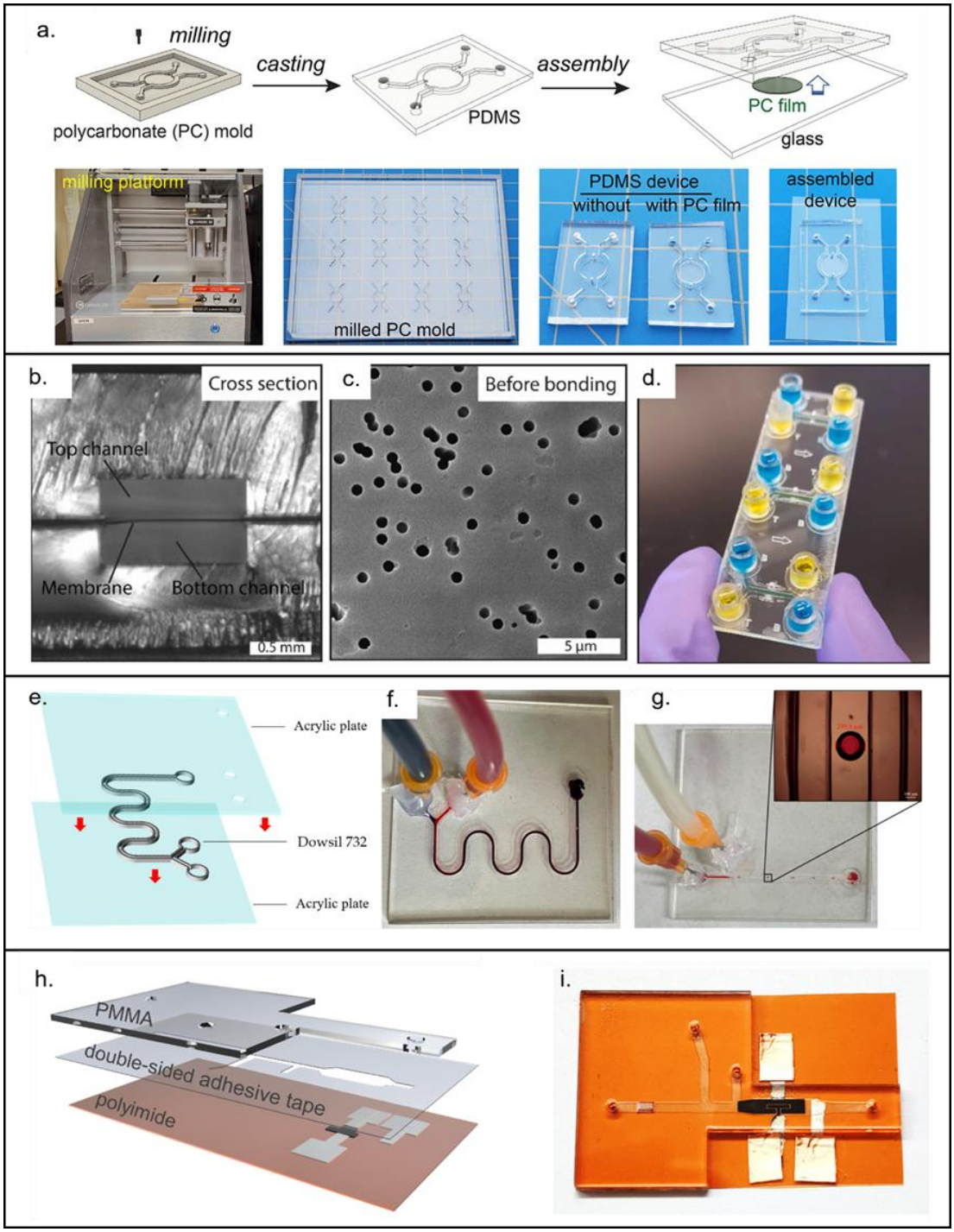

Figure 1.4. Materials used for the fabrication of low-cost non-porous microfluidic devices. A. Microfluidic device made from PDMS casted in a micromilled mold [132]. B. Organ on a chip using micromilling and laser cutting [133]. This time the micromilling was used for end-use platforms instead of being used for mold fabrication. C. Laser cutted PETE membrane [133]. D. Final assembled device [133]. E. 3D printed device made out of novel resin (Dowsil 732) that enables end-use devices [134]. F. Micromixer used to test Dowsil 732 [134]. G. Droplet generator used to test Dowsil 732 [134]. H. Laser cut microfluidic device made of PMMA and double-sided adhesive tape [135]. I. Final assembled device [135].

2.2.1. Fabrication methods for porous materials

Since µPADs, µTADs and µCADs have similar structures, they do share similar fabrication approaches [77,136]. One of the straightforward approaches is to cut paper into strips with desired dimensions, followed by loading essential reagents [70,80,137]. Here, the capillary action serves as the driving pump to spread samples from one end to another [71,138]. Hydrophobic fluid barriers can also be used to control the fluid flow in porous devices, turning a single piece of paper into a fluid managing platform [65,139,140]. Different printers can be used to create hydrophobic walls that confine the fluid transport in between, most printers are simple, inexpensive, and suitable for large volume creation (mass production) [37,70]. Inkjet printing is a popular printing fabrication technology, consisting of two main categories: powder based, or photopolymer based [141–144]. Using this technique, hydrophobic inks are used to create the channel walls on paper-based devices [64,145,146]. Note that inkjet printing is applicable for multiple types of paper, while laser printers provide rapid and large volume printing processes [71,147].

In addition, flexographic printing has also been used for creating µPADs. This method provides a continuous nature of fabrication, which is critical in mass production [148,149]. The screen-printing process has also been used yet it requires multiple steps and has low resolution [65,150–152]. Moreover, wax screen printing is a technology that combines the advantages of wax printing and screen printing, offering a simple 2-step process at much lower costs than traditional wax printing technology [151]. Wax printing has been widely used for creating channel walls in paper-based devices [153,154], however, there are still some limitations for this technology such as the difficulty

to create smaller size channels [48,155,156]. The solvents may also soak into the wax and paper boundaries, thus compromising the functionality of the device [157–160]. Using stamps (ink imprinting) and pen writing (handwriting) are easy yet non-precise techniques to pattern 2D channels [68,161,162]. Plasma treatment can also be used to pattern channels using handheld corona treater [38,163]. The cross-sectional area of porous devices can be adjusted to control the flow motion [65,164], it is possible to cut paper and cloth with different inexpensive tools (*i.e.,* scissors, razor blade) [37,68]. Those tools already exist in commercial versions, coupled to CNC machines and are able to execute a predefined cutting path based on the drawings [165–167]. Similarly, xurography (digital craft cutter) can be used to cut other materials (*e.g.,* polymeric sheet), as long as the material thickness is small [166,168,169].

2.2.2. 3D printing

3D printing technology has proven to be a cost-effective method for prototyping and engineering studies [129,134]. With the improvements of 3D printers, filaments and CAD technologies, 3D printing has emerged as a great tool to create microfluidic devices [30,48,129]. Additive manufacturing constructs three-dimensional objects directly from the CAD designs using techniques such as fused deposition modeling (FDM) and stereolithography (SLA) [48,129,131]. Moreover, this technique allows for the fabrication of the final enclosed device directly from the resin and also for the development of PDMS molds using specific resins [121,129,170]. The printed parts may also be bonded to other substrates or 3D printed parts using adhesive tapes or treatments such as UV bonding [121,171,172]. Owing to the fact that 3D printing does not require a cleanroom setting nor the skilled personnel, this

method holds great promise for low-cost microfluidics, especially when non-conventional designs and multi-layered structures are needed [121,173,174]. However, current 3D printing techniques still have limitations such as clogging of the channels, poor quality of the surfaces and low resolution [129,170]. Despite having lower resolution than conventional cleanroom techniques, the resolution of 3D printers is already suitable for multiple microfluidic applications [129,170]. Although the selection of resins for printing transparent parts and molds is limited, with the rapid advances in this technology, 3D printing resins that promote better resolution, surface finishing and transparency would further enhance the capabilities of microfluidic devices; in fact, there are resins currently being developed with the specific purpose of fabricating microfluidic devices (*e.g.,* figure 4.1e) [170,175]. For further discussion on 3D printing technologies applied to microfluidic devices manufacturing, the readers are encouraged to review the following references: [39,129,170,175–178].

2.2.3. Micromilling

Unlike 3D printing, micromilling is a subtractive manufacturing technique that removes the materials from the bulk to create the desired structures. The prepared parts can be bonded to a substrate to create the final enclosed microfluidic device [179,180], or it can be used as a mold for PDMS [181,182]. Similar to many other low-cost fabrication methods, micromilling does not require a cleanroom and is relatively fast, greatly expediting the manufacturing processes especially for prototyping tests [25,183]. Currently, many materials have been explored to create microfluidic devices using micromilling, among which PMMA and aluminum are two most popular materials [181–185]. The

micromilled molds made of aluminum can be used for casting multiple times, which could further reduce the cost of the final device [183,186].

On the other hand, micromilling has several limitations that should be considered. For example, the milling bits used in micromilling are prone to breaking especially when high resolution (*e.g.,* 25 µm) is required [187,188]. In addition, complex 3D features and designs may not be suitable for micromilling, even though customized milling bits may be able to create structures with preset shapes [181,189]. Micromilling only removes the materials from external surfaces, therefore bonding with other substrates is inevitable to create enclosed microchannels. The bonding could be done mechanically (*i.e.,* using screws), thermally (*i.e.,* bonding two PMMA plates when heated up), or using surface treatments and adhesives such as the tapes [190–193].

2.2.4. Laser micromachining

Laser micromachining has also been employed for low-cost microfluidics [133,194]. For example, CO2 laser is a widely used microfabrication method [71,123,195,196]. During the fabrication process, the laser energy is focused on the region of interest of the workpieces, causing the materials to melt and evaporate. Typically, a CO2 laser with a wavelength of 10.6 µm are used [133,194]. Indeed, sophisticated laser machine or reduced wavelength (*e.g.,* femtosecond lasers) can be applied to further improve the cutting resolution, yet these methods are not suitable for low-cost microfluidics since extra costs are inevitably required [197–199]. When it comes to the materials used in laser micromachining, both hard materials such as glass and soft materials such as PMMA, cyclic olefin copolymer (COC) and even paper could be used [200,201]. Note that to avoid the cracks caused by thermal stress, surface coating could

be applied on the glass slides [202] . In addition, laser micromachining can be used to create both molds and final devices after bonding [53,66,203]. The bonding and assembly techniques used for laser cut devices are similar to those used for micromilled devices [25,133,183,194].

2.2.5. Other fabrication methods

Thin plastic films can also be directly made into final devices via screen printing technology, or as simple as hand cutting [48,71]. Films and thin plastics can be fabricated at large scale using laminate manufacturing or roller imprinting [126,204]. Note that PMMA has been widely used in low-cost microfluidics, it has been used to create devices by micromilling, laser ablation, and by the injection molding [122,205], thus holding promise in mass production [122,124]. It is also worth mentioning that the methods such as roller imprinting, injection molding and hot embossing do require a high-resolution mold, which increases the initial cost but eventually can compensate towards low unit price [206–208]. Indeed, there are other fabrication methods explored for microfluidics, for example, microwire has been used to create devices but the performance is not as high as that of 3D printing [209,210]. Interested readers are encouraged to read the references [25,31,37].

Table 1.1. Advantages and disadvantages comparisons, and cost estimations for the aforementioned low-cost fabrication technologies.

Method	Advantages	Disadvantages	Fabrication Cost	References
3D printing	Prints on demand Robust mechanical properties Easy adaption for electromechanics detectors	Low resolution Limited minimal feature size Lack of transparency Biocompatibility issues	Microfluidic 3D printer: >$3000 Cost per part: ~$5	[39,211]
Wax printing	Hydrophobic channel walls Eco-friendly Suitable for mass production	Low resolution Time-consuming	Wax printer: >$1000 $0.001 per device of 1 cm^2	[68,212]
Inkjet printing	High resolution Easy adaptivity to various substrates Multi-material printing Rapid process Suitable for mass production	Not eco-friendly Requires frequent maintenance	Inkjet printer: ~$300	[204,213–215]

Screen printing	Capable of printing a variety of conductive materials Simple process Suitable for mass production	Low resolution Different screens are needed for different patterns Not suitable for mass production	Screen printer: ~$300	[216]
Micromilling	Capable of making complex features Rapid prototyping method	High surface roughness	CNC mills: ~$1000 Substrate: ~$10	[186]
Laser cutting	Easy integration with electronics High precision	High energy consumption Not suitable for mass production	Laser cutter: >$400 Substrate: ~$10	[117,194,217]
Xurography	Eco-friendly Simple prototyping method	Edge warping and tearing Not suitable for mass production Low precision	Knife plotter: >$300 Accessories: ~$10	[218]
Laser printing	User friendly	Requires special inks	Laserjet printer: ~$300	[219]
Manual cutting	Simple operation	Low resolution	Inexpensive	[71]

Flexographic printing	Continuous printing	Requires frequent maintenance	Depends on the design	[220]
Hot embossing	Good for mass production	Requires mould fabrication	Requires mould price evaluation	[221]
Injection molding	Good for mass production	Requires mould fabrication	Requires mould price evaluation	[222]

3. Latest environmental applications

In this section, we will review the latest low-cost microfluidic advancements in the field of environmental monitoring. There are three main subsections to summarize and discuss the devices used for water, air, and soil contamination detection.

3.1. Water quality monitoring

Effective water quality monitoring and assessment are of great importance and essential to public health. Low-cost microfluidic devices offer competitive performance as compared to sophisticated equipment in centralized laboratories yet are more cost-effective and provide simpler operation and more rapid analytical analysis [34,223]. As a result, much effort has been made to develop more effective and low-cost microfluidic devices for efficient water quality monitoring for the assessment of different types of contaminants. This section provides the readers with an overview of the most recent advancements in this regard.

3.1.1. Heavy metal pollutants

Heavy metal pollution in water has received increasing attention over the past decades [36,224,225]. It is reported that even at low concentrations, these contaminants can pose a great threat to the aquatic environment, ecosystem, and human health [119,226]. Given such growing concerns, low-cost microfluidic devices can be an affordable tool for continuous water monitoring regarding heavy metal contamination worldwide. The burgeoning advancements are distinct as evidenced by continuous developments made over the past years, with many applications built on top of paper microfluidics

[36]. To name a few, Wang et al. developed a μPAD with high detection accuracy and selectivity for lead ions (Pb2+) in drinking water. The device realized rapid visual quantitative detection by examining the extension length of the color bar in the particle dam [227]. A similar device was designed to quantify silver (Ag+) contamination in freshwater, and it was reported to have a detection limit of 453.7 nM, high selectivity, and a high recovery rate of 96.8% [228]. Jarujamrus et al. developed a μPAD to detect mercury (Hg2+) in various water samples with the ability to instantly report Hg2+ concentration on-site by using a smartphone. The smartphone analyzer is responsive and user-friendly, which has enabled unskilled users to use this device to conduct sample analysis [229]. Similar applications used μPADs for the detection of Cu2+ [230,231].

Besides the detection of a single type of heavy metal, μPADs were also developed for the identification of multiple heavy metals simultaneously. Khoshbin et al. developed a paper-based aptasensor to detect Ag+ and Hg2+ within 10 minutes based on conformational changes of Ag+ -and Hg2+ specific aptamers. The concentration of the ions can be indicated by fluorescence recovery rate, with a limit of detection of 1.33 pM for Hg2+ and 1.01 pM for Ag+ [232]. Idros et al. used a μPAD to detect several major heavy metals, including Hg2+, Pb2+, Cr3+, Ni2+, Cu2+, and Fe3+ by applying different ligands loaded onto the test paper [233] (Figure 5.1a). Similarly, Kamnoet et al. capitalized on the colorimetric assays to identify multiple heavy metals including Cu2+, Co2+, Ni2+, Hg2+, and Mn2+ with a corresponding limit of detection of 0.32, 0.59, 5.87, 0.20, and 0.11 mg/L, respectively [153].

The porous nature of papers and capillary driving can limit associated fluid and particle manipulation. Herein, other materials such as polymers are also applied to fabricate microfluidic devices for more accurate heavy metal detection. For example, an epitaxial graphene sensor was combined with a 3D-printed microfluidic chip to detect Pb2+ and Cd2+ [224]. In another study, a porous conductive carbon cloth was integrated with a microfluidic device to desalinate and recover valuable metal ions (Cu2+, Zn2+, Ni2+, Ag+, and Zn2+/ Cu2+ mixtures) from wastewater samples [234]. Ding et al. successfully conducted heavy metal analysis by using a sponge-based microfluidic device that was integrated with ion-selective electrodes for sampling heavy metal ions (Cd2+ and Pb2+) and non-metal clinically related chemical ions, namely K+, Na+, and Cl− [235] (Figure 5.1b). Furthermore, a combined μCPAD was developed to detect mercury and lead ions in water samples. The groups used cloth's ductility and durability to endure the oscillation during fabrication to improve the producibility and life span of the device [227].

3.1.2. Non-metallic pollutants

Non-metal substances are more abundant pollutants in water and are highly complex by nature. Nowadays, portable microfluidic devices are playing a critical role in water quality analysis for a large variety of toxins, such as pharmaceutical residues, due to their many advantages [119]. Scala-Benuzzi et al. developed an electrochemical paper-based immunocapture assay (EPIA) to assess Ethinylestradiol quantitively in water samples. It was reported the test achieved a low detection limit of 0.1 ng/L and a linearity range of 0.5–120 ng/L [236]. In another study, chlorpyrifos pesticide was detected by using a lipase-embedded paper-based device [237]. The limit of detection and limit of

quantification was found to be 0.065 mg/L and 0.198 mg/L, respectively. Interestingly, the wash water of cauliflower, grapes, coriander leaves, brinjal, and bitter guard could be used as samples [237]. Jemmeli et al. developed a highly sensitive paper-based electrochemical sensor to detect bisphenol A (BPA) in drinking water [238]. Mako et al. developed a μPAD to detect nitrite levels in drinking water [239]. Peters et al., developed a μPAD to monitor total ammonia levels in freshwater [240]. Similarly, μPAD was used for detecting phosphate in water samples [241,242]. Besides paper-based devices, Carvalho et al. developed a fully 3D printed thread-based microfluidic device to detect Nitrite in well water samples with high precision [243]. Caetano et al. developed a textile thread-based microfluidic device combined with an electrochemical biosensor to detect phenol concentration in tap water [149].

It is worth noting that, among all the non-metallic pollutants, microplastics have been drawing lots of research attention recently. Microfluidic devices can benefit microplastic-related research in many ways, such as microplastic identification and separation. However, only a few low-cost microfluidic devices have been developed for these applications. Pollard et al. developed a low-cost and high-throughput three-dimensional printed microfluidic resistive pulse sensor for characterizing algae with spherical and rod structures as well as microplastics from tea bags. The device can rapidly screen liquids at a volume rate of 1L/min in the presence of microplastic and algae [244] (Figure 5.1c). Mesquita et al. developed a 3D printed microfluidic device for microplastic identification that improved the Nile Red staining process [245]. It is suggested that researchers use the full potential of low-cost microfluidic devices to achieve reproducible and reliable long-term assessment of environmental microplastics.

3.1.3. Waterborne microorganisms

The presence of waterborne pathogens can cause severe illnesses. Continuous monitoring and in-situ studies of waterborne microorganisms are another rapidly growing research interest. In a recent study, Yin et al. developed a 3D-printed integrated microfluidic chip for colorimetric detection of SARS-CoV-2 and other human enteric pathogens in wastewater. The sensitivity of detection was reported to be 100 genome equivalent (GE)/mL for SARS-CoV-2 and 500 colony-forming units (CFU)/mL for other targeted human enteric pathogens [246] (Figure 5.1d). Schaumburg et al. designed a μPAD for waterborne bacteria detection which consists of two sequential pre-concentration steps. The detection limit of concentration was as low as 9.2 CFU/mL in laboratory samples and 920 CFU/mL in apple juice samples within ~90 min [247]. Several studies successfully used μPAD and 3D printed microfluidic devices to detect E. coli in various water samples and achieved low detection limit, high sensitivity, and quick analysis [226,248–250].

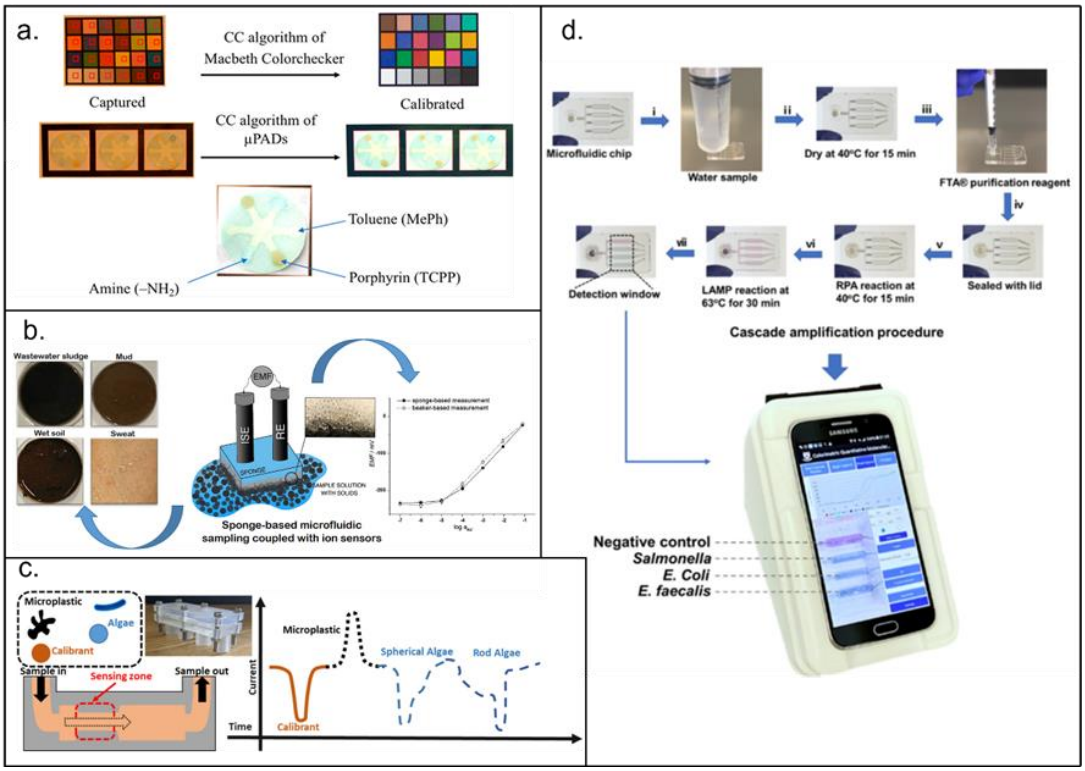

Figure 1.5. Low-cost microfluidic platform for water quality monitoring. A. Detection of Hg2+, Pb2+, Cr3+, Ni2+, Cu2+, and Fe3+ by applying different ligands loaded onto the test paper [233]. B. Detection of heavy metal ions (Cd2+ and Pb2+) and non-metal clinically related chemical ions, namely K+, Na+, and Cl− with a sponge-based device [235]. C. Characterizing algae with spherical and microplastics from tea bags with a 3D printed device [244]. D. Detection of SARS-CoV-2 and other human enteric pathogens in wastewater with a 3D printed device [246].

3.2. Air quality monitoring

Monitoring and controlling airborne microparticles are drawing attention due to the decreasing air quality across the globe. Microfluidic devices have proven the ability to sort and separate microparticles effectively, which shall be used in air quality monitoring for particle trapping and real-time concentration analysis. In this section, recent applications of low-cost microfluidic devices in the assessment of airborne micro particles are discussed.

3.2.1. Metallic and non-metallic pollutants

Airborne metal particles are one of the most representative harmful elements. Several studies have used μPAD to detect some typical airborne metal particles. Sun et al. developed a μPAD that realized on-site multiaxial quantification of airborne trace metals by implementing unmanned aerial vehicle in-air sampling (UAV). Data can be easily processed by a smartphone within 30 minutes [251]. The same group later applied graphene oxide (GO) coating onto the paper and improved the detection limits for Fe, Cu, and Ni to 6.6, 5.1, and 9.9 ng respectively, which is comparable to the commercial coupled plasma (ICP) instruments [252] (Figure 6.1a). Jia et al. successfully used a μPAD to detect cobalt (Co), copper (Cu), and iron (Fe) in ambient air and street sediments with detection limits of 8.2, 45.8, and 186.0 ng [253].

Unlike water applications, only a few devices used low-cost microfluidic devices for the detection of non-metallic airborne pollutants. For example, Guo et al. developed a smartphone-based microfluidic sensor to detect gaseous formaldehyde in the ambient. The microfluidic chip consists of two reagent reservoirs, a reaction reservoir, and a mixing column. The PTFE membrane was used to prevent the fluid from flowing out while the gas molecules enter. The system showed great selectivity against other ambient gas [254]. Zhao et al. developed a 3D printed based microfluidic impactor for particular matter classification and concentration detection [255] (Figure 6.1b). However, most of these applications used costly fabrication techniques, such as photolithography, and the integration with multiple sensors also increased the overall cost [256].

3.2.2. Airborne microorganisms

Dias et al. used a μPAD to detect levoglucosan concentration in the ambient with a colorimetric method. The linear detection range is 0 to 64.8 μg m/L and the detection limit is 2 and 6 μg m/L. The device showed selectivity for levoglucosan with variation in colorimetric signal intensity lower than 8% [257] (Figure 6.1c). Seok et al. developed a μPAD combined with a 3D printed analysis kit for detection of airborne bacteria by collecting aerosols [258] (Figure 6.1d).

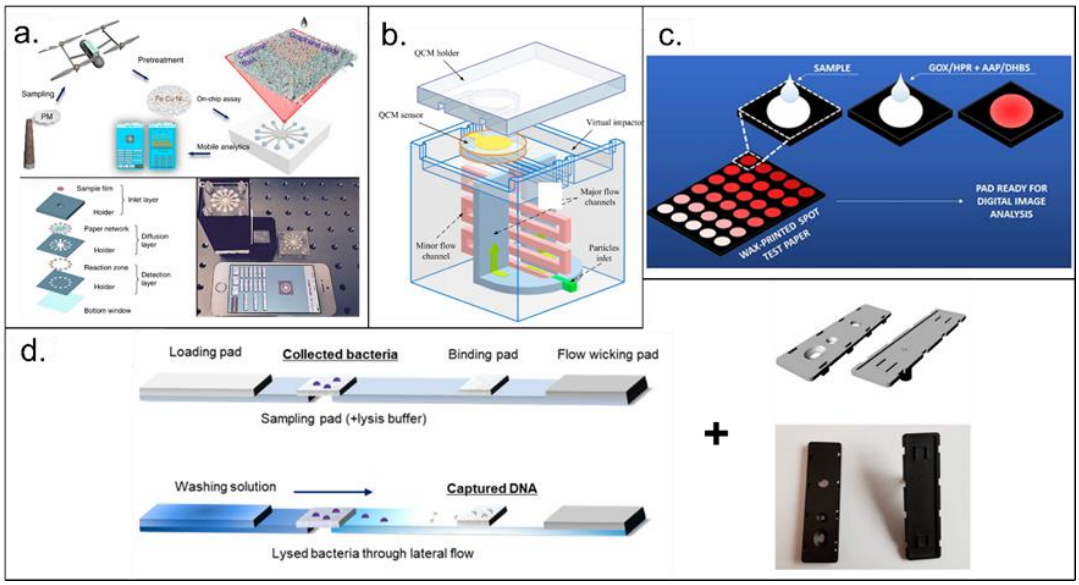

Figure 1.6. Low-cost microfluidic platforms for air quality monitoring. A. Quantification of airborne trace metals, such as Fe, Cu, and Ni with μPAD [252]. B. Particular matter classification and concentration detection with a 3D printed device [255]. C. Levoglucosan concentration detection in the ambient air with μPAD [257]. D. Detection of airborne bacteria with μPAD and a 3D printed device [258].

3.3. Soil quality monitoring

Soil is home to many types of microorganisms and nutrients and contains many types of toxic pollutants. Simplified detection methods and analysis devices for soil quality management are beneficial to agricultural development,

ecosystem, and human health. This section reviews the recent applications of low-cost microfluidic approaches used for soil quality assessments.

3.3.1. Heavy metals and non-metallic pollutants

Ding et al. used an acidified μPAD integrated with potentiometric sensors for the detection of multiple heavy metal ions in the soil, street run-off, and multiple environmental samples [235] (Figure 7.1a). Similarly, an eco-friendlier metal-modified μPAD was developed for the same purpose [101] (Figure 7.1b). Xi et al. developed a centrifugal microfluidic system for pyrene extraction from soil [259]. A similar centrifugal microfluidic device was also used for the detection of pesticide residues in vegetables and soil [260]. Other soil nutrients can be detected using colorimetric microfluidic devices, most of these applications used μPAD, 3D printed devices, and a combination of low-cost fabrication techniques [261].

3.3.2. Soil microorganisms

With the advantages of microfluidic platforms, the development of soil-on-a-chip has been growing to study soil biofilms and microorganisms' ecological and biological impacts [262,263] (Figure 7.1c). However, challenges and limitations still exist, such as the controlling of hydrophilic and hydrophobic surfaces in PDMS based devices, which highlighted the potential benefits of using porous membrane microchannels, which are normally fabricated with low costs.

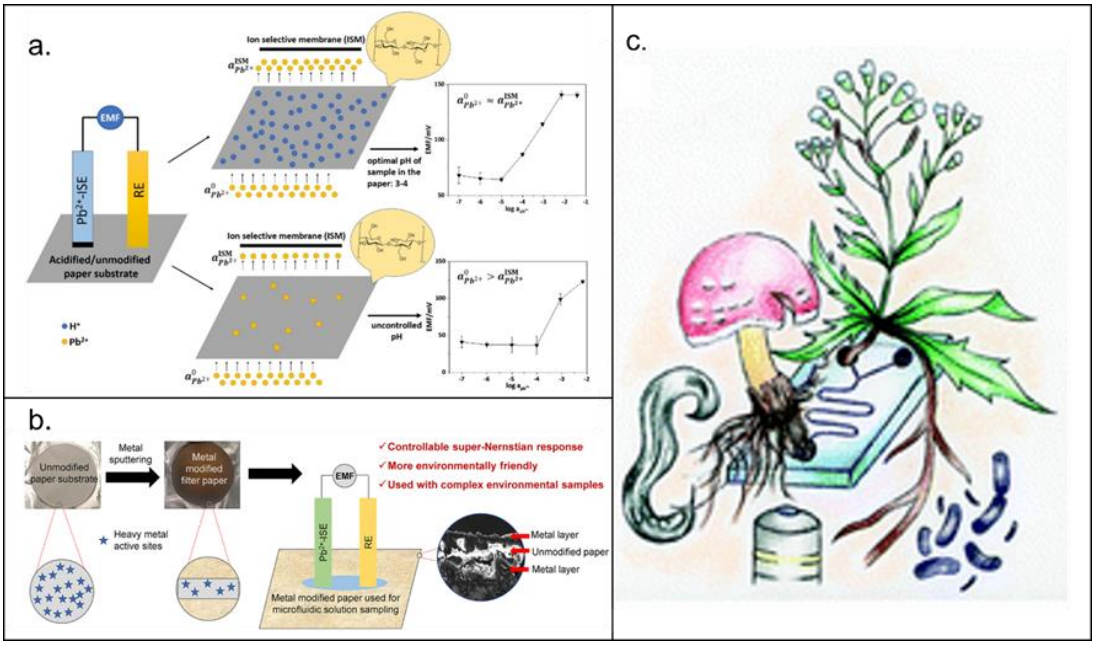

Figure 1.7. Low-cost microfluidic platform for soil quality monitoring. A. Detection of multiple heavy metal ions using acidified μPAD [235]. B. Detection of multiple heavy metal ions using metal modified μPAD [101]. C. Soil-on-chip concept [262].

3.4. Other microfluidic platform environmental applications

Microfluidic devices can be used for many other environmental applications. The burgeoning demand for reliable and reproducible devices that can be mass-produced makes low-cost microfluidic approaches more appealing. Readers are encouraged to read review papers in this regard and further implement low-cost fabrication techniques by combining different methodologies or converting existing designs to low-cost versions [12,15,264]. Table 2 summarizes the low-cost microfluidic platforms for environmental monitoring mentioned in this review regarding their substrate material, fabrication method, detection methods, and significant contributions and results.

Table 1.2. Summary of environmental applications using microfluidic technologies.

Applications	Substrates (fabrication)	Detection technique	Contributions and results	References
Detection of Hg^{2+} concentration in water samples	μPAD	Colorimetric	High sensitivity; low LOD (0.003 mg/L, 3SD blank/slope of the calibration curve); small sample volume uptake; short analysis time	[229]
Detection of Cu^{2+} concentration in water samples	μPAD	Colorimetric	Can be adapted to measure a wide range of Cu concentrations (from approximately 20 to 500 000 ppb)	[230,231]
Detection of Ag^{+} and Hg2+ in water samples	μPAD	Fluorescence recovery changes from reaction with GO surface	LODs of 1.33 and 1.01 pM; rapid analysis	[232]
Detection of Hg^{2+}, Pb^{2+}, Cr^{3+}, Ni^{2+}, Cu^{2+}, and Fe^{3+} in water samples	μPAD	Colorimetric	Integration of digital image processing with color calibration technique and paper-based sensor	[233]
Detection of Cu^{2+}, Co^{2+}, Ni^{2+}, Hg^{2+}, and Mn^{2+} in the water sample	μPAD, wax printing	Colorimetric	Lowest detectable concentrations of 0.32, 0.59, 5.87, 0.20, and 0.11 mg/L for	[153]

			Cu, Co, Ni, Hg, and Mn, respectively	
Detection of Pb^{2+} and Cd^{2+} in the water sample	3D printed chip	Epitaxial Graphene Conductivity	High sensitivity detection to low concentration Pb	[224]
Recover metal ions (Cu^{2+}, Zn^{2+}, Ni^{2+}, Ag^{+}, and Zn^{2+}/$Cu2^{+}$ mixtures) from water sample	Carbon cloth	Electro-oxidation process	Can be used as controlled decoration of materials with metal nanoparticle patterns; Regeneration of rare earth trace contaminants	[224,234]
Detection of heavy metal ions (Cd^{2+} and Pb^{2+}) and non-metal chemical ions, K^{+}, Na^{+}, and Cl^{-} from the water sample	Polyurethane based sponge	Potentiometric measurements between electrodes; Liquid wicking capacity testing	Measurements of heavy metals without prior to modification of the sampling substrate	[100]
Detection of mercury and lead ions in the water	μCPAD	Fluorescence sensing	LODs were 0.18 and 0.07 μg/L; can be used in point-of-care testing of heavy metal ions in environmental monitoring fields	[227]
Quantification of ethinylestradiol in water samples	Paper-based immunocapture assay (EPIA), screen	Electrochemical reaction	LOD 0.1 ng/L; linear range value 0.5–120 ng/L; high recovery rate	[236]

	printed carbon electrodes			
Detection of chlorpyrifos pesticide in water samples	µPAD	Colorimetric	LOD of 0.065 mg/L; LOQ of 0.198 mg/L	[237]
Detection of bisphenol A (BPA) in drinking water	µPAD, ink-printed carbon electrodes	Electrochemical reaction	LOD of 0.03 µM	[238]
Detection of nitrite levels in drinking water	µPAD	N-(1-Naphthyl) ethylenediamine-Grafted Cellulose, Colorimetric	LOD in synthetic freshwater is 0.26 µM; in real seawater is 0.22 µM	[239]
Detection of ammonia levels in drinking water	µPAD	Colorimetric	LOD of 0.32 mg N/L, working concentration ranges of 0.5–3.0 mg N/L using NY; 0.47 mg N/L and working concentration ranges of 2.0–10 mg N/L using BTB indicators	[240]

Detection of phosphate levels in drinking water	µPAD	Colorimetric	LOD between 1.3 and 2.8 ppm in various aqueous media	[241,242]
Detection of Nitrite in well water	Thread-based, 3D printed electrodes	Electrochemical reaction	LOD of 2.39 µmol/L; good repeatability and reproducibility	[243]
Detection of phenol concentration in tap water	Textile thread-based, Screen-printed electrodes	Electrochemical reaction	LOD of 2.94 nmol/L; limit of quantification 8.92 nmol/L	[149]
Characterization of algae and microplastics from tea bags	3D printed	Flow resistive pulse sensor	Particles range from 2 to 30 µm; can be used at high flow rate	[244]
Identification of microplastics in water samples	3D printed	Fluorescence sensing	Study of Nile red staining capability for microplastic identification	[245]
Detection of SARS-CoV-2 and other human enteric pathogens in wastewater	3D printed	Colorimetric	SARS-CoV-2 sensitivities of 100 genome equivalent (GE)/mL; human enteric pathogens sensitivities of 500 colony-forming units (CFU)/mL	[246]

Detection of waterborne bacteria	μPAD	Polymerase chain reaction (PCR)	Low detection concentration of 9.2 CFU/mL in lab; 920 CFU/mL in apple juice samples	[247]
Detection of E. coli in various water samples	3D printed	Bacteriophage-based bioluminescence assay	Can identify 4.1 E. coli CFU in 100 mL of drinking water within 5.5 hours	[22,226,248,250]
Quantification of airborne trace metals	μPAD with GO-nanosheet-coating	Colorimetric	LOD of 16.6, 5.1, and 9.9 ng for metals Fe, Cu, and Ni, respectively; rapid real-time analysis	[252]
Detection of cobalt (Co), copper (Cu), and iron (Fe) in ambient air and street sediments	μPAD	Colorimetric	LOD for Co, Cu, and Fe were determined to be 8.2, 45.8, and 186.0 ng, respectively	[253]
Detection of gaseous formaldehyde in the ambient	PTFE membrane	Colorimetric	LOD of 0.01 ppm; high selectivity	[254]
Detection of levoglucosan	μPAD	Colorimetric	LOD is 2 6 μg/mL; limit of quantification is 6 μg/mL; average recovery was 105 ± 9%	[257]

concentration in the ambient				
Detection of airborne bacteria	µPAD + 3D printed channel	Polymerase chain reaction (PCR)	Fast analysis; simple, cost effective	[258]
Detection of multiple heavy metal ions in the soil, street run-off, and multiple environmental samples	µPAD	Potentiometric response	Improved response time; can be used for complex samples containing high number of solids to liquids	[101,235]
Extraction of pyrene from soil	µPAD	UV absorbance measurement	LOD of 1 ppm (0.03 microg absolute detection limit)	[259]
Detection of pesticide residues in vegetables and soil	µPAD	Enzyme Inhibition	LOD of 0.1 ppm or 0.1 µg/g (5 ng absolute LOD); Less expensive reagents	[260]

4. Discussion and conclusion

Low-cost microfluidic technologies have grown over the years, especially because the materials and fabrication methods summarized here are useful to aid places with limited resources, proving to be a reliable substitute to expensive equipment and complex operation processes [37,265]. Among all the low-cost devices, paper is one of the most widely used, given its high availability and easy manufacturing techniques [68,70]. In addition, porous devices are attractive because they are user friendly, its capillary nature made it possible to eliminate the dependency on external flow control equipment (*i.e.,* no necessity of pumps), easing the operation [70,71]. However, porous devices lack the ability to provide equivalent abilities in fluid and particle manipulation as non-porous devices due to the passive nature of fluid wicking [70,121].

In addition, a variety of methods have been successfully used to create polymeric devices, including 3D printing, micromilling, laser cutting, xurography, injection moulding, and hot embossing [121,133,183,218,222]. Specifically, 3D printing has emerged as an inexpensive fabrication approach, providing acceptable resolution that is beneficial for the creation of complex microchannels [121,266]. Xurography employs a knife cutter to cut structures in the materials, this simple method is useful for the fabrication of rapid tests through the employment of laminated devices [165,169,267]. However, the resolution is highly limited by the blade sizes and the method lacks the capabilities to fabricate thick devices [133,194,218]. Laser micromachining has its resolution heavily reliant on the laser quality and wavelength, in order to increase the resolution, expensive lasers are

necessary, limiting its applications in low-cost microfluidics [71,196,268]. Mass production remains a key approach to reduce the final cost of a single unit, in this regard, several methods such as injection molding and hot embossing are good candidates [115,221].

Despite great achievements made over the past years for low-cost microfluidics, current devices still do not possess competitive performance compared to devices made using traditional methods especially those based on the clean room fabrication techniques. In summary, the selection of the most appropriate material for certain applications is critical to achieve the desired performance for microfluidic devices. Though there is a large pool of potential materials available for selection, the goal of achieving low-cost, good quality, and efficient high-volume production remains to be the challenging triple constraints for creating a more competitive force for low-cost microfluidics regarding capability, reproducibility, and sustainability [170,269].

Environmental monitoring is a field that demands costly analysis techniques and have been benefited from low-cost microfluidic devices [270,271]. Water quality monitoring is an important application of low-cost microfluidic devices, as freshwater management is essential to human life, although still limited in some places [10,272]. In case of water contamination, low-cost microfluidic devices can assist tracking diseases since multiple tests can be performed using disposable or reusable devices (*e.g.,* Covid on wastewater using 3D printed devices [246]). Instead of outsourcing tests, it is possible to continuously monitor water quality using portable tests [273,274]. Heavy metal detection in water samples using

paper-based devices have been demonstrated in different devices: multiple heavy metals in coastal waters [275]; in situ cadmium [276] and mercury [272] detection, indicating that most heavy metals can be identified using low-cost devices. Micromilling and 3D printed devices were explored for heavy metal detection [224,277] and though these devices were successful experimentally and demonstrated enough accuracy to be used in the lab, the dependency on external pumping systems and trained personnel still limits their market potential. When it comes to processing samples with large volumes, injection molded devices have emerged as a major player. For example, the detection of E. coli in earlier stages was performed using an injection molded device capable of processing 100 mL of water [248].

Air and soil quality are other important fields of environmental monitoring due to their direct relation with humans [278,279]. Different µPADs have been developed for heavy metal detection in soil street run-off samples [235], and air samples [253]. Non-porous technologies have also been used for soil analysis, such as centrifugal microfluidic device for the detection of pesticide residues in vegetables and soil [259,260]. Despite many successful applications in the air and soil monitoring areas, as evidenced in research publications, low-cost devices have yet to be widely commercially available in the market due to complexity of air and soil samples [271,280]. Samples are normally filtered and washed, which is time consuming (especially for air samples, which have to be captured in open space) hindering the use of low-cost technologies by the general public [251,281]. Though microfluidic devices have been widely used for environmental applications,

not all devices can be considered user-friendly and low-cost [25,37]. Especially for air and soil environmental analysis, as discussed above, this can be mainly due to the sample pre-processing and device operation (*e.g.,* pump operation in 3D printed devices). More applications related to air and soil quality monitoring are encouraged and should be developed. Most of the low-cost devices reviewed in the paper used colorimetric detection method [68,80,282]. Though water is related to a lot of applications, there is a lack of standardization that could be beneficial to boost commercialization.

Cost reduction is critical to expand the usage of microfluidic devices in environmental monitoring. A combination of a few low-cost techniques (hybrid devices) was attempted for different purposes and should be further explored [120,129,136]. Hybrid devices can take advantage of commercially available technologies [120,129,227]. Smartphones have been used along with low-cost microfluidic devices to enhance accuracy and overall performance [242,246,283]. Smartphones were coupled with paper-based inkjet-printed devices for Cr3+ and Al3+ identification on water [284], as well as Pb2+ [285]. For the case of air quality control, drones were used to collect samples in different location and heights and used smartphones for data processing within 30 minutes at a cost of $1.92 [251]. The samples still needed to be pre-processed with acid solutions for final analysis, showing that this step requires more simplification. A filtration system was developed to be used in the field (hand powered), which is a good option to substitute pumping systems in devices that do not require flow rate precision [230]. With the advantages of microfluidic platforms, the development of soil-on-a-chip

devices has been growing to study soil biofilms and ecological and biological impacts of microorganisms, which is of fundamental importance for the constant development of novel and better performing agricultural practices [262,263]. Overall, low-cost microfluidic devices have proven their capability to perform environmental monitoring assessment, furthermore, low-cost microfluidics have been contributing to the worldwide spread of microfluidic technologies, indicating that researchers should keep innovating towards more reliable cost-effective devices [262,271,272].

Acknowledgments

We acknowledge financial support from Rhode Island Foundation (8429_20210963).

5. References

1. Podgorski, J.; Berg, M. Global Threat of Arsenic in Groundwater. Science (80-.). 2020, 368, 845–850.

2. Santos, R.G.; Machovsky-Capuska, G.E.; Andrades, R. Plastic Ingestion as an Evolutionary Trap: Toward a Holistic Understanding. Science (80-.). 2021, 373, 56–60.

3. Xu, X.; Nie, S.; Ding, H.; Hou, F.F. Environmental Pollution and Kidney Diseases. Nat. Rev. Nephrol. 2018, 14, 313–324.

4. Lau, W.W.Y.; Shiran, Y.; Bailey, R.M.; Cook, E.; Stuchtey, M.R.; Koskella, J.; Velis, C.A.; Godfrey, L.; Boucher, J.; Murphy, M.B. Evaluating Scenarios toward Zero Plastic Pollution. Science (80-.). 2020, 369, 1455–1461.

5. Evans, E.; Gabriel, E.F.M.; Coltro, W.K.T.; Garcia, C.D. Rational Selection of Substrates to Improve Color Intensity and Uniformity on Microfluidic Paper-Based Analytical Devices. Analyst 2014, 139, 2127–2132.

6. Yang, X.; Zhang, T.; Zhang, X.; Chu, C.; Sang, S. Global Burden of Lung Cancer Attributable to Ambient Fine Particulate Matter Pollution in 204 Countries and Territories, 1990–2019. Environ. Res. 2022, 204, 112023.

7. Mahaqi, A.; Mehiqi, M.; Moheghy, M.A.; Moheghi, M.M.; Hussainzadeh, J. Nitrate Pollution in Kabul Water Supplies, Afghanistan; Sources and Chemical Reactions: A Review. Int. J. Environ. Sci. Technol. 2021, 1–10.

8. Colford, J.M.J.; Roy, S.; Beach, M.J.; Hightower, A.; Shaw, S.E.; Wade, T.J. A Review of Household Drinking Water Intervention Trials and an Approach to the Estimation of Endemic Waterborne Gastroenteritis in the United States. J. Water Health 2006, 4 Suppl 2, 71–88, doi:10.2166/wh.2006.018.

9. Hamilton, A.J.; Stagnitti, F.; Premier, R.; Boland, A.-M.; Hale, G. Quantitative Microbial Risk Assessment Models for Consumption of Raw Vegetables Irrigated with Reclaimed Water. Appl. Environ. Microbiol. 2006, 72, 3284–3290.

10. Komolafe, A.A.; Adegboyega, S.A.-A.; Anifowose, A.Y.B.; Akinluyi, F.O.; Awoniran, D.R. Air Pollution and Climate Change in Lagos, Nigeria: Needs for Proactive Approaches to Risk Management and Adaptation. Am. J. Environ. Sci. 2014, 10, 412.

11. Yew, M.; Ren, Y.; Koh, K.S.; Sun, C.; Snape, C. A Review of State-of-the-Art Microfluidic Technologies for Environmental Applications: Detection and Remediation. Glob. Challenges 2019, 3, 1800060.

12. Pol, R.; Céspedes, F.; Gabriel, D.; Baeza, M. Microfluidic Lab-on-a-Chip Platforms for Environmental Monitoring. TrAC Trends Anal. Chem. 2017, 95, 62–68.

13. Ritchie, J.C.; Zimba, P. V; Everitt, J.H. Remote Sensing Techniques to Assess Water Quality. Photogramm. Eng. Remote Sens. 2003, 69, 695–704.

14. Pena-Pereira, F.; Bendicho, C.; Pavlović, D.M.; Martín-Esteban, A.; Díaz-Álvarez, M.; Pan, Y.; Cooper, J.; Yang, Z.; Safarik, I.; Pospiskova, K. Miniaturized Analytical Methods for Determination of Environmental Contaminants of Emerging Concern–a Review. Anal. Chim. Acta 2021, 1158, 238108.

15. Dhar, B.C.; Lee, N.Y. Lab-on-a-Chip Technology for Environmental Monitoring of Microorganisms. BioChip J. 2018, 12, 173–183.

16. Gao, Y.; Wu, M.; Lin, Y.; Xu, J. Acoustic Microfluidic Separation Techniques and Bioapplications: A Review. Micromachines 2020, 11, 921.

17. McNeely, M.R.; Spute, M.K.; Tusneem, N.A.; Oliphant, A.R. Hydrophobic Microfluidics. In Proceedings of the Microfluidic Devices and Systems II; International Society for Optics and Photonics, 1999; Vol. 3877, pp. 210–220.

18. Zhu, Y.; Fang, Q. Analytical Detection Techniques for Droplet Microfluidics—A Review. Anal. Chim. Acta 2013, 787, 24–35.

19. Moreau, W.M. Semiconductor Lithography: Principles, Practices, and Materials; Springer Science & Business Media, 2012; ISBN 1461308852.

20. Rai-Choudhury, P. Handbook of Microlithography, Micromachining, and Microfabrication: Microlithography; SPIE press, 1997; Vol. 1; ISBN 0819423785.

21. Song, Y.; Lin, B.; Tian, T.; Xu, X.; Wang, W.; Ruan, Q.; Guo, J.; Zhu, Z.; Yang, C. Recent Progress in Microfluidics-Based Biosensing. Anal. Chem. 2018, 91, 388–404.

22. Lin, S.; Yu, Z.; Chen, D.; Wang, Z.; Miao, J.; Li, Q.; Zhang, D.; Song, J.; Cui, D. Progress in Microfluidics-based Exosome Separation and Detection Technologies for Diagnostic Applications. Small 2020, 16, 1903916.

23. Mao, X.; Huang, T.J. Microfluidic Diagnostics for the Developing World. Lab Chip 2012, 12, 1412–1416.

24. Lin, Y.; Gao, Y.; Wu, M.; Zhou, R.; Chung, D.; Caraveo, G.; Xu, J. Acoustofluidic Stick-and-Play Micropump Built on Foil for Single-Cell Trapping. Lab Chip 2019, 19, 3045–3053.

25. Faustino, V.; Catarino, S.O.; Lima, R.; Minas, G. Biomedical Microfluidic Devices by Using Low-Cost Fabrication Techniques: A Review. J. Biomech. 2016, 49, 2280–2292, doi:https://doi.org/10.1016/j.jbiomech.2015.11.031.

26. Fan, Y. Low-cost Microfluidics: Materials and Methods. Micro Nano Lett. 2018, 13, 1367–1372.

27. Lin, Y.; Gritsenko, D.; Feng, S.; Teh, Y.C.; Lu, X.; Xu, J. Detection of Heavy Metal by Paper-Based Microfluidics. Biosens. Bioelectron. 2016, 83, 256–266.

28. Zhang, C.; Su, Y.; Liang, Y.; Lai, W. Microfluidic Cloth-Based Analytical Devices: Emerging Technologies and Applications. Biosens. Bioelectron. 2020, 168, 112391.

29. Yazdi, A.A.; Popma, A.; Wong, W.; Nguyen, T.; Pan, Y.; Xu, J. 3D Printing: An Emerging Tool for Novel Microfluidics and Lab-on-a-Chip Applications. Microfluid. Nanofluidics 2016, 20, 1–18.

30. Bhattacharjee, N.; Urrios, A.; Kang, S.; Folch, A. The Upcoming 3D-Printing Revolution in Microfluidics. Lab Chip 2016, 16, 1720–1742.

31. Raj M, K.; Chakraborty, S. PDMS Microfluidics: A Mini Review. J. Appl. Polym. Sci. 2020, 137, 48958.

32. Nightingale, A.M.; Beaton, A.D.; Mowlem, M.C. Trends in Microfluidic Systems for in Situ Chemical Analysis of Natural Waters. Sensors Actuators B Chem. 2015, 221, 1398–1405.

33. Volpatti, L.R.; Yetisen, A.K. Commercialization of Microfluidic Devices. Trends Biotechnol. 2014, 32, 347–350.

34. Jaywant, S.A.; Arif, K.M. A Comprehensive Review of Microfluidic Water Quality Monitoring Sensors. Sensors 2019, 19, 4781.

35. Manisha, H.; Priya Shwetha, P.D.; Prasad, K.S. Low-Cost Paper Analytical Devices for Environmental and Biomedical Sensing Applications. In Environmental, Chemical and Medical Sensors; Springer, 2018; pp. 315–341.

36. Almeida, M.I.G.S.; Jayawardane, B.M.; Kolev, S.D.; McKelvie, I.D. Developments of Microfluidic Paper-Based Analytical Devices (MPADs) for Water Analysis: A Review. Talanta 2018, 177, 176–190, doi:https://doi.org/10.1016/j.talanta.2017.08.072.

37. Tomazelli Coltro, W.K.; Cheng, C.-M.; Carrilho, E.; de Jesus, D.P. Recent Advances in Low-Cost Microfluidic Platforms for Diagnostic Applications. Electrophoresis 2014, 35, 2309–2324, doi:https://doi.org/10.1002/elps.201400006.

38. He, Y.; Wu, Y.; Fu, J.-Z.; Wu, W.-B. Fabrication of Paper-Based Microfluidic Analysis Devices: A Review. Rsc Adv. 2015, 5, 78109–78127.

39. Chen, C.; Mehl, B.T.; Munshi, A.S.; Townsend, A.D.; Spence, D.M.; Martin, R.S. 3D-Printed Microfluidic Devices: Fabrication, Advantages and Limitations-a Mini Review. Anal. Methods 2016, 8, 6005–6012, doi:10.1039/C6AY01671E.

40. Martinez, A.W.; Phillips, S.T.; Butte, M.J.; Whitesides, G.M. Patterned Paper as a Platform for Inexpensive, Low-volume, Portable Bioassays. Angew. Chemie 2007, 119, 1340–1342.

41. Silva, A.L.P.; Prata, J.C.; Walker, T.R.; Duarte, A.C.; Ouyang, W.; Barcelò, D.; Rocha-Santos, T. Increased Plastic Pollution Due to COVID-19 Pandemic: Challenges and Recommendations. Chem. Eng. J. 2021, 405, 126683.

42. Adyel, T.M. Accumulation of Plastic Waste during COVID-19. Science (80-.). 2020, 369, 1314–1315.

43. Sanitary Safety of the 2021 French Intensive Care Society Medical Conference: A Case/Control Study. Ann. Intensive Care 2022, 12, 11.

44. McMillan, A.H.; Thomée, E.K.; Dellaquila, A.; Nassman, H.; Segura, T.; Lesher-Pérez, S.C. Rapid Fabrication of Membrane-Integrated Thermoplastic Elastomer Microfluidic Devices. Micromachines 2020, 11, 731.

45. Tien, J.; Dance, Y.W. Microfluidic Biomaterials. Adv. Healthc. Mater. 2021, 10, 2001028.

46. Niculescu, A.-G.; Chircov, C.; Bîrcă, A.C.; Grumezescu, A.M. Fabrication and Applications of Microfluidic Devices: A Review. Int. J. Mol. Sci. 2021, 22, 2011.

47. Scott, S.M.; Ali, Z. Fabrication Methods for Microfluidic Devices: An Overview. Micromachines 2021, 12, 319.

48. Gale, B.K.; Jafek, A.R.; Lambert, C.J.; Goenner, B.L.; Moghimifam, H.; Nze, U.C.; Kamarapu, S.K. A Review of Current Methods in Microfluidic Device Fabrication and Future Commercialization Prospects. Invent. 2018, 3.

49. Yamada, K.; Henares, T.G.; Suzuki, K.; Citterio, D. Paper-based Inkjet-printed Microfluidic Analytical Devices. Angew. Chemie Int. Ed. 2015, 54, 5294–5310.

50. Rumaner, M.; Horowitz, L.; Ovadya, A.; Folch, A. Thread as a Low-Cost Material for Microfluidic Assays on Intact Tumor Slices. Micromachines 2019, 10, 481.

51. Au, A.K.; Huynh, W.; Horowitz, L.F.; Folch, A. 3D-Printed Microfluidics. Angew. Chemie Int. Ed. 2016, 55, 3862–3881, doi:https://doi.org/10.1002/anie.201504382.

52. de Tarso Garcia, P.; Cardoso, T.M.G.; Garcia, C.D.; Carrilho, E.; Coltro, W.K.T. A Handheld Stamping Process to Fabricate Microfluidic Paper-Based Analytical Devices with Chemically Modified Surface for Clinical Assays. Rsc Adv. 2014, 4, 37637–37644.

53. Gao, B.; Li, X.; Yang, Y.; Chu, J.; He, B. Emerging Paper Microfluidic Devices. Analyst 2019, 144, 6497–6511.

54. Li, Q.; Yuan, Z.; Zhang, C.; Hu, S.; Chen, Z.; Wu, Y.; Chen, P.; Qi, H.; Ye, D. Tough, Highly Oriented, Super Thermal Insulating Regenerated All-Cellulose Sponge-Aerogel Fibers Integrating a Graded Aligned Nanostructure. Nano Lett. 2022, 22, 3516–3524.

55. Zhou, M.; Shi, X.; Li, X.; Xiao, G.; Liang, L.; Ju, J.; Wang, F.; Xia, Q.; Sun, W.; Qiao, Y. Constructing Silk Fibroin-Based Three-Dimensional Microfluidic Devices via a Tape Mask-Assisted Multiple-Step Etching Technique. ACS Appl. Bio Mater. 2021, 4, 8039–8048.

56. Arroyo, M.J.; Erenas, M.M.; de Orbe-Paya, I.; Cantrell, K.; Dobado, J.A.; Ballester, P.; Blondeau, P.; Salinas-Castillo, A.; Capitán-Vallvey, L.F. Thread Based Microfluidic Platform for Urinary Creatinine Analysis. Sensors Actuators B Chem. 2020, 305, 127407.

57. Fallahi, H.; Zhang, J.; Phan, H.-P.; Nguyen, N.-T. Flexible Microfluidics: Fundamentals, Recent Developments, and Applications. Micromachines 2019, 10, 830.

58. Nielsen, J.B.; Hanson, R.L.; Almughamsi, H.M.; Pang, C.; Fish, T.R.; Woolley, A.T. Microfluidics: Innovations in Materials and Their Fabrication and Functionalization. Anal. Chem. 2019, 92, 150–168.

59. Santana, Á.L.; Meireles, M.A.A. New Starches Are the Trend for Industry Applications: A Review. Food public Heal. 2014, 4, 229–241.

60. Gupta, P.K.; Raghunath, S.S.; Prasanna, D.V.; Venkat, P.; Shree, V.; Chithananthan, C.; Choudhary, S.; Surender, K.; Geetha, K. An Update on Overview of Cellulose, Its Structure and Applications. Cellulose 2019, 201.

61. Gao, B.; Yang, Y.; Liao, J.; He, B.; Liu, H. Bioinspired Multistructured Paper Microfluidics for POCT. Lab Chip 2019, 19, 3602–3608.

62. Glavan, A.C.; Martinez, R. V; Maxwell, E.J.; Subramaniam, A.B.; Nunes, R.M.D.; Soh, S.; Whitesides, G.M. Rapid Fabrication of Pressure-Driven Open-Channel Microfluidic Devices in Omniphobic RF Paper. Lab Chip 2013, 13, 2922–2930.

63. Böhm, A.; Carstens, F.; Trieb, C.; Schabel, S.; Biesalski, M. Engineering Microfluidic Papers: Effect of Fiber Source and Paper Sheet Properties on Capillary-Driven Fluid Flow. Microfluid. Nanofluidics 2014, 16, 789–799.

64. Lim, H.; Jafry, A.T.; Lee, J. Fabrication, Flow Control, and Applications of Microfluidic Paper-Based Analytical Devices. Molecules 2019, 24, 2869.

65. Soum, V.; Park, S.; Brilian, A.I.; Kwon, O.-S.; Shin, K. Programmable Paper-Based Microfluidic Devices for Biomarker Detections. Micromachines 2019, 10, 516.

66. Ma, J.; Yan, S.; Miao, C.; Li, L.; Shi, W.; Liu, X.; Luo, Y.; Liu, T.; Lin, B.; Wu, W. Paper Microfluidics for Cell Analysis. Adv. Healthc. Mater. 2019, 8, 1801084.

67. Chitnis, G.; Ding, Z.; Chang, C.-L.; Savran, C.A.; Ziaie, B. Laser-Treated Hydrophobic Paper: An Inexpensive Microfluidic Platform. Lab Chip 2011, 11, 1161–1165.

68. Xia, Y.; Si, J.; Li, Z. Fabrication Techniques for Microfluidic Paper-Based Analytical Devices and Their Applications for Biological Testing: A Review. Biosens. Bioelectron. 2016, 77, 774–789, doi:https://doi.org/10.1016/j.bios.2015.10.032.

69. Tang, R.; Xie, M.Y.; Li, M.; Cao, L.; Feng, S.; Li, Z.; Xu, F. Nitrocellulose Membrane for Paper-Based Biosensor. Appl. Mater. Today 2022, 26, 101305.

70. Adkins, J.; Boehle, K.; Henry, C. Electrochemical Paper-Based Microfluidic Devices. Electrophoresis 2015, 36, 1811–1824, doi:https://doi.org/10.1002/elps.201500084.

71. Nishat, S.; Jafry, A.T.; Martinez, A.W.; Awan, F.R. Paper-Based Microfluidics: Simplified Fabrication and Assay Methods. Sensors Actuators B Chem. 2021, 336, 129681, doi:https://doi.org/10.1016/j.snb.2021.129681.

72. Li, W.; Zhang, X.; Li, T.; Ji, Y.; Li, R. Molecularly Imprinted Polymer-Enhanced Biomimetic Paper-Based Analytical Devices: A Review. Anal. Chim. Acta 2021, 1148, 238196.

73. Fu, L.-M.; Wang, Y.-N. Detection Methods and Applications of Microfluidic Paper-Based Analytical Devices. TrAC Trends Anal. Chem. 2018, 107, 196–211.

74. Kaneta, T.; Alahmad, W.; Varanusupakul, P. Microfluidic Paper-Based Analytical Devices with Instrument-Free Detection and Miniaturized Portable Detectors. Appl. Spectrosc. Rev. 2019, 54, 117–141.

75. Zheng, W.; Wang, K.; Xu, H.; Zheng, C.; Cao, B.; Qin, Q.; Jin, Q.; Cui, D. Strategies for the Detection of Target Analytes Using Microfluidic Paper-Based Analytical Devices. Anal. Bioanal. Chem. 2021, 413, 2429–2445.

76. Carrell, C.; Kava, A.; Nguyen, M.; Menger, R.; Munshi, Z.; Call, Z.; Nussbaum, M.; Henry, C. Beyond the Lateral Flow Assay: A Review of Paper-Based Microfluidics. Microelectron. Eng. 2019, 206, 45–54, doi:https://doi.org/10.1016/j.mee.2018.12.002.

77. Tan, W.; Powles, E.; Zhang, L.; Shen, W. Go with the Capillary Flow. Simple Thread-Based Microfluidics. Sensors Actuators B Chem. 2021, 334, 129670, doi:https://doi.org/10.1016/j.snb.2021.129670.

78. Agustini, D.; Bergamini, M.F.; Marcolino-Junior, L.H. Low Cost Microfluidic Device Based on Cotton Threads for Electroanalytical Application. Lab Chip 2016, 16, 345–352.

79. Farajikhah, S.; Cabot, J.M.; Innis, P.C.; Paull, B.; Wallace, G. Life-Saving Threads: Advances in Textile-Based Analytical Devices. ACS Comb. Sci. 2019, 21, 229–240.

80. Weng, X.; Kang, Y.; Guo, Q.; Peng, B.; Jiang, H. Recent Advances in Thread-Based Microfluidics for Diagnostic Applications. Biosens. Bioelectron. 2019, 132, 171–185, doi:https://doi.org/10.1016/j.bios.2019.03.009.

81. Oliveira, A.C.M.; Araújo, D.A.G.; Pradela-Filho, L.A.; Takeuchi, R.M.; Trindade, M.A.G.; Dos Santos, A.L. Threads in Tubing: An Innovative Approach towards Improved Electrochemical Thread-Based Microfluidic Devices. Lab Chip 2022, 22, 3045–3054.

82. Berthier, J.; Brakke, K.A.; Gosselin, D.; Berthier, E.; Navarro, F. Thread-Based Microfluidics: Flow Patterns in Homogeneous and Heterogeneous Microfiber Bundles. Med. Eng. Phys. 2017, 48, 55–61, doi:https://doi.org/10.1016/j.medengphy.2017.08.004.

83. Xiao, G.; He, J.; Chen, X.; Qiao, Y.; Wang, F.; Xia, Q.; Yu, L.; Lu, Z. A Wearable, Cotton Thread/Paper-Based Microfluidic Device Coupled with Smartphone for Sweat Glucose Sensing. Cellulose 2019, 26, 4553–4562.

84. Xia, J.; Khaliliazar, S.; Hamedi, M.M.; Sonkusale, S. Thread-Based Wearable Devices. MRS Bull. 2021, 46, 502–511.

85. Agustini, D.; Caetano, F.R.; Quero, R.F.; da Silva, J.A.F.; Bergamini, M.F.; Júnior, L.H.M.; de Jesus, D.P. Microfluidic Devices Based on Textile Threads for Analytical Applications: State of the Art and Perspectives. Anal. Methods 2021.

86. Alsaeed, B.; Mansour, F.R. Distance-Based Paper Microfluidics; Principle, Technical Aspects and Applications. Microchem. J. 2020, 155, 104664, doi:https://doi.org/10.1016/j.microc.2020.104664.

87. Shimazu, R.; Tomimuro, K.; Ni, Y.; Malegori, C.; Hamedpour, V.; Hiruta, Y.; Oliveri, P.; Merkx, M.; Citterio, D. Microfluidic Thread-Based Analytical Devices for Point-of-Care Detection of Therapeutic Antibody in Blood. Sensors Actuators B Chem. 2022, 352, 131002.

88. Jarujamrus, P.; Prakobkij, A.; Puchum, S.; Chaisamdaeng, S.; Meelapsom, R.; Anutrasakda, W.; Amatatongchai, M.; Chairam, S.; Citterio, D. Acid–Base Titration Using a Microfluidic Thread-Based Analytical Device (MTAD). Analyst 2020, 145, 4457–4466.

89. Nilghaz, A.; Zhang, L.; Li, M.; Ballerini, D.R.; Shen, W. Understanding Thread Properties for Red Blood Cell Antigen Assays: Weak ABO Blood Typing. ACS Appl. Mater. Interfaces 2014, 6, 22209–22215.

90. Xu, B.; Qin, T.; Zhang, J.; Ding, Y.; Su, Y.; Wu, J.; Pan, D.; Zhang, Y.; Shen, Z. Cloth-Based Microfluidic Analytical Devices by Laser-Induced Hydrophilization Technique. Sensors Actuators B Chem. 2021, 341, 129998.

91. Zheng, L.; Liu, Y.; Zhang, C. A Sample-to-Answer, Wearable Cloth-Based Electrochemical Sensor (WCECS) for Point-of-Care Detection of Glucose in Sweat. Sensors Actuators B Chem. 2021, 343, 130131.

92. Bagherbaigi, S.; Córcoles, E.P.; Wicaksono, D.H.B. Cotton Fabric as an Immobilization Matrix for Low-Cost and Quick Colorimetric Enzyme-Linked Immunosorbent Assay (ELISA). Anal. Methods 2014, 6, 7175–7180.

93. Tasaengtong, B.; Sameenoi, Y. A One-Step Polymer Screen-Printing Method for Fabrication of Microfluidic Cloth-Based Analytical Devices. Microchem. J. 2020, 158, 105078.

94. Li, H.; Liu, C.; Wang, D.; Zhang, C. Programmable Fluid Transport on Photolithographically Micropatterned Cloth Devices: Towards the Development of Facile, Multifunctional Colorimetric Diagnostic Platforms. Sensors Actuators B Chem. 2018, 255, 2416–2430.

95. Nilghaz, A.; Bagherbaigi, S.; Lam, C.L.; Mousavi, S.M.; Córcoles, E.P.; Wicaksono, D.H.B. Multiple Semi-Quantitative Colorimetric Assays in Compact Embeddable Microfluidic Cloth-Based Analytical Device (MCAD) for Effective Point-of-Care Diagnostic. Microfluid. Nanofluidics 2015, 19, 317–333.

96. Shang, Q.; Su, Y.; Liang, Y.; Lai, W.; Jiang, J.; Wu, H.; Zhang, C. Correction to: Ultrasensitive Cloth-Based Microfluidic Chemiluminescence Detection of Listeria Monocytogenes HlyA Gene by Hemin/G-Quadruplex DNAzyme and Hybridization Chain Reaction Signal Amplification. Anal. Bioanal. Chem. 2022, 414, 4011.

97. Shang, Q.; Su, Y.; Liang, Y.; Lai, W.; Jiang, J.; Wu, H.; Zhang, C. Ultrasensitive Cloth-Based Microfluidic Chemiluminescence Detection of Listeria Monocytogenes HlyA Gene by Hemin/G-Quadruplex DNAzyme and Hybridization Chain Reaction Signal Amplification. Anal. Bioanal. Chem. 2020, 412, 3787–3797.

98. Jiang, J.; Wu, H.; Su, Y.; Liang, Y.; Shu, B.; Zhang, C. Electrochemical Cloth-Based DNA Sensors (ECDSs): A New Class of Electrochemical Gene Sensors. Anal. Chem. 2020, 92, 7708–7716.

99. Nilghaz, A.; Ballerini, D.R.; Shen, W. Exploration of Microfluidic Devices Based on Multi-Filament Threads and Textiles: A Review. Biomicrofluidics 2013, 7, 51501, doi:10.1063/1.4820413.

100. Ding, R.; Lisak, G. Sponge-Based Microfluidic Sampling for Potentiometric Ion Sensing. Anal. Chim. Acta 2019, 1091, 103–111.

101. Silva, R.; Ahamed, A.; Cheong, Y.H.; Zhao, K.; Ding, R.; Lisak, G. Non-Equilibrium Potentiometric Sensors Integrated with Metal Modified Paper-Based Microfluidic Solution Sampling Substrates for Determination of Heavy Metals in Complex Environmental Samples. Anal. Chim. Acta 2022, 1197, 339495.

102. Hu, K.; Ma, L.; Wang, Z.; Fernandez-Delgado, O.; Garay, Y.E.; Lopez, J.A.; Li, X. Facile Synthesis and Integration of Poly (Vinyl Alcohol) Sponge-Supported Metal Nanocatalysts on a Microfluidic Chip Enable a New Continuous Flow Multireactor Nanocatalysis Platform for High Efficiency and Reusability Catalysis. ACS Sustain. Chem. Eng. 2022, 10, 10579–10589.

103. Mogera, U.; Guo, H.; Namkoong, M.; Rahman, M.S.; Nguyen, T.; Tian, L. Wearable Plasmonic Paper–Based Microfluidics for Continuous Sweat Analysis. Sci. Adv. 2022, 8, eabn1736, doi:10.1126/sciadv.abn1736.

104. Bae, C.W.; Chinnamani, M.V.; Lee, E.H.; Lee, N.-E. Stretchable Non-Enzymatic Fuel Cell-Based Sensor Patch Integrated with Thread-Embedded Microfluidics for Self-Powered Wearable Glucose Monitoring. Adv. Mater. Interfaces 2022, 9, 2200492, doi:https://doi.org/10.1002/admi.202200492.

105. Mao, X.; Zhang, C. A Microfluidic Cloth-Based Photoelectrochemical Analytical Device for the Detection of Glucose in Saliva. Talanta 2022, 238, 123052, doi:https://doi.org/10.1016/j.talanta.2021.123052.

106. Prabowo, B.A.; Fernandes, E.; Freitas, P. A Pump-Free Microfluidic Device for Fast Magnetic Labeling of Ischemic Stroke Biomarkers. Anal. Bioanal. Chem. 2022, 414, 2571–2583, doi:10.1007/s00216-022-03915-w.

107. Young, R.J.; Lovell, P.A. Introduction to Polymers; CRC press, 2011; ISBN 0429109482.

108. Strobl, G.R.; Strobl, G.R. The Physics of Polymers; Springer, 1997; Vol. 2;.

109. Mark, J.; Ngai, K.; Graessley, W.; Mandelkern, L.; Samulski, E.; Wignall, G.; Koenig, J. Physical Properties of Polymers; Cambridge University Press, 2004; ISBN 0521530180.

110. Carothers, W.H. Polymers and Polyfunctionality. Trans. Faraday Soc. 1936, 32, 39–49.

111. Rose, M.; Palkovits, R. Cellulose-based Sustainable Polymers: State of the Art and Future Trends. Macromol. Rapid Commun. 2011, 32, 1299–1311.

112. Seoud, O.A. El; Heinze, T. Organic Esters of Cellulose: New Perspectives for Old Polymers. Polysaccharides I 2005, 103–149.

113. Hacker, M.C.; Krieghoff, J.; Mikos, A.G. Synthetic Polymers. In Principles of regenerative medicine; Elsevier, 2019; pp. 559–590.

114. Maitz, M.F. Applications of Synthetic Polymers in Clinical Medicine. Biosurface and Biotribology 2015, 1, 161–176.

115. Chan, H.N.; Chen, Y.; Shu, Y.; Chen, Y.; Tian, Q.; Wu, H. Direct, One-Step Molding of 3D-Printed Structures for Convenient Fabrication of Truly 3D PDMS Microfluidic Chips. Microfluid. Nanofluidics 2015, 19, 9–18, doi:10.1007/s10404-014-1542-4.

116. Haubert, K.; Drier, T.; Beebe, D. PDMS Bonding by Means of a Portable, Low-Cost Corona System. Lab Chip 2006, 6, 1548–1549.

117. Li, M.; Li, S.; Wu, J.; Wen, W.; Li, W.; Alici, G. A Simple and Cost-Effective Method for Fabrication of Integrated Electronic-Microfluidic Devices Using a Laser-Patterned PDMS Layer. Microfluid. Nanofluidics 2012, 12, 751–760, doi:10.1007/s10404-011-0917-z.

118. Miranda, I.; Souza, A.; Sousa, P.; Ribeiro, J.; Castanheira, E.M.S.; Lima, R.; Minas, G. Properties and Applications of PDMS for Biomedical Engineering: A Review. J. Funct. Biomater. 2021, 13, 2.

119. Barocio, M.E.; Hidalgo-Vázquez, E.; Kim, Y.; Rodas-Zuluaga, L.I.; Chen, W.-N.; Barceló, D.; Iqbal, H.N.M.; Parra-Saldívar, R.; Castillo-Zacarías, C. Portable Microfluidic Devices for In-Field Detection of Pharmaceutical Residues in Water: Recent Outcomes and Current Technological Situation – A Short Review. Case Stud. Chem. Environ. Eng. 2021, 3, 100069, doi:https://doi.org/10.1016/j.cscee.2020.100069.

120. Ruiz, C.; Kadimisetty, K.; Yin, K.; Mauk, M.G.; Zhao, H.; Liu, C. Fabrication of Hard–Soft Microfluidic Devices Using Hybrid 3D Printing. Micromachines 2020, 11, 567.

121. Razavi Bazaz, S.; Rouhi, O.; Raoufi, M.A.; Ejeian, F.; Asadnia, M.; Jin, D.; Ebrahimi Warkiani, M. 3D Printing of Inertial Microfluidic Devices. Sci. Rep. 2020, 10, 5929, doi:10.1038/s41598-020-62569-9.

122. Ma, X.; Li, R.; Jin, Z.; Fan, Y.; Zhou, X.; Zhang, Y. Injection Molding and Characterization of PMMA-Based Microfluidic Devices. Microsyst. Technol. 2020, 26, 1317–1324.

123. Chen, X.; Li, T.; Gao, Q.I. A Novel Method for Rapid Fabrication of PMMA Microfluidic Chip by Laser Cutting and Sealing Integration. Surf. Rev. Lett. 2019, 26, 1950042.

124. Trotta, G.; Volpe, A.; Ancona, A.; Fassi, I. Flexible Micro Manufacturing Platform for the Fabrication of PMMA Microfluidic Devices. J. Manuf. Process. 2018, 35, 107–117.

125. Fan, Y.; Liu, Y.; Li, H.; Foulds, I.G. Printed Wax Masks for 254 Nm Deep-UV Pattering of PMMA-Based Microfluidics. J. Micromechanics Microengineering 2012, 22, 27001.

126. Focke, M.; Kosse, D.; Müller, C.; Reinecke, H.; Zengerle, R.; von Stetten, F. Lab-on-a-Foil: Microfluidics on Thin and Flexible Films. Lab Chip 2010, 10, 1365–1386.

127. Bertana, V.; Potrich, C.; Scordo, G.; Scaltrito, L.; Ferrero, S.; Lamberti, A.; Perrucci, F.; Pirri, C.F.; Pederzolli, C.; Cocuzza, M. 3D-Printed Microfluidics on Thin Poly (Methyl Methacrylate) Substrates for Genetic Applications. J. Vac. Sci. Technol. B, Nanotechnol. Microelectron. Mater. Process. Meas. Phenom. 2018, 36, 01A106.

128. Heuer, C.; Preuß, J.; Habib, T.; Enders, A.; Bahnemann, J. 3D Printing in Biotechnology—An Insight into Miniaturized and Microfluidic Systems for Applications from Cell Culture to Bioanalytics. Eng. Life Sci. 2021.

129. Mehta, V.; Rath, S.N. 3D Printed Microfluidic Devices: A Review Focused on Four Fundamental Manufacturing Approaches and Implications on the Field of Healthcare. Bio-Design Manuf. 2021, 4, 311–343, doi:10.1007/s42242-020-00112-5.

130. Pranzo, D.; Larizza, P.; Filippini, D.; Percoco, G. Extrusion-Based 3D Printing of Microfluidic Devices for Chemical and Biomedical Applications: A Topical Review. Micromachines 2018, 9, 374.

131. Weisgrab, G.; Ovsianikov, A.; Costa, P.F. Functional 3D Printing for Microfluidic Chips. Adv. Mater. Technol. 2019, 4, 1900275.

132. Oh, J.M.; Begum, H.M.; Liu, Y.L.; Ren, Y.; Shen, K. Recapitulating Tumor Hypoxia in a Cleanroom-Free, Liquid-Pinning-Based Microfluidic Tumor Model. ACS Biomater. Sci. Eng. 2022, 8, 3107–3121, doi:10.1021/acsbiomaterials.2c00207.

133. Persson, H.; Park, S.; Mohan, M.; Cheung, K.K.; Simmons, C.A.; Young, E.W.K. Rapid Assembly of PMMA Microfluidic Devices with PETE Membranes for Studying the Endothelium. Sensors Actuators B Chem. 2022, 356, 131342, doi:https://doi.org/10.1016/j.snb.2021.131342.

134. Jin, Y.; Xiong, P.; Xu, T.; Wang, J. Time-Efficient Fabrication Method for 3D-Printed Microfluidic Devices. Sci. Rep. 2022, 12, 1233, doi:10.1038/s41598-022-05350-4.

135. Gerstl, F.; Pongkitdachoti, U.; Unob, F.; Baeumner, A.J. Miniaturized Sensor for Electroanalytical and Electrochemiluminescent Detection of Pathogens Enabled through Laser-Induced Graphene Electrodes Embedded in Microfluidic Channels. Lab Chip 2022.

136. Dou, M.; Sanjay, S.T.; Benhabib, M.; Xu, F.; Li, X. Low-Cost Bioanalysis on Paper-Based and Its Hybrid Microfluidic Platforms. Talanta 2015, 145, 43–54, doi:https://doi.org/10.1016/j.talanta.2015.04.068.

137. Akyazi, T.; Basabe-Desmonts, L.; Benito-Lopez, F. Review on Microfluidic Paper-Based Analytical Devices towards Commercialisation. Anal. Chim. Acta 2018, 1001, 1–17, doi:https://doi.org/10.1016/j.aca.2017.11.010.

138. Xie, L.; Zi, X.; Zeng, H.; Sun, J.; Xu, L.; Chen, S. Low-Cost Fabrication of a Paper-Based Microfluidic Using a Folded Pattern Paper. Anal. Chim. Acta 2019, 1053, 131–138.

139. Liu, J.; Kong, X.; Wang, H.; Zhang, Y.; Fan, Y. Roll-to-Roll Wax Transfer for Rapid and Batch Fabrication of Paper-Based Microfluidics. Microfluid. Nanofluidics 2020, 24, 1–7.

140. Liu, J.; Zhang, B.; Zhang, Y.; Fan, Y. Fluid Control with Hydrophobic Pillars in Paper-Based Microfluidics. J. Micromechanics Microengineering 2021, 31, 127002.

141. Olmos, C.M.; Vaca, A.; Rosero, G.; Peñaherrera, A.; Perez, C.; de Sá Carneiro, I.; Vizuete, K.; Arroyo, C.R.; Debut, A.; Pérez, M.S. Epoxy Resin Mold and PDMS Microfluidic Devices through Photopolymer Flexographic Printing Plate. Sensors Actuators B Chem. 2019, 288, 742–748.

142. Aladese, A.D.; Jeong, H.-H. Recent Developments in 3D Printing of Droplet-Based Microfluidics. BioChip J. 2021, 1–21.

143. Loo, J.F.C.; Ho, A.H.P.; Turner, A.P.F.; Mak, W.C. Integrated Printed Microfluidic Biosensors. Trends Biotechnol. 2019, 37, 1104–1120.

144. Khorsandi, D.; Nodehi, M.; Waqar, T.; Shabani, M.; Kamare, B.; Zare, E.N.; Ersoy, S.; Annabestani, M.; Çelebi, M.F.; Kafadenk, A. Manufacturing of Microfluidic Sensors Utilizing 3d Printing Technologies: A Production System. J. Nanomater. 2021, 2021.

145. Fan, Y.; Wang, H.; Liu, S.; Zhang, B.; Zhang, Y. Milk Carton with Integrated Paper-based Microfluidics for Milk Quality Rapid Test. J. Food Saf. 2018, 38, e12548.

146. Wang, Y.; Deng, R.; Yang, L.; Bain, C.D. Fabrication of Monolayers of Uniform Polymeric Particles by Inkjet Printing of Monodisperse Emulsions Produced by Microfluidics. Lab Chip 2019, 19, 3077–3085.

147. Bamshad, A.; Cho, H.J. Laserjet Printed Micro/Nano Sensors and Microfluidic Systems: A Simple and Facile Digital Platform for Inexpensive, Flexible, and Low-volume Devices. Adv. Mater. Technol. 2021, 6, 2100401.

148. Qian, S.; Han, Y.; Xu, F.; Feng, D.; Yang, X.; Wu, X.; Hao, L.; Yuan, M. A Fast, Sensitive, Low-Cost Electrochemical Paper-Based Chip for Real-Time Simultaneous Detection of Cadmium (Ⅱ) and Lead (Ⅱ) via Aptamer. Talanta 2022, 247, 123548, doi:https://doi.org/10.1016/j.talanta.2022.123548.

149. Caetano, F.R.; Carneiro, E.A.; Agustini, D.; Figueiredo-Filho, L.C.S.; Banks, C.E.; Bergamini, M.F.; Marcolino-Junior, L.H. Combination of Electrochemical Biosensor and Textile Threads: A Microfluidic Device for Phenol Determination in Tap Water. Biosens. Bioelectron. 2018, 99, 382–388, doi:https://doi.org/10.1016/j.bios.2017.07.070.

150. Dixon, C. Printed Digital Microfluidics for Diagnosis of Disease 2020.

151. Morbioli, G.G.; Mazzu-Nascimento, T.; Stockton, A.M.; Carrilho, E. How Are These Devices Manufactured? In Paper-based Diagnostics; Springer, 2019; pp. 89–122.

152. Yehia, A.M.; Saad, A.S.; Tantawy, M.A. USB Multiplex Analyzer Employing Screen-Printed Silver Electrodes on Paper Substrate; a Developed Design for Dissolution Testing. J. Pharm. Biomed. Anal. 2020, 186, 113272.

153. Kamnoet, P.; Aeungmaitrepirom, W.; Menger, R.F.; Henry, C.S. Highly Selective Simultaneous Determination of Cu(Ii), Co(Ii), Ni(Ii), Hg(Ii), and Mn(Ii) in Water Samples Using Microfluidic Paper-Based Analytical Devices. Analyst 2021, 146, 2229–2239, doi:10.1039/D0AN02200D.

154. Liu, M.; Zhang, C.; Liu, F. Understanding Wax Screen-Printing: A Novel Patterning Process for Microfluidic Cloth-Based Analytical Devices. Anal. Chim. Acta 2015, 891, 234–246.

155. Lin, D.; Li, B.; Fu, L.; Qi, J.; Xia, C.; Zhang, Y.; Chen, J.; Choo, J.; Chen, L. A Novel Polymer-Based Nitrocellulose Platform for Implementing a Multiplexed Microfluidic Paper-Based Enzyme-Linked Immunosorbent Assay. Microsystems Nanoeng. 2022, 8, 1–10.

156. Tesfaye, T.; Hussen, A. Microfluidic Paper-Based Analytical Device (MPAD) Fabricated by Wax Screen Printing Technique for the Determination of Nitrite and Nitrate Ion in Water Samples. Microfluid. Nanofluidics 2022, 26, 1–13.

157. Ruiz, R.A.; Gonzalez, J.L.; Vazquez-Alvarado, M.; Martinez, N.W.; Martinez, A.W. Beyond Wax Printing: Fabrication of Paper-Based Microfluidic Devices Using a Thermal Transfer Printer. Anal. Chem. 2022, 94, 8833–8837.

158. Chen, C.; Meng, H.; Guo, T.; Deshpande, S.; Chen, H. Development of Paper Microfluidics with 3D-Printed PDMS Barriers for Flow Control. ACS Appl. Mater. Interfaces 2022.

159. Tran, B.T.; Rijiravanich, P.; Puttaraksa, N.; Surareungchai, W. Wax Gates in Laminated Microfluidic Paper-Based Immunosensors. Microchem. J. 2022, 178, 107343.

160. Szabo, E.; Hess-Dunning, A. Irreversible, Self-Aligned Microfluidic Packaging for Chronic Implant Applications. J. Micromechanics Microengineering 2021, 31, 95011.

161. Noviana, E.; Carrão, D.B.; Pratiwi, R.; Henry, C.S. Emerging Applications of Paper-Based Analytical Devices for Drug Analysis: A Review. Anal. Chim. Acta 2020, 1116, 70–90, doi:https://doi.org/10.1016/j.aca.2020.03.013.

162. Dornelas, K.L.; Dossi, N.; Piccin, E. A Simple Method for Patterning Poly (Dimethylsiloxane) Barriers in Paper Using Contact-Printing with Low-Cost Rubber Stamps. Anal. Chim. Acta 2015, 858, 82–90.

163. Zhu, Z.; Chen, P.; Liu, K.; Escobedo, C. A Versatile Bonding Method for PDMS and SU-8 and Its Application towards a Multifunctional Microfluidic Device. Micromachines 2016, 7, 230.

164. Modha, S.; Castro, C.; Tsutsui, H. Recent Developments in Flow Modeling and Fluid Control for Paper-Based Microfluidic Biosensors. Biosens. Bioelectron. 2021, 178, 113026.

165. Gosset, A.; Durrieu, C.; Renaud, L.; Deman, A.-L.; Barbe, P.; Bayard, R.; Chateaux, J.-F. Xurography-Based Microfluidic Algal Biosensor and Dedicated Portable Measurement Station for Online Monitoring of Urban Polluted Samples. Biosens. Bioelectron. 2018, 117, 669–677.

166. Guo, W.; Hansson, J.; Gustafsson, L.; van der Wijngaart, W. “ Bend-and-Bond” Polymer Microfluidic Origami. In Proceedings of the 2021 IEEE 34th International Conference on Micro Electro Mechanical Systems (MEMS); IEEE, 2021; pp. 222–225.

167. Cortes-Medina, M.; Avendano, A.; Bushman, A.; Chang, C.-W.; Menyhert, M.; Song, J.W. Microfluidic Prototyping by Xurography to Engineer Fully-Lumenized Microvessels In Vitro. FASEB J. 2020, 34, 1.

168. Caffiyar, M.Y.; Lim, K.P.; Basha, I.H.K.; Hamid, N.H.; Cheong, S.C.; Ho, E.T.W. Label-Free, High-Throughput Assay of Human Dendritic Cells from Whole-Blood Samples with Microfluidic Inertial Separation Suitable for Resource-Limited Manufacturing. Micromachines 2020, 11, 514.

169. Speller, N.C.; Morbioli, G.G.; Cato, M.E.; Cantrell, T.P.; Leydon, E.M.; Schmidt, B.E.; Stockton, A.M. Cutting Edge Microfluidics: Xurography and a Microwave. Sensors Actuators B Chem. 2019, 291, 250–256, doi:https://doi.org/10.1016/j.snb.2019.04.004.

170. He, Y.; Wu, Y.; Fu, J.; Gao, Q.; Qiu, J. Developments of 3D Printing Microfluidics and Applications in Chemistry and Biology: A Review. Electroanalysis 2016, 28, 1658–1678, doi:https://doi.org/10.1002/elan.201600043.

171. Bressan, L.P.; Adamo, C.B.; Quero, R.F.; de Jesus, D.P.; da Silva, J.A.F. A Simple Procedure to Produce FDM-Based 3D-Printed Microfluidic Devices with an Integrated PMMA Optical Window. Anal. Methods 2019, 11, 1014–1020.

172. Wei, L.; Fang, G.; Kuang, Z.; Cheng, L.; Wu, H.; Guo, D.; Liu, A. 3D-Printed Low-Cost Fabrication and Facile Integration of Flexible Epidermal Microfluidics Platform. Sensors Actuators B Chem. 2022, 353, 131085.

173. Raoufi, M.A.; Bazaz, S.R.; Niazmand, H.; Rouhi, O.; Asadnia, M.; Razmjou, A.; Warkiani, M.E. Fabrication of Unconventional Inertial Microfluidic Channels Using Wax 3D Printing. Soft Matter 2020, 16, 2448–2459.

174. Su, R.; Wen, J.; Su, Q.; Wiederoder, M.S.; Koester, S.J.; Uzarski, J.R.; McAlpine, M.C. 3D Printed Self-Supporting Elastomeric Structures for Multifunctional Microfluidics. Sci. Adv. 2020, 6, eabc9846.

175. Nielsen, A. V; Beauchamp, M.J.; Nordin, G.P.; Woolley, A.T. 3D Printed Microfluidics. Annu. Rev. Anal. Chem. 2020, 13, 45–65.

176. Enders, A.; Siller, I.G.; Urmann, K.; Hoffmann, M.R.; Bahnemann, J. 3D Printed Microfluidic Mixers—A Comparative Study on Mixing Unit Performances. Small 2019, 15, 1804326.

177. Gonzalez, G.; Chiappone, A.; Dietliker, K.; Pirri, C.F.; Roppolo, I. Fabrication and Functionalization of 3D Printed Polydimethylsiloxane-Based Microfluidic Devices Obtained through Digital Light Processing. Adv. Mater. Technol. 2020, 5, 2000374.

178. de Almeida Monteiro Melo Ferraz, M.; Nagashima, J.B.; Venzac, B.; Le Gac, S.; Songsasen, N. 3D Printed Mold Leachates in PDMS Microfluidic Devices. Sci. Rep. 2020, 10, 1–9.

179. Rahim, M.S.; Ehsan, A.A. Micro Milling Process for the Rapid Prototyping of Microfluidic Devices. Adv. Microfluid. Nanofluids 2021.

180. Hossain, M.M.; Rahman, T. Low Cost Micro Milling Machine for Prototyping Plastic Microfluidic Devices. Multidiscip. Digit. Publ. Inst. Proc. 2018, 2, 707.

181. Javidanbardan, A.; Azevedo, A.M.; Chu, V.; Conde, J.P. A Systematic Approach for Developing 3D High-Quality PDMS Microfluidic Chips Based on Micromilling Technology. Micromachines 2021, 13, 6.

182. Jiménez-Díaz, E.; Cano-Jorge, M.; Zamarrón-Hernández, D.; Cabriales, L.; Páez-Larios, F.; Cruz-Ramírez, A.; Vázquez-Victorio, G.; Fiordelisio, T.; Hautefeuille, M. Micro–Macro: Selective Integration of Microfeatures Inside Low-Cost Macromolds for PDMS Microfluidics Fabrication. Micromachines 2019, 10, 576.

183. Nguyen, T.-Q.; Mah, J.; Park, W.-T.; Lee, S. Rapid and Versatile Micromold Fabrication Using Micromilling and Nanopolishing for Microfluidic Devices. In Proceedings of the Fluids Engineering Division Summer Meeting; American Society of Mechanical Engineers, 2019; Vol. 59070, p. V004T06A011.

184. Saptaji, K.; Triawan, F.; Sai, T.K.; Gebremariam, A. Deburring Method of Aluminum Mould Produced by Milling Process for Microfluidic Device Fabrication. Indones. J. Sci. Technol. 2021, 6, 123–140.

185. Behroodi, E.; Latifi, H.; Bagheri, Z.; Ermis, E.; Roshani, S.; Salehi Moghaddam, M. A Combined 3D Printing/CNC Micro-Milling Method to Fabricate a Large-Scale Microfluidic Device with the Small Size 3D Architectures: An Application for Tumor Spheroid Production. Sci. Rep. 2020, 10, 1–14.

186. Guckenberger, D.J.; de Groot, T.E.; Wan, A.M.D.; Beebe, D.J.; Young, E.W.K. Micromilling: A Method for Ultra-Rapid Prototyping of Plastic Microfluidic Devices. Lab Chip 2015, 15, 2364–2378.

187. Leclerc, C. Experimental and Computational Analyses of a Microfluidic Chip Fabricated Through Computer Numerical Control Micromilling of Stressed Polystyrene Sheets 2021.

188. Charles, P.T.; Wadhwa, V.; Kouyate, A.; Mesa-Donado, K.J.; Adams, A.A.; Deschamps, J.R.; Kusterbeck, A.W. A High Aspect Ratio Bifurcated 128-Microchannel Microfluidic Device for Environmental Monitoring of Explosives. Sensors 2018, 18, 1568.

189. Ku, X.; Zhang, Z.; Liu, X.; Chen, L.; Li, G. Low-Cost Rapid Prototyping of Glass Microfluidic Devices Using a Micromilling Technique. Microfluid. Nanofluidics 2018, 22, 1–8.

190. Madureira, M.; Faustino, V.; Schütte, H.; Pinho, D.; Minas, G.; Gassmann, S.; Lima, R. Red Blood Cells Separation in a Curved T-Shaped Microchannel Fabricated by a Micromilling Technique. In Proceedings of the ECCOMAS Thematic Conference on Computational Vision and Medical Image Processing; Springer, 2019; pp. 585–593.

191. Owens, C.E.; Hart, A.J. High-Precision Modular Microfluidics by Micromilling of Interlocking Injection-Molded Blocks. Lab Chip 2018, 18, 890–901.

192. Gonçalves, I.M.; Madureira, M.; Miranda, I.; Schütte, H.; Moita, A.; Minas, G.; Gassmann, S.; Lima, R. Separation Microfluidic Device Fabricated by Micromilling Techniques. Eng. Proc. 2021, 4, 37.

193. Kosoff, D.; Yu, J.; Suresh, V.; Beebe, D.J.; Lang, J.M. Surface Topography and Hydrophilicity Regulate Macrophage Phenotype in Milled Microfluidic Systems. Lab Chip 2018, 18, 3011–3017.

194. Mohammed, M.I.; Alam, M.N.H.Z.; Kouzani, A.; Gibson, I. Fabrication of Microfluidic Devices: Improvement of Surface Quality of CO2laser Machined Poly(Methylmethacrylate) Polymer. J. Micromechanics Microengineering 2016, 27, 15021, doi:10.1088/0960-1317/27/1/015021.

195. Buchroithner, B.; Mayr, S.; Hauser, F.; Priglinger, E.; Stangl, H.; Santa-Maria, A.R.; Deli, M.A.; Der, A.; Klar, T.A.; Axmann, M. Dual Channel Microfluidics for Mimicking the Blood–Brain Barrier. ACS Nano 2021, 15, 2984–2993.

196. Shin, J.H.; Choi, S. Open-Source and Do-It-Yourself Microfluidics. Sensors Actuators B Chem. 2021, 347, 130624.

197. Elgohary, A.; Block, E.; Squier, J.; Koneshloo, M.; Shaha, R.K.; Frick, C.; Oakey, J.; Aryana, S.A. Fabrication of Sealed Sapphire Microfluidic Devices Using Femtosecond Laser Micromachining. Appl. Opt. 2020, 59, 9285–9291.

198. Andriukaitis, D.; Vargalis, R.; Šerpytis, L.; Drevinskas, T.; Kornyšova, O.; Stankevičius, M.; Bimbiraitė-Survilienė, K.; Kaškonienė, V.; Maruškas, A.S.; Jonušauskas, L. Fabrication of Microfluidic Tesla Valve Employing Femtosecond Bursts. Micromachines 2022, 13, 1180.

199. Saadat, M.; Taylor, M.; Hughes, A.; Hajiyavand, A.M. Rapid Prototyping Method for 3D PDMS Microfluidic Devices Using a Red Femtosecond Laser. Adv. Mech. Eng. 2020, 12, 1687814020982713.

200. Islam, M.; Loewen, A.; Allen, P.B. Simple, Low-Cost Fabrication of Acrylic Based Droplet Microfluidics and Its Use to Generate DNA-Coated Particles. Sci. Rep. 2018, 8, 1–11.

201. Lin, H.; Zhao, Y.; Lin, S.; Wang, B.; Yeung, C.; Cheng, X.; Wang, Z.; Cai, T.; Yu, W.; King, K. A Rapid and Low-Cost Fabrication and Integration Scheme to Render 3D Microfluidic Architectures for Wearable Biofluid Sampling, Manipulation, and Sensing. Lab Chip 2019, 19, 2844–2853.

202. Chung, C.-K.; Chang, H.C.; Shih, T.R.; Lin, S.L.; Hsiao, E.J.; Chen, Y.S.; Chang, E.C.; Chen, C.C.; Lin, C.C. Water-Assisted CO2 Laser Ablated Glass

and Modified Thermal Bonding for Capillary-Driven Bio-Fluidic Application. Biomed. Microdevices 2010, 12, 107–114.

203. Mahmud, M.A.; Blondeel, E.J.M.; Kaddoura, M.; MacDonald, B.D. Features in Microfluidic Paper-Based Devices Made by Laser Cutting: How Small Can They Be? Micromachines 2018, 9, 220.

204. Su, W.; Cook, B.S.; Fang, Y.; Tentzeris, M.M. Fully Inkjet-Printed Microfluidics: A Solution to Low-Cost Rapid Three-Dimensional Microfluidics Fabrication with Numerous Electrical and Sensing Applications. Sci. Rep. 2016, 6, 35111, doi:10.1038/srep35111.

205. Kotz, F.; Mader, M.; Dellen, N.; Risch, P.; Kick, A.; Helmer, D.; Rapp, B.E. Fused Deposition Modeling of Microfluidic Chips in Polymethylmethacrylate. Micromachines 2020, 11, 873.

206. Shiu, P.P.; Knopf, G.K.; Ostojic, M.; Nikumb, S. Rapid Fabrication of Tooling for Microfluidic Devices via Laser Micromachining and Hot Embossing. J. Micromechanics Microengineering 2008, 18, 25012.

207. Zhang, H.; Fang, F.; Gilchrist, M.D.; Zhang, N. Filling of High Aspect Ratio Micro Features of a Microfluidic Flow Cytometer Chip Using Micro Injection Moulding. J. Micromechanics Microengineering 2018, 28, 75005.

208. Zhang, N.; Liu, J.; Zhang, H.; Kent, N.J.; Diamond, D.; D. Gilchrist, M. 3D Printing of Metallic Microstructured Mould Using Selective Laser Melting for Injection Moulding of Plastic Microfluidic Devices. Micromachines 2019, 10, 595.

209. Jia, Y.; Jiang, J.; Ma, X.; Li, Y.; Huang, H.; Cai, K.; Cai, S.; Wu, Y. PDMS Microchannel Fabrication Technique Based on Microwire-Molding. Chinese Sci. Bull. 2008, 53, 3928–3936.

210. Kuo, J.T.W.; Kim, B.J.; Hara, S.A.; Lee, C.D.; Gutierrez, C.A.; Hoang, T.Q.; Meng, E. Novel Flexible Parylene Neural Probe with 3D Sheath Structure for Enhancing Tissue Integration. Lab Chip 2013, 13, 554–561.

211. Chen, H.; Yang, B.; Yang, Z. Chapter 1 - Fabrication of Microfluidic Chips. Multidiscip. Microfluid. Nanofluidic Lab-on-a-chip 2022, 3–35.

212. Altundemir, S.; Uguz, A.K.; Ulgen, K. A Review on Wax Printed Microfluidic Paper-Based Devices for International Health. Biomicrofluidics 2017, 11, 41501, doi:10.1063/1.4991504.

213. Lohse, D. Fundamental Fluid Dynamics Challenges in Inkjet Printing. Annu. Rev. Fluid Mech. 2021, 11, 42, doi:10.1146/annurev-fluid-022321.

214. Maejima, K.; Tomikawa, S.; Suzuki, K.; Citterio, D. Inkjet Printing: An Integrated and Green Chemical Approach to Microfluidic Paper-Based Analytical Devices. RSC Adv. 2013, 3, 9258–9263, doi:10.1039/C3RA40828K.

215. Waheed, S.; Cabot, J.M.; Macdonald, N.P.; Lewis, T.; Guijt, R.M.; Paull, B.; Breadmore, M.C. 3D Printed Microfluidic Devices: Enablers and Barriers. Lab Chip 2016, 16, 1993–2013.

216. Yafia, M.; Shukla, S.; Najjaran, H. Fabrication of Digital Microfluidic Devices on Flexible Paper-Based and Rigid Substrates via Screen Printing. J. Micromechanics Microengineering 2015, 25, 57001, doi:10.1088/0960-1317/25/5/057001.

217. Cate, D.M.; Adkins, J.A.; Mettakoonpitak, J.; Henry, C.S. Recent Developments in Paper-Based Microfluidic Devices. Anal. Chem. 2015, 87, 19–41.

218. Martínez-López, J.I.; Mojica, M.; Rodríguez, C.A.; Siller, H.R. Xurography as a Rapid Fabrication Alternative for Point-of-Care Devices: Assessment of Passive Micromixers. Sensors 2016, 16, doi:10.3390/s16050705.

219. Thomas, M.S.; Millare, B.; Clift, J.M.; Bao, D.; Hong, C.; Vullev, V.I. Print-and-Peel Fabrication for Microfluidics: What's in It for Biomedical Applications? Ann. Biomed. Eng. 2010, 38, 21–32.

220. Olkkonen, J.; Lehtinen, K.; Erho, T. Flexographically Printed Fluidic Structures in Paper. Anal. Chem. 2010, 82, 10246–10250.

221. Li, J.M.; Liu, C.; Qiao, H.C.; Zhu, L.Y.; Chen, G.; Dai, X.D. Hot Embossing/Bonding of a Poly (Ethylene Terephthalate)(PET) Microfluidic Chip. J. Micromechanics Microengineering 2007, 18, 15008.

222. Attia, U.M.; Marson, S.; Alcock, J.R. Micro-Injection Moulding of Polymer Microfluidic Devices. Microfluid. Nanofluidics 2009, 7, 1–28.

223. Saez, J.; Catalan-Carrio, R.; Owens, R.M.; Basabe-Desmonts, L.; Benito-Lopez, F. Microfluidics and Materials for Smart Water Monitoring: A Review. Anal. Chim. Acta 2021, 1186, 338392, doi:https://doi.org/10.1016/j.aca.2021.338392.

224. Santangelo, M.F.; Shtepliuk, I.; Filippini, D.; Puglisi, D.; Vagin, M.; Yakimova, R.; Eriksson, J. Epitaxial Graphene Sensors Combined with 3D-Printed Microfluidic Chip for Heavy Metals Detection. Sensors 2019, 19, doi:10.3390/s19102393.

225. Kinuthia, G.K.; Ngure, V.; Beti, D.; Lugalia, R.; Wangila, A.; Kamau, L. Levels of Heavy Metals in Wastewater and Soil Samples from Open Drainage Channels in Nairobi, Kenya: Community Health Implication. Sci. Rep. 2020, 10, 8434, doi:10.1038/s41598-020-65359-5.

226. Snyder, S.A.; Boban, M.; Li, C.; VanEpps, J.S.; Mehta, G.; Tuteja, A. Lysis and Direct Detection of Coliforms on Printed Paper-Based Microfluidic Devices. Lab Chip 2020, 20, 4413–4419, doi:10.1039/D0LC00665C.

227. Wang, L.; Li, B.; Wang, J.; Qi, J.; Li, J.; Ma, J.; Chen, L. A Rotary Multi-Positioned Cloth/Paper Hybrid Microfluidic Device for Simultaneous Fluorescence Sensing of Mercury and Lead Ions by Using Ion Imprinted Technologies. J. Hazard. Mater. 2022, 428, 128165, doi:https://doi.org/10.1016/j.jhazmat.2021.128165.

228. Wang, G.; Chu, L.T.; Hartanto, H.; Utomo, W.B.; Pravasta, R.A.; Chen, T.-H. Microfluidic Particle Dam for Visual and Quantitative Detection of Lead Ions. ACS Sensors 2020, 5, 19–23, doi:10.1021/acssensors.9b01945.

229. JARUJAMRUS, P.; MEELAPSOM, R.; PENCHAREE, S.; OBMA, A.; AMATATONGCHAI, M.; DITCHAROEN, N.; CHAIRAM, S.; TAMUANG, S. Use of a Smartphone as a Colorimetric Analyzer in Paper-Based Devices for Sensitive and Selective Determination of Mercury in Water Samples. Anal. Sci. 2018, 34, 75–81, doi:10.2116/analsci.34.75.

230. Quinn, C.W.; Cate, D.M.; Miller-Lionberg, D.D.; Reilly, T.; Volckens, J.; Henry, C.S. Solid-Phase Extraction Coupled to a Paper-Based Technique for Trace Copper Detection in Drinking Water. Environ. Sci. Technol. 2018, 52, 3567–3573, doi:10.1021/acs.est.7b05436.

231. Sharifi, H.; Tashkhourian, J.; Hemmateenejad, B. A 3D Origami Paper-Based Analytical Device Combined with PVC Membrane for Colorimetric Assay of Heavy Metal Ions: Application to Determination of Cu(II) in Water Samples. Anal. Chim. Acta 2020, 1126, 114–123, doi:https://doi.org/10.1016/j.aca.2020.06.006.

232. Khoshbin, Z.; Housaindokht, M.R.; Verdian, A. A Low-Cost Paper-Based Aptasensor for Simultaneous Trace-Level Monitoring of Mercury (II) and Silver (I) Ions. Anal. Biochem. 2020, 597, 113689, doi:https://doi.org/10.1016/j.ab.2020.113689.

233. Idros, N.; Chu, D. Triple-Indicator-Based Multidimensional Colorimetric Sensing Platform for Heavy Metal Ion Detections. ACS Sensors 2018, 3, 1756–1764, doi:10.1021/acssensors.8b00490.

234. Allioux, F.-M.; Kapruwan, P.; Milne, N.; Kong, L.; Fattaccioli, J.; Chen, Y.; Dumée, L.F. Electro-Capture of Heavy Metal Ions with Carbon Cloth Integrated Microfluidic Devices. Sep. Purif. Technol. 2018, 194, 26–32, doi:https://doi.org/10.1016/j.seppur.2017.10.064.

235. Ding, R.; Cheong, Y.H.; Zhao, K.; Lisak, G. Acidified Paper Substrates for Microfluidic Solution Sampling Integrated with Potentiometric

Sensors for Determination of Heavy Metals. Sensors Actuators B Chem. 2021, 347, 130567, doi:https://doi.org/10.1016/j.snb.2021.130567.

236. Scala-Benuzzi, M.L.; Raba, J.; Soler-Illia, G.J.A.A.; Schneider, R.J.; Messina, G.A. Novel Electrochemical Paper-Based Immunocapture Assay for the Quantitative Determination of Ethinylestradiol in Water Samples. Anal. Chem. 2018, 90, 4104–4111, doi:10.1021/acs.analchem.8b00028.

237. Sankar, K.; Lenisha, D.; Janaki, G.; Juliana, J.; Kumar, R.S.; Selvi, M.C.; Srinivasan, G. Digital Image-Based Quantification of Chlorpyrifos in Water Samples Using a Lipase Embedded Paper Based Device. Talanta 2020, 208, 120408, doi:https://doi.org/10.1016/j.talanta.2019.120408.

238. Jemmeli, D.; Marcoccio, E.; Moscone, D.; Dridi, C.; Arduini, F. Highly Sensitive Paper-Based Electrochemical Sensor for Reagent Free Detection of Bisphenol A. Talanta 2020, 216, 120924, doi:https://doi.org/10.1016/j.talanta.2020.120924.

239. Mako, T.L.; Levenson, A.M.; Levine, M. Ultrasensitive Detection of Nitrite through Implementation of N-(1-Naphthyl)Ethylenediamine-Grafted Cellulose into a Paper-Based Device. ACS Sensors 2020, 5, 1207–1215, doi:10.1021/acssensors.0c00291.

240. Peters, J.J.; Almeida, M.I.G.S.; Šraj, L.O.; McKelvie, I.D.; Kolev, S.D. Development of a Micro-Distillation Microfluidic Paper-Based Analytical Device as a Screening Tool for Total Ammonia Monitoring in Freshwaters. Anal. Chim. Acta 2019, 1079, 120–128, doi:https://doi.org/10.1016/j.aca.2019.05.050.

241. Racicot, J.M.; Mako, T.L.; Olivelli, A.; Levine, M. A Paper-Based Device for Ultrasensitive, Colorimetric Phosphate Detection in Seawater. Sensors 2020, 20, doi:10.3390/s20102766.

242. Sarwar, M.; Leichner, J.; Naja, G.M.; Li, C.-Z. Smart-Phone, Paper-Based Fluorescent Sensor for Ultra-Low Inorganic Phosphate Detection in Environmental Samples. Microsystems Nanoeng. 2019, 5, 56, doi:10.1038/s41378-019-0096-8.

243. Carvalho, R.M.; Ferreira, V.S.; Lucca, B.G. A Novel All-3D-Printed Thread-Based Microfluidic Device with an Embedded Electrochemical Detector: First Application in Environmental Analysis of Nitrite. Anal. Methods 2021, 13, 1349–1357, doi:10.1039/D1AY00070E.

244. Pollard, M.; Hunsicker, E.; Platt, M. A Tunable Three-Dimensional Printed Microfluidic Resistive Pulse Sensor for the Characterization of Algae and Microplastics. ACS Sensors 2020, 5, 2578–2586, doi:10.1021/acssensors.0c00987.

245. Mesquita, P.; Gong, L.; Lin, Y. A Low-Cost Microfluidic Method for Microplastics Identification: Towards Continuous Recognition. Micromachines 2022, 13, 499.

246. Yin, K.; Ding, X.; Xu, Z.; Li, Z.; Wang, X.; Zhao, H.; Otis, C.; Li, B.; Liu, C. Multiplexed Colorimetric Detection of SARS-CoV-2 and Other Pathogens in Wastewater on a 3D Printed Integrated Microfluidic Chip. Sensors Actuators B Chem. 2021, 344, 130242, doi:https://doi.org/10.1016/j.snb.2021.130242.

247. Schaumburg, F.; Carrell, C.S.; Henry, C.S. Rapid Bacteria Detection at Low Concentrations Using Sequential Immunomagnetic Separation and Paper-Based Isotachophoresis. Anal. Chem. 2019, 91, 9623–9630, doi:10.1021/acs.analchem.9b01002.

248. Alonzo, L.F.; Hinkley, T.C.; Miller, A.; Calderon, R.; Garing, S.; Williford, J.; Clute-Reinig, N.; Spencer, E.; Friend, M.; Madan, D.; et al. A Microfluidic Device and Instrument Prototypes for the Detection of Escherichia Coli in Water Samples Using a Phage-Based Bioluminescence Assay. Lab Chip 2022, 22, 2155–2164, doi:10.1039/D1LC00888A.

249. Lin, D.; Li, B.; Qi, J.; Ji, X.; Yang, S.; Wang, W.; Chen, L. Low Cost Fabrication of Microfluidic Paper-Based Analytical Devices with Water-Based Polyurethane Acrylate and Their Application for Bacterial Detection. Sensors Actuators B Chem. 2020, 303, 127213, doi:https://doi.org/10.1016/j.snb.2019.127213.

250. Sweet, E.C.; Liu, N.; Chen, J.; Lin, L. Entirely-3D Printed Microfluidic Platform for On-Site Detection of Drinking Waterborne Pathogens. In Proceedings of the 2019 IEEE 32nd International Conference on Micro Electro Mechanical Systems (MEMS); 2019; pp. 79–82.

251. Sun, H.; Jia, Y.; Dong, H.; Fan, L.; Zheng, J. Multiplex Quantification of Metals in Airborne Particulate Matter via Smartphone and Paper-Based Microfluidics. Anal. Chim. Acta 2018, 1044, 110–118, doi:https://doi.org/10.1016/j.aca.2018.07.053.

252. Sun, H.; Jia, Y.; Dong, H.; Fan, L. Graphene Oxide Nanosheets Coupled with Paper Microfluidics for Enhanced On-Site Airborne Trace Metal Detection. Microsystems Nanoeng. 2019, 5, 4, doi:10.1038/s41378-018-0044-z.

253. Jia, Y.; Dong, H.; Zheng, J.; Sun, H. Portable Detection of Trace Metals in Airborne Particulates and Sediments via MPADs and Smartphone. Biomicrofluidics 2017, 11, 64101, doi:10.1063/1.5003308.

254. Guo, X.-L.; Chen, Y.; Jiang, H.-L.; Qiu, X.-B.; Yu, D.-L. Smartphone-Based Microfluidic Colorimetric Sensor for Gaseous Formaldehyde Determination with High Sensitivity and Selectivity. Sensors 2018, 18, doi:10.3390/s18093141.

255. Zhao, J.; Liu, M.; Liang, L.; Wang, W.; Xie, J. Airborne Particulate Matter Classification and Concentration Detection Based on 3D Printed Virtual Impactor and Quartz Crystal Microbalance Sensor. Sensors Actuators A Phys. 2016, 238, 379–388, doi:https://doi.org/10.1016/j.sna.2015.12.029.

256. Poenar, D.P. Microfluidic and Micromachined/MEMS Devices for Separation, Discrimination and Detection of Airborne Particles for Pollution Monitoring. Micromachines 2019, 10, doi:10.3390/mi10070483.

257. Dias, I.M.; Cardoso, T.M.G.; Coltro, W.K.T.; Urban, R.C. Paper-Based Analytical Devices with Colorimetric Detection for Determining Levoglucosan in Atmospheric Particulate Matter. Atmos. Environ. 2019, 213, 463–469, doi:https://doi.org/10.1016/j.atmosenv.2019.06.040.

258. Seok, Y.; Lee, J.; Kim, M.-G. Paper-Based Airborne Bacteria Collection and DNA Extraction Kit. Biosensors 2021, 11, doi:10.3390/bios11100375.

259. Xi, Y.; Duford, D.A.; Salin, E.D. Automated Liquid–Solid Extraction of Pyrene from Soil on Centrifugal Microfluidic Devices. Talanta 2010, 82, 1072–1076, doi:https://doi.org/10.1016/j.talanta.2010.06.007.

260. Duford, D.A.; Xi, Y.; Salin, E.D. Enzyme Inhibition-Based Determination of Pesticide Residues in Vegetable and Soil in Centrifugal Microfluidic Devices. Anal. Chem. 2013, 85, 7834–7841, doi:10.1021/ac401416w.

261. Cheng, Y.; Yang, R.M.H.; Alejandro, F.M.; Li, F.; Balavandy, S.K.; Wang, L.; Breadmore, M.; Doyle, R.; Naidu, R. 7 - Current Applications of Colourimetric Microfluidic Devices (Smart Phone Based) for Soil Nutrient Determination. Smartphone-Based Detect. Devices 2021, 103–128.

262. Stanley, C.E.; Grossmann, G.; i Solvas, X.; deMello, A.J. Soil-on-a-Chip: Microfluidic Platforms for Environmental Organismal Studies. Lab Chip 2016, 16, 228–241, doi:10.1039/C5LC01285F.

263. Wu, S.; Wu, Y.; Cao, B.; Huang, Q.; Cai, P. An Invisible Workforce in Soil: The Neglected Role of Soil Biofilms in Conjugative Transfer of Antibiotic Resistance Genes. Crit. Rev. Environ. Sci. Technol. 2022, 52, 2720–2748, doi:10.1080/10643389.2021.1892015.

264. Pouyanfar, N.; Harofte, S.Z.; Soltani, M.; Siavashy, S.; Asadian, E.; Ghorbani-Bidkorbeh, F.; Keçili, R.; Hussain, C.M. Artificial Intelligence-Based Microfluidic Platforms for the Sensitive Detection of Environmental Pollutants: Recent Advances and Prospects. Trends Environ. Anal. Chem. 2022, 34, e00160, doi:https://doi.org/10.1016/j.teac.2022.e00160.

265. Morbioli, G.G.; Mazzu-Nascimento, T.; Stockton, A.M.; Carrilho, E. Technical Aspects and Challenges of Colorimetric Detection with Microfluidic

Paper-Based Analytical Devices (MPADs) - A Review. Anal. Chim. Acta 2017, 970, 1–22, doi:https://doi.org/10.1016/j.aca.2017.03.037.

266. Carrasco-Correa, E.J.; Simó-Alfonso, E.F.; Herrero-Martínez, J.M.; Miró, M. The Emerging Role of 3D Printing in the Fabrication of Detection Systems. TrAC Trends Anal. Chem. 2021, 136, 116177.

267. Phan, T.H.T.; Kim, S.-J. Super-Hydrophobic Microfluidic Channels Fabricated via Xurography-Based Polydimethylsiloxane (PDMS) Micromolding. Chem. Eng. Sci. 2022, 117768.

268. Chen, C.; Townsend, A.D.; Hayter, E.A.; Birk, H.M.; Sell, S.A.; Martin, R.S. Insert-Based Microfluidics for 3D Cell Culture with Analysis. Anal. Bioanal. Chem. 2018, 410, 3025–3035.

269. Amin, R.; Joshi, A.; Tasoglu, S. Commercialization of 3D-Printed Microfluidic Devices. J. 3D Print. Med. 2017, 1, 85–89, doi:10.2217/3dp-2016-0010.

270. Kung, C.-T.; Hou, C.-Y.; Wang, Y.-N.; Fu, L.-M. Microfluidic Paper-Based Analytical Devices for Environmental Analysis of Soil, Air, Ecology and River Water. Sensors Actuators B Chem. 2019, 301, 126855.

271. Jokerst, J.C.; Emory, J.M.; Henry, C.S. Advances in Microfluidics for Environmental Analysis. Analyst 2012, 137, 24–34.

272. Budlayan, M.L.; Dalagan, J.; Lagare-Oracion, J.P.; Patricio, J.; Arco, S.; Latayada, F.; Vales, T.; Baje, B.; Alguno, A.; Capangpangan, R. Detecting Mercury Ions in Water Using a Low-Cost Colorimetric Sensor Derived from Immobilized Silver Nanoparticles on a Paper Substrate. Environ. Nanotechnology, Monit. Manag. 2022, 18, 100736, doi:https://doi.org/10.1016/j.enmm.2022.100736.

273. Rizzo, P. Water and Wastewater Pipe Nondestructive Evaluation and Health Monitoring: A Review. Adv. Civ. Eng. 2010, 2010.

274. Berardi, L.; Giustolisi, O.; Kapelan, Z.; Savic, D.A. Development of Pipe Deterioration Models for Water Distribution Systems Using EPR. J. Hydroinformatics 2008, 10, 113–126.

275. Wang, M.; Song, Z.; Jiang, Y.; Zhang, X.; Wang, L.; Zhao, H.; Cui, Y.; Gu, F.; Wang, Y.; Zheng, G. A Three-Dimensional Pinwheel-Shaped Paper-Based Microfluidic Analytical Device for Fluorescence Detection of Multiple Heavy Metals in Coastal Waters by Rational Device Design. Anal. Bioanal. Chem. 2021, 413, 3299–3313, doi:10.1007/s00216-021-03269-9.

276. Yuan, Y.; Jia, H.; Wang, J. A Microfluidic Electrochemical Sensing Platform for in Situ Detection of Trace Cadmium Ions. Anal. Methods 2022.

277. Huang, W.-H.; Mai, V.-P.; Wu, R.-Y.; Yeh, K.-L.; Yang, R.-J. A Microfluidic Aptamer-Based Sensor for Detection of Mercury(II) and Lead(II) Ions in Water. Micromachines 2021, 12.

278. Akimoto, H. Global Air Quality and Pollution. Science (80-.). 2003, 302, 1716–1719.

279. Fenger, J. Urban Air Quality. Atmos. Environ. 1999, 33, 4877–4900.

280. Schulze, F.; Gao, X.; Virzonis, D.; Damiati, S.; Schneider, M.R.; Kodzius, R. Air Quality Effects on Human Health and Approaches for Its Assessment through Microfluidic Chips. Genes (Basel). 2017, 8, 244.

281. Zhu, X.; Wang, K.; Yan, H.; Liu, C.; Zhu, X.; Chen, B. Microfluidics as an Emerging Platform for Exploring Soil Environmental Processes: A Critical Review. Environ. Sci. Technol. 2022, 56, 711–731, doi:10.1021/acs.est.1c03899.

282. Tabani, H.; Samkumpim, T.; Alahmad, W.; Dorabadizare, F.; Varanusupakul, P. In-Tube Gel Electro-Membrane Combined with Microfluidic Paper-Based Device: A Green and Miniaturized Extraction Mode for the Chromium Speciation. Adv. Sample Prep. 2022, 3, 100036, doi:https://doi.org/10.1016/j.sampre.2022.100036.

283. Lopez-Ruiz, N.; Curto, V.F.; Erenas, M.M.; Benito-Lopez, F.; Diamond, D.; Palma, A.J.; Capitan-Vallvey, L.F. Smartphone-Based Simultaneous PH and Nitrite Colorimetric Determination for Paper Microfluidic Devices. Anal. Chem. 2014, 86, 9554–9562.

284. Taheri, H.; Khayatian, G. Smartphone-Based Microfluidic Chip Modified Using Pyrrolidine-1-Dithiocarboxylic Acid for Simultaneous Colorimetric Determination of Cr3+ and Al3+ Ions. Spectrochim. Acta Part A Mol. Biomol. Spectrosc. 2022, 272, 121000.

285. Cui, Y.; Wang, R.; Brady, B.; Wang, X. Fully Inkjet-Printed Paper-Based Pb2+ Optodes for Water Analysis without Interference from the Chloramine Disinfectant. Anal. Bioanal. Chem. 2022, doi:10.1007/s00216-022-04286-y.

CHAPTER 2. A low-cost microfluidic method for microplastics identification: Towards continuous recognition

by

Pedro Mesquita, Liyuan Gong, Yang Lin

Department of Mechanical, Industrial and Systems Engineering, University of Rhode Island, Kingston, Rhode Island, USA

Published in Micromachines

Mesquita, P., Gong, L. and Lin, Y., 2022. A Low-Cost Microfluidic Method for Microplastics Identification: Towards Continuous Recognition. Micromachines, 13(4), p.499. https://doi.org/10.3390/mi13040499

ABSTRACT

Plastic pollution has emerged as a growing concern worldwide. In particular, the most abundant plastic debris, microplastics, has necessitated the development of rapid and effective identification methods to track down the stages and evidence of the pollution. In this paper, we combine low-cost plastic staining technologies using Nile Red with the continuous feature offered by microfluidics to propose a low-cost 3D printed device for the identification of microplastics. It is observed that the microfluidic devices indicate comparable staining and identification performance compared to conventional Nile Red staining processes while offering the advantages of continuous recognition for long-term environmental monitoring. The results also show that concentration, temperature, and residency time possess strong effects on the identification performance. Finally, various microplastics have been applied to further demonstrate the effectiveness of the proposed devices. It is found that, among different types of microplastics, non-spherical microplastics show the maximal fluorescence level. Meanwhile, natural fibers indicate better staining quality when compared to synthetic ones.

1. Introduction

It has been estimated that the ongoing COVID-19 pandemic has exceedingly increased the demand for the use of plastics [1]. As of August 23, 2021, more than 8.4 million tons of pandemic-associated plastic debris was released to the oceans [2]. Among them, most of the plastic debris is microplastics with a size smaller than 5 mm [3,4], and it can be classified into primary and secondary microplastics. Generally, primary microplastics are the microscopic plastics that were intentionally made small (*e.g.,* microbeads used in cosmetics) [5–7], while secondary microplastics are particles resulting from the breakdown of macroscopic pieces due to the conjoint environmental effects (*i.e.,* photo-oxidation, hydrolysis, microorganism degradation, mechanical shear, *etc.*) [8,9]. Despite the fact that a variety of plastic types have been identified in microplastics, most of the microplastics in seawater originate from packaging materials (*e.g.,* polyethylene, and polypropylene) [10]. Owing to their small density, these microplastics tend to float on the surface of water, thus they can spread worldwide (in opposition to denser plastics that tend to settle down) and are more difficult to remove [11,12].

Nevertheless, current understanding of the plastic pollution in terms of the quantity, type, lifetime, and associated health effects largely remain unknown. As a result, microplastic separation and identification serves as an important approach to providing evidence and metrics of the pressing environmental issues caused by plastic pollution [13]. For example, worldwide microplastics assessment is possible to identify hot pollution spots and determine the historical trends which may lead to novel strategies for fighting debris spread [14–16]. At present, quite a few

identification techniques have been explored for microplastic identification. Among them, common methods include visual inspection, Fourier-transform infrared spectroscopy (FTIR), Raman spectroscopy and scanning electron microscopy (SEM) [17,18]. Despite their effectiveness, these techniques, except visual inspection, rely on expensive apparatus and time-consuming detection methods that are limited to trained personnel, thus hindering the expansion of these methods for high-throughput detection [19–21].

As a result, visual inspection, though not as effective as other sophisticated counterparts, is still widely applied for faster recognition [22,23]. Currently, a variety of sampling and identification technologies have been used to improve the performance of visual inspection, of which a commonly used one is the combination of filtration and staining [24,25]. However, filtration often leads to false positives due to potential interference from organic matters in the samples [26,27]. More importantly, its performance is highly reliant on the size of the filters, thus limiting its capabilities in sampling small microplastics. In addition, particles are also prone to adhere to the filters, resulting in ineffective separation of the microplastics for identification [28,29]. In addition, staining of the microplastics relies on staining agents that turn microplastics into prominently visible particles [30,31]. Currently, it is unsurprising that quite a few staining agents (*e.g.,* Rhodamine B, Rose Bengal, Trypan Blue, *etc.)* have been explored for this purpose. Among them, Nile Red was reported to be one of the most effective agents due to its favorable binding performance with lipophilic substances [30,32,33].

Nevertheless, the focus of current studies on microplastic staining and identification has been largely given to batch-by-batch or case-by-case analysis [25,34–36]. Therefore, sample collection is still inevitable and remains a time-consuming step in the whole sampling process. Moreover, temporal information is hardly achievable. Given the needs of acquiring in-depth studies of microplastic pollution in oceans and other water bodies, long-term monitoring or continuous monitoring is essential and a low-cost, simple while effective method should be developed. Thanks to the burgeoning developments of the microfluidic technologies over the past decades, microfluidic devices can be a promising solution to address this need due to its powerful particle control capabilities and the ease of integration in modern electronic systems [37,38]. For example, microfluidics has been used for long-term monitoring of algae in the past [39]. Tumor responses to hypoxia conditions were also analyzed continuously in a microfluidic platform [40]. Indeed, microplastic identification is also not a new research area for microfluidics [41,42], yet to the best knowledge of the authors, microfluidics has not been applied for long-term microplastics assessment and we believe the combination of low-cost Nile Red staining and microfluidic fluid control would provide a novel venue to confront the ever-deteriorating plastic issues without complicated analysis and costly instrumentations. Low-cost fabrication methods such as 3D printing and molding can be applied to further minimize the cost associated with this method, and the miniaturized devices may also be integrated in the monitoring stations near seashores, along with data collection of other water quality metrics on a continuous basis.

Herein, we further explored the staining capabilities of Nile Red through a microfluidic device capable of continuously staining microplastics for rapid identification. The proposed device has two inlets for respective Nile Red and sample injection (Figure 1.2A), and a serpentine channel that allows for sufficient mixing of the staining agent and the sample. In this paper, we studied the effects of dominating parameters on the identification performance, including Nile Red concentration, temperature, and residency time. Note that prior to performing microfluidic studies, static studies that resemble traditional Nile Red staining processes were adopted and served as a baseline for comparison.

2. Materials and Methods

In this paper, the process of static microplastic identification using Nile Red was carried out without a filter. Specifically, the staining Nile Red solution was added directly into an Eppendorf tube containing the microplastics sample and placed inside an oven (Figure 1.2B). On the other hand, microfluidic experiments followed a similar procedure: mixing Nile Red and microplastics in the device (which was placed inside oven). Since the mixing process is passively induced without human operation, this process holds promise for continuous staining.

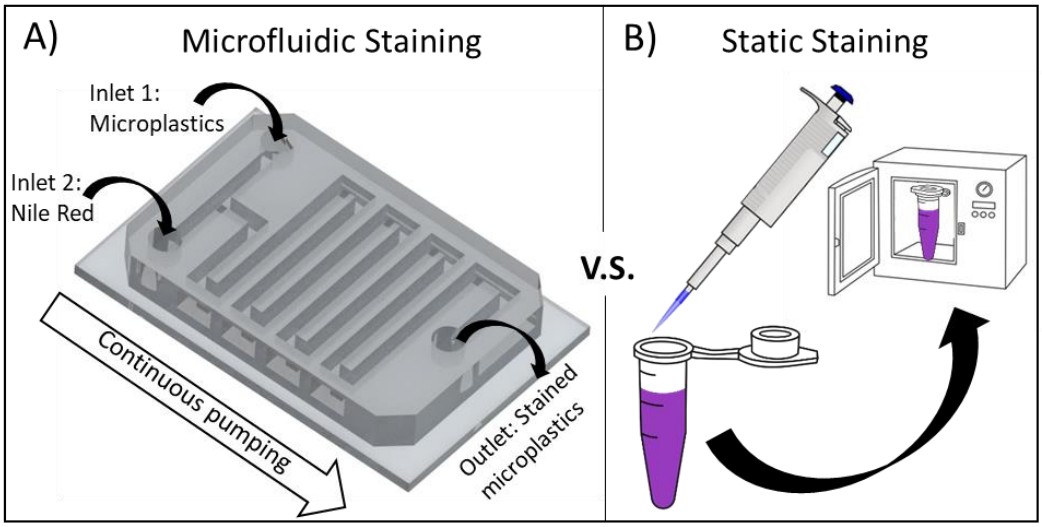

Figure 2.1. Schematic illustration of the staining processes studied in this paper. A) process of microfluidics-based continuous staining of microplastics using Nile Red. B) process of static staining of microplastics. Compared to microfluidic staining, the static process is laborious as it requires multiple batches and manual operation.

2.1. Nile Red preparation

The staining solution was prepared by dissolving Nile Red (technical grade, N3013, Sigma-Aldrich) in methanol to different concentrations. We have considered the limit of solubility of Nile Red in methanol (1 mg/mL) to be the stock solution for further dilution, from which the solution was diluted into 50X, 100X, 250X, 500X, and 1000X samples.

2.2. Microplastics sample preparation

In this paper, lab-prepared and commercially available microplastics were adopted in lieu of naturally formed microplastics. More specifically, microspheres made of polyethylene (PE), ranging from 10 - 45 µm (Cospheric, Inc.) were applied to determine the optimal parameters for staining. Other plastics including the microspheres made of polystyrene (PS) with sizes from 9.5-11.5 µm (Cospheric,

Inc.), cotton and acrylic fabric acquired from clothing, polypropylene (PP) and non-spherical PE prepared from plastic storage containers were also applied to test the versability of the proposed method. All the samples were mixed with deionized (DI) water prior to staining. Note that commercial microspheres were diluted in a concentration of 10 mg/mL, while the other samples were diluted to 1 mg/mL, that is because the commercial particles were more available than the ones obtained from other sources.

2.3. Static experiments

To prepare the samples for static experiments, 100 µL of Nile Red solution was thoroughly mixed with 100 µL of PE microplastics solution inside an Eppendorf tube, followed by baking inside an oven (Quincy Lab, model 10). On the other hand, all static experiments were performed using PE microspheres. To investigate the effect of Nile Red concentration on staining performance, different concentrations were tested: 100X, 250X, 500X, and 1000X; in addition, different temperatures (*i.e.,* 25, 40, 50, 60, 70, and 80 °C) were applied to study the effects of temperature. All the samples were placed inside the oven for 10 minutes, and analysis was conducted immediately after baking.

2.4. Microfluidic experiments

To create the microfluidic devices, soft lithography, a commonly used method in microfluidics, was applied. Specifically, a 3D printer (CADWorks 3D, µMicrofluidics edition) was used to create the molds for casting polydimethylsiloxane (PDMS) to obtain the final devices. After curing the PDMS mixture in an oven over night at 65 °C, a corona treater (BD-20AC Laboratory

Corona Treater) was used to permanently bond the device onto a glass slide. Finally, the device was placed inside the oven and a syringe pump (Chemyx, Fusion 200) was used to run the samples as well as the staining agents inside the device.

2.5. Sample observation

For both static and microfluidic staining, an inverted microscope (Zeiss Axio Vert.A1) was used. To visualize the fluorescent signal from the samples, an illumination system (Excelitas X-Cite mini+) with a wavelength of 365 nm was used. All the images were recorded using a camera attached to the microscope (Phantom VEO E310L). ImageJ (https://imagej.nih.gov/ij/) was used to analyze and quantify the results. Each experiment was performed four times for statistical analysis. We have not filtered the particles prior to observation, instead, we have directly placed a droplet of the diluted sample on top of a glass slide.

3. Results

3.1. Static results

It is worth mentioning that high concentration Nile Red can lead to undesired aggregation [43,44], which may clog microfluidic channels and mask signals from stained microplastics. Moreover, the aggregation may destroy the samples into unrealistic microplastics (once aggregated the original size and shape are lost) and induce misleading conclusions [45,46]. We have observed that aggregations occurred for Nile Red solutions diluted up to 50X. Therefore, Nile Red solutions diluted to a minimum of 100X were used in our experiments to guarantee that no

induced aggregations would happen. Figure 2.2 illustrates how aggregation occurs over time. Specially, 50X Nile Red solution was placed onto a glass slide containing PE microspheres, and aggregation process was recorded at 3000 fps. Figure 2.2A shows the initial frame (0.0003 s), it is possible to observe that particles are separated. The other images show the subsequent frames (from 0.0006 s to 0.0013 s), where the aggregation is showed. In this image it is possible to see how fast aggregations are induced in microplastics due to the excess of Nile Red. Also, the original features of the particles are lost, if someone were to study the size distribution or the shape of this sample, the outcome would certainly not be accurate due to the aggregation.

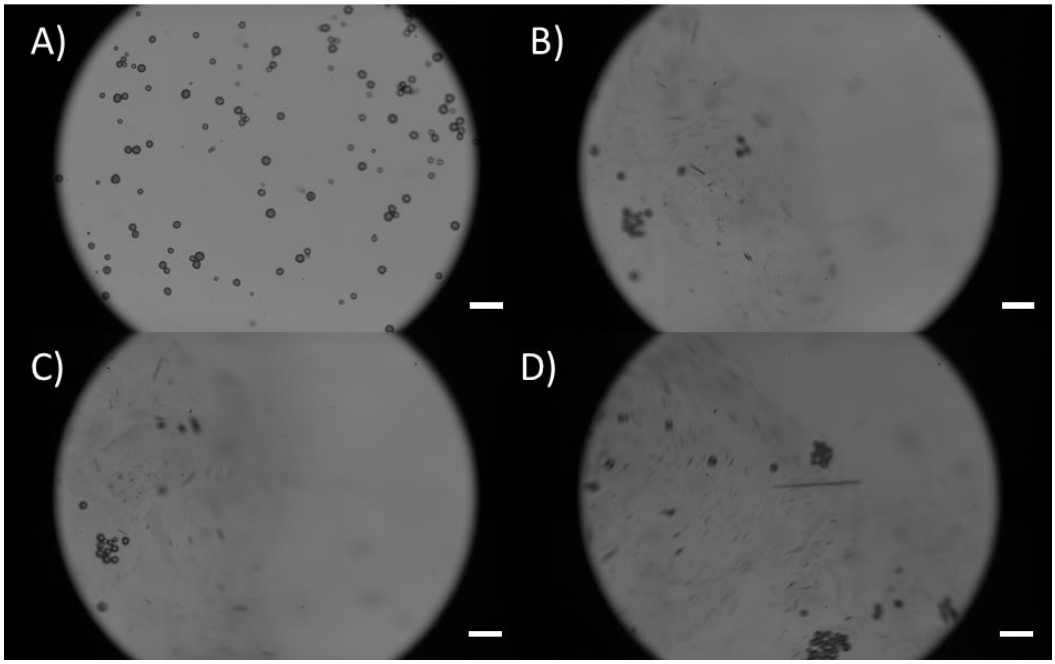

Figure 2.2. Aggregation induced due to high Nile Red concentrations. A) First frame (0.0003 s) – Moment in which the Nile Red solution is placed on the glass slide right after the preparation; B) Second frame (0.0006 s) – Beginning of the aggregation; C) Third frame (0.0010 s) – Initial particle clusters can be observed; D) Fourth frame (0.0013 s) – Higher levels of aggregation are observed; Scale bars are 100 µm.

Once the threshold for the Nile Red concentration was defined, static experiments were conducted to determine the effects of Nile Red concentration, and temperature on staining efficiency. It was already known that temperature, residency time and ambient lights were important for the staining quality, however, no systematic study was available [30,47]. We have observed that for an infinitely long time (72 hours) the highest pixel intensity of a sample containing 100X Nile Red at 25 °C is 150, thus we defined this intensity to be the reference for results normalization (all results shown in this paper are normalized with respect to this result). Figure 3.2 shows the results for the concentration and temperature static analysis, indicating that higher concentrations associated with higher temperatures provide better staining results, which is in accordance with the results from other groups [47,48]. However, it is difficult to identify relevant fluorescent signal at 25°C, thus we have added arrows to indicate the particle positions.

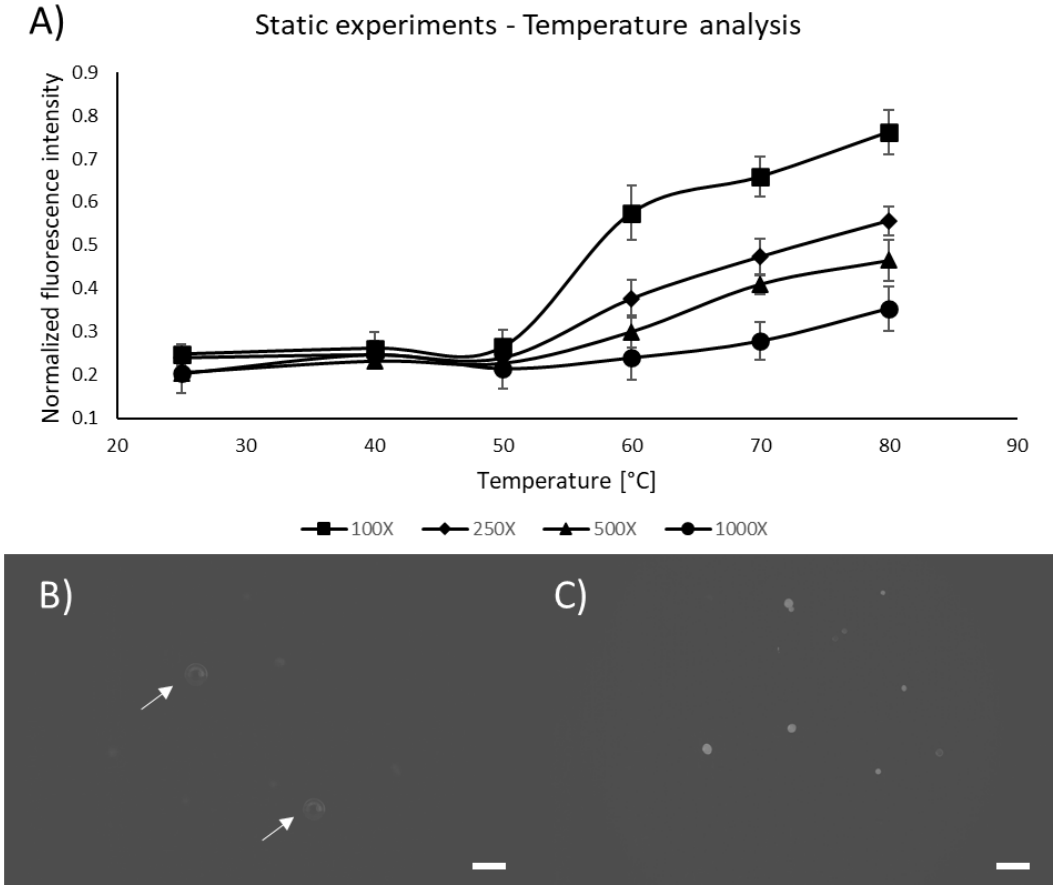

Figure 2.3. Effect of Nile Red concentration and temperature for static samples placed inside the oven for 10 minutes. A) Graph showing the influence of different Nile Red concentrations and oven temperatures on staining performance; B) PE microspheres stained using 100X Nile Red at 25 °C; C) PE microspheres stained using 100X Nile Red at 80 °C; Scale bars are 100 µm.

Following the concentration and temperature experiments, we determined the effect of time on the staining quality (Figure 4.2). To do so, samples were kept inside the oven at a fixed temperature and Nile Red concentration, varying only the time. Since the previous results indicate that 100X and 250X Nile Red solutions at 80 °C are the most prominent combinations, thus these parameters were chosen along with variation in time: 5, 6, 7, 8, 9, 10, 11, and 12 minutes. As shown in Figure 4.2A, after 10 minutes, no significant changes in fluorescence level were observed, which means that this is enough time to extract the maximum

performance from the staining agent. Figures 4.2B and 4.2C show the differences between the minimum and maximum staining time, where it is possible to observe that more time produces stronger fluorescence signal in the particles.

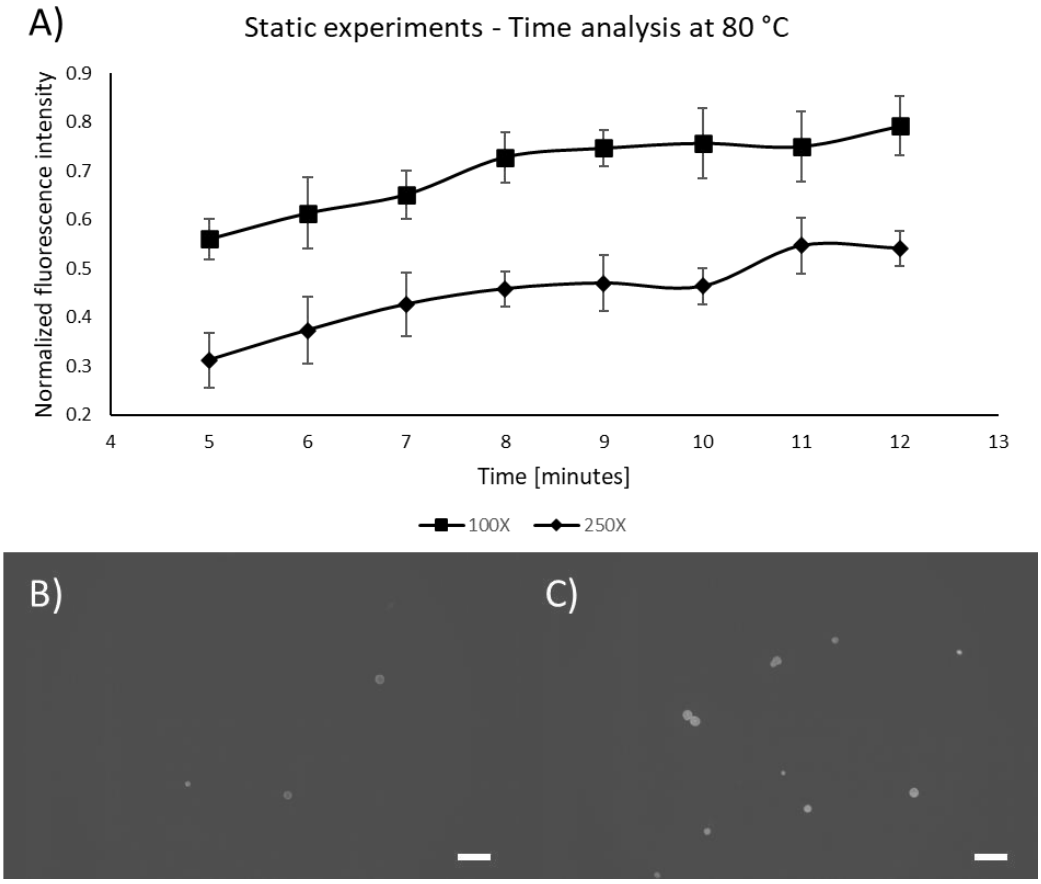

Figure 2.4. Effect of time for 100X and 250X Nile Red solutions at 80 °C. A) Graph showing the influence of time; B) PE microspheres stained using 100X Nile Red for 5 minutes; C) PE microspheres stained using 100X Nile Red for 12 minutes; Scale bars are 100 µm.

3.2. Microfluidic results

As aforementioned, microfluidics holds great potentials in providing continuous monitoring of microplastics in various water bodies. In this section, we applied the parameters under optimal conditions obtained from static experiments

to explore the possibilities of using microfluidics for continuous microplastic identification.

As aforementioned, concentration and temperature are important parameters, thus their optimized values were adopted for the microfluidic device. When it comes to the flowing conditions, residency time becomes another important parameter which is subject to the external devices (*i.e.,* syringe pump). In this paper, the total microchannel length was 400 mm, and its cross-sectional area was 2x2 mm. Using this design, we could achieve 5, 6, 7, 8, 9, 10, 11, and 12 minutes of residency time by applying corresponding flow rates of 7.82, 6.52, 5.58, 4.89, 4.34, 3.91, 3.55, and 3.26 µL/min, respectively. Note that the microfluidic device was placed inside the oven while the syringe pump was kept outside. The input and output hoses were long enough to enable for sample collection and syringe manipulation outside the oven. Figure 5.2 shows the set-up arrangement.

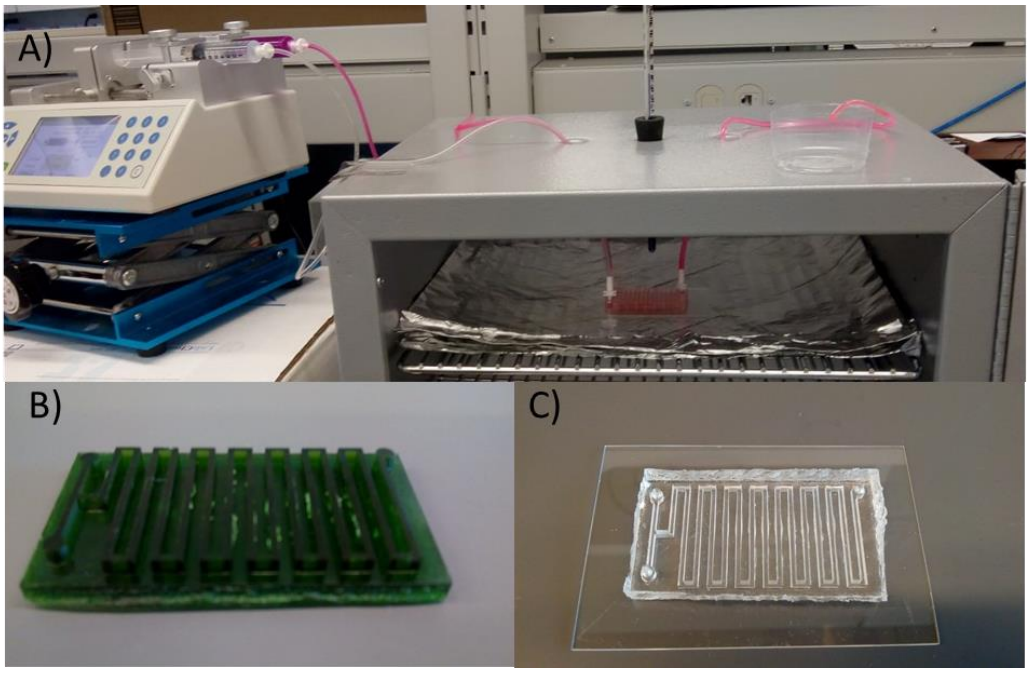

Figure 2.5. Operational set-up for microfluidic staining. A) Microfluidic device placed inside oven with inlet and outlet tubings; B) Photo of the mold used for PDMS casting; C) Photo of the final bonded device.

From the information acquired during the static experiments, we have performed the microfluidic experiments with the most promising configurations with respect to concentration and temperature (*i.e.,* 100X and 250X; at 80 °C). Different flow rates were tested to compare the performance of static and microfluidic staining regarding the residency time. As expected, lower flow rates provided better results, which is in accordance with the static experiments [46,49]. Nonetheless, it is possible to observe that for the lowest flow rate (and highest residency time) the static staining had superior fluorescence levels (~ 37% higher). This behavior could be attributed to the lower mixing quality governed by diffusion inside the device, since the static samples were actively shaken prior to oven insertion [50–52]. Even though the microfluidic results exhibited lower fluorescence levels compared to the static experiments, it provides passive mixing

and staining without tedious and time-consuming manual sample preparation. Nonetheless, it is worth mentioning that for higher flow rates, identification becomes difficult due to low fluorescence levels arising from short residency time. Figure 6.2 shows the results for microfluidic staining of the PE microspheres.

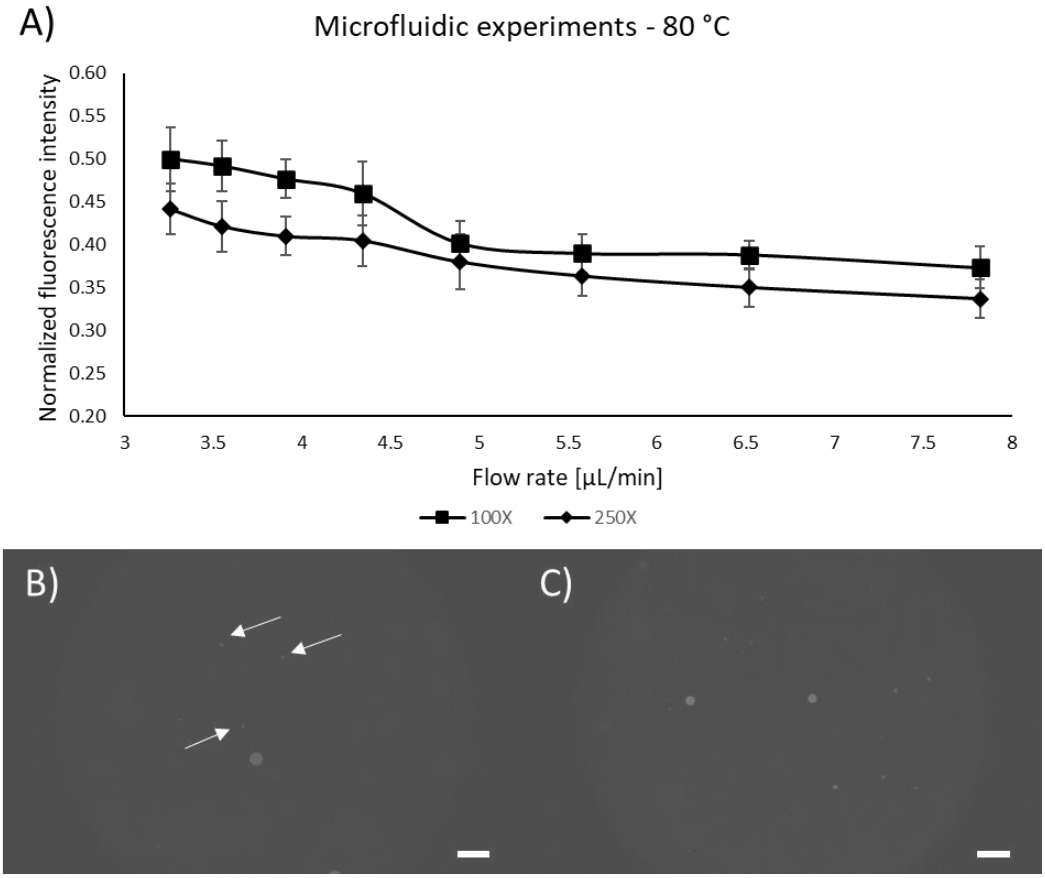

Figure 2.6. Microfluidic staining. A) Effect of flow rate for fixed temperature; B) PE microspheres stained using 100X Nile Red at 5.58 µL/min; C) PE microspheres stained using 100X Nile Red at 3.26 µL/min; Scale bars are 100 µm.

Besides PE microspheres, we further demonstrated the capabilities of our device for identifying other types of plastic. In this regard, multiple types of microplastics were applied, including microspheres (PS), fibers (cotton and acrylic), plastic parts scratched from storage containers (PP and PE). Moreover, yeast was adopted as a model of potential organic particles in seawater. Figure 7.2 shows

the results of microfluidic staining for these samples. Note that PS microspheres showed better results when compared to the PE microspheres stained by the microfluidic device. Amongst the fibers, cotton indicated stronger fluorescence levels compared to acrylic, yet both were identifiable. Surprisingly, we found that all results obtained using PP and PE samples indicated the highest pixel intensity (*i.e.,* 255, though larger than the threshold, it is indeed a strong indicator). However, as a recognized downside of staining identification, our method still suffers from the incapabilities of distinguishing microplastics from other natural particles, which can be seen from the results obtained using yeasts. It showed comparable fluorescence levels with respect to the plastics, highlighting the necessity for eliminating organic matter prior sample analysis. Nevertheless, our results have demonstrated that continuous staining is achievable in microfluidic devices.

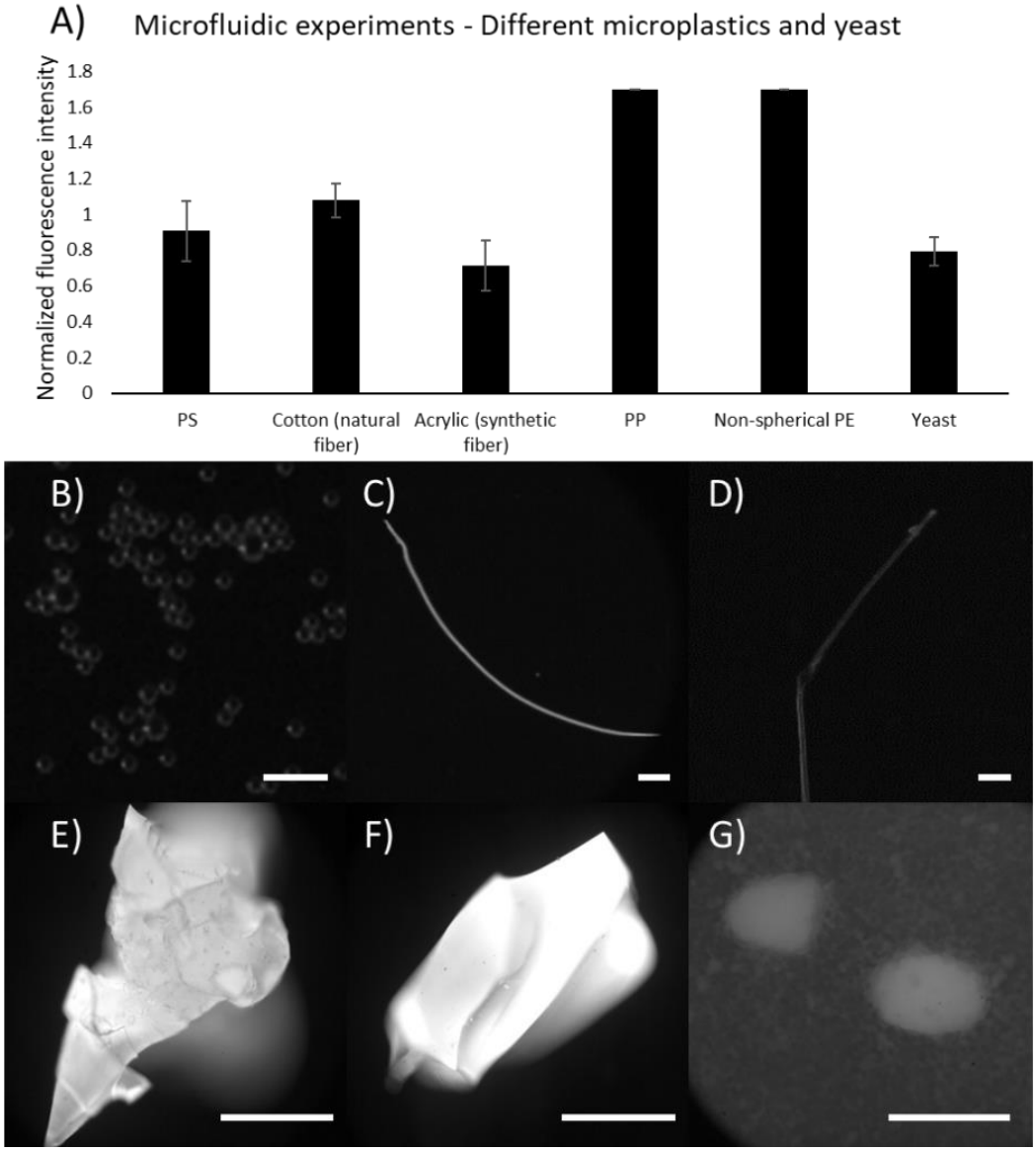

Figure 2.7. Microfluidic staining for different plastics and yeast. A) Fluorescence levels for different microplastics and yeast; B) PS microspheres; Scale bar is 50 µm; C) Cotton (natural fiber); D) Acrylic (synthetic fiber); Scale bars are 1 mm; E) PP from storage container; Scale bars are 50 µm. F) PE from storage container; Scale bars are 50 µm. G) Yeast; Scale bars are 50 µm.

4. Discussion

In this paper, we have presented a novel microfluidic identification method towards the continuous recognition of microplastics in water. Our method

combines the Nile Red staining protocols with the high-throughput advantages imposed by microfluidics [45,47,51]. We acknowledge that the flow rates used must be small in order to achieve reasonable residency time, which has a negative effect on the throughput; however, the use of multiple (parallel) devices is feasible (especially due to its miniaturized size) which can enhance the throughput significantly [53,54]. In addition, the devices could be further improved and integrated in water monitoring stations in the future for continuous sampling and identification. According to the results obtained, the best staining quality is at the lowest flow rate (3.26 µL/min), which was expected since the static experiments showed that the lowest residency time performed the best.

In addition, though microfluidic results are still not as good as the static ones, future improvements can be carried out by adopting a better mixing strategy for Nile Red and samples [50–52]. Currently, a myriad of mixing methods has been developed for microfluidic devices, including both passive and active mixing. For example, better mixing performance could be addressed by adding pillars inside the channels [55,56]. Active mixers such as acoustofluidic mixers are alternatives and often provide more rapid mixing due to their superior particle control abilities [57].

The device can be further improved by coupling an on-chip heater, eliminating the need for an oven [58], thus reducing costs and enhancing its integrability. Once fully miniaturized, the device could be used for in situ analysis of water samples [47,48]. In situ analysis could also benefit from the use of smartphones, possibly

for both identification and for device operation (pump and active mixers control) [59–61].

Note that, the concentration of microplastics in seawater samples varies widely, being less concentrated off-shore (down to 8 particles/m^3) [62]. In addition, global plastic distribution also changes significantly from one place to another, thereby a rapid and continuous identification prior to in-depth analysis would be beneficial. Though the staining method is not capable of distinguish different types of microplastics, including other particles such as marine organisms, but it indeed provides a simple, low-cost and effective method to confirm the presence of microplastics prior to more in-depth analysis including type differentiation [63]. Moreover, compared to regular visual inspection that bypasses the fluorescence staining, this proposed method turns microplastics into more prominent particles for better identification [64].

5. Conclusions

Overall, we have suggested the adoption of a microfluidic device for the continuous analysis and further detection of microplastics. Nile Red has proven to be effective for the identification of microplastics. Static experiments were performed to systematically assess the influence of staining agent concentration, temperature, and residency time. Based on the results, the microfluidic configuration for continuous staining was optimized, leading to the best fluorescence results among the tested configurations. Our method demonstrated to be feasible for the identification of different types of microplastics with the

advantage of continuous staining and with the possibility of future integration for in situ identification along with higher throughputs. This platform demonstrated to successfully identify microplastics in a continuous manner, representing a valuable option for the environmental management.

Acknowledgements

This research was supported by Y. Lin's start up fund at URI. P. Mesquita acknowledge the "Enhancement of Graduate Research Awards" grant support from the Graduate School at URI.

6. References

1. Binda, G.; Bellasi, A.; Spanu, D.; Pozzi, A.; Cavallo, D.; Bettinetti, R. Evaluating the Environmental Impacts of Personal Protective Equipment Use by the General Population during the COVID-19 Pandemic: A Case Study of Lombardy (Northern Italy). Environ. 2021, 8.

2. Peng, Y.; Wu, P.; Schartup, A.T.; Zhang, Y. Plastic Waste Release Caused by COVID-19 and Its Fate in the Global Ocean. Proc. Natl. Acad. Sci. 2021, 118.

3. Cózar, A.; Sanz-Martín, M.; Martí, E.; González-Gordillo, J.I.; Ubeda, B.; Gálvez, J.Á.; Irigoien, X.; Duarte, C.M. Plastic Accumulation in the Mediterranean Sea. PLoS One 2015, 10, e0121762.

4. Eriksen, M.; Lebreton, L.C.M.; Carson, H.S.; Thiel, M.; Moore, C.J.; Borerro, J.C.; Galgani, F.; Ryan, P.G.; Reisser, J. Plastic Pollution in the World's Oceans: More than 5 Trillion Plastic Pieces Weighing over 250,000 Tons Afloat at Sea. PLoS One 2014, 9, e111913.

5. Yurtsever, M. Glitters as a Source of Primary Microplastics: An Approach to Environmental Responsibility and Ethics. J. Agric. Environ. Ethics 2019, 32, 459–478.

6. van Wezel, A.; Caris, I.; Kools, S.A.E. Release of Primary Microplastics from Consumer Products to Wastewater in the Netherlands. Environ. Toxicol. Chem. 2016, 35, 1627–1631.

7. Boucher, J.; Friot, D. Primary Microplastics in the Oceans: A Global Evaluation of Sources; Iucn Gland, Switzerland, 2017; Vol. 10;.

8. Enfrin, M.; Lee, J.; Gibert, Y.; Basheer, F.; Kong, L.; Dumée, L.F. Release of Hazardous Nanoplastic Contaminants Due to Microplastics Fragmentation under Shear Stress Forces. J. Hazard. Mater. 2020, 384, 121393.

9. Julienne, F.; Delorme, N.; Lagarde, F. From Macroplastics to Microplastics: Role of Water in the Fragmentation of Polyethylene. Chemosphere 2019, 236, 124409.

10. Emblem, A. Plastics Properties for Packaging Materials. In Packaging Technology; Elsevier, 2012; pp. 287–309.

11. Pedrotti, M.L.; Petit, S.; Elineau, A.; Bruzaud, S.; Crebassa, J.-C.; Dumontet, B.; Martí, E.; Gorsky, G.; Cózar, A. Changes in the Floating Plastic Pollution of the Mediterranean Sea in Relation to the Distance to Land. PLoS One 2016, 11, e0161581.

12. Woodall, L.C.; Sanchez-Vidal, A.; Canals, M.; Paterson, G.L.J.; Coppock, R.; Sleight, V.; Calafat, A.; Rogers, A.D.; Narayanaswamy, B.E.; Thompson, R.C. The Deep Sea Is a Major Sink for Microplastic Debris. R. Soc. open Sci. 2014, 1, 140317.

13. do Sul, J.A.I. Why It Is Important to Analyze the Chemical Composition of Microplastics in Environmental Samples. Mar. Pollut. Bull. 2021, 165, 112086.

14. De Sá, L.C.; Oliveira, M.; Ribeiro, F.; Rocha, T.L.; Futter, M.N. Studies of the Effects of Microplastics on Aquatic Organisms: What Do We Know and Where Should We Focus Our Efforts in the Future? Sci. Total Environ. 2018, 645, 1029–1039.

15. Wagner, M.; Scherer, C.; Alvarez-Muñoz, D.; Brennholt, N.; Bourrain, X.; Buchinger, S.; Fries, E.; Grosbois, C.; Klasmeier, J.; Marti, T. Microplastics in Freshwater Ecosystems: What We Know and What We Need to Know. Environ. Sci. Eur. 2014, 26, 1–9.

16. Shim, W.J.; Hong, S.H.; Eo, S.E. Identification Methods in Microplastic Analysis: A Review. Anal. methods 2017, 9, 1384–1391.

17. Elkhatib, D.; Oyanedel-Craver, V. A Critical Review of Extraction and Identification Methods of Microplastics in Wastewater and Drinking Water. Environ. Sci. Technol. 2020, 54, 7037–7049.

18. Turan, N.B.; Erkan, H.S.; Engin, G.O. Microplastics in Wastewater Treatment Plants: Occurrence, Fate and Identification. Process Saf. Environ. Prot. 2021, 146, 77–84.

19. Kumar, B.N.V.; Löschel, L.A.; Imhof, H.K.; Löder, M.G.J.; Laforsch, C. Analysis of Microplastics of a Broad Size Range in Commercially Important Mussels by Combining FTIR and Raman Spectroscopy Approaches. Environ. Pollut. 2021, 269, 116147.

20. Prata, J.C.; Paço, A.; Reis, V.; da Costa, J.P.; Fernandes, A.J.S.; da Costa, F.M.; Duarte, A.C.; Rocha-Santos, T. Identification of Microplastics in White Wines Capped with Polyethylene Stoppers Using Micro-Raman Spectroscopy. Food Chem. 2020, 331, 127323.

21. Prata, J.C.; da Costa, J.P.; Fernandes, A.J.S.; da Costa, F.M.; Duarte, A.C.; Rocha-Santos, T. Selection of Microplastics by Nile Red Staining Increases Environmental Sample Throughput by Micro-Raman Spectroscopy. Sci. Total Environ. 2021, 783, 146979.

22. Cutroneo, L.; Reboa, A.; Besio, G.; Borgogno, F.; Canesi, L.; Canuto, S.; Dara, M.; Enrile, F.; Forioso, I.; Greco, G. Microplastics in Seawater: Sampling Strategies, Laboratory Methodologies, and Identification Techniques Applied to Port Environment. Environ. Sci. Pollut. Res. 2020, 27, 8938–8952.

23. Chen, G.; Fu, Z.; Yang, H.; Wang, J. An Overview of Analytical Methods for Detecting Microplastics in the Atmosphere. TrAC Trends Anal. Chem. 2020, 115981.

24. Stanton, T.; Johnson, M.; Nathanail, P.; Gomes, R.L.; Needham, T.; Burson, A. Exploring the Efficacy of Nile Red in Microplastic Quantification: A Costaining Approach. Environ. Sci. Technol. Lett. 2019, 6, 606–611.

25. Nalbone, L.; Panebianco, A.; Giarratana, F.; Russell, M. Nile Red Staining for Detecting Microplastics in Biota: Preliminary Evidence. Mar. Pollut. Bull. 2021, 172, 112888.

26. Karlsson, T.M.; Kärrman, A.; Rotander, A.; Hassellöv, M. Comparison between Manta Trawl and in Situ Pump Filtration Methods, and Guidance for Visual Identification of Microplastics in Surface Waters. Environ. Sci. Pollut. Res. 2020, 27, 5559–5571.

27. Funck, M.; Yildirim, A.; Nickel, C.; Schram, J.; Schmidt, T.C.; Tuerk, J. Identification of Microplastics in Wastewater after Cascade Filtration Using Pyrolysis-GC–MS. MethodsX 2020, 7, 100778.

28. Bayo, J.; López-Castellanos, J.; Olmos, S. Membrane Bioreactor and Rapid Sand Filtration for the Removal of Microplastics in an Urban Wastewater Treatment Plant. Mar. Pollut. Bull. 2020, 156, 111211.

29. Zhu, X. Optimization of Elutriation Device for Filtration of Microplastic Particles from Sediment. Mar. Pollut. Bull. 2015, 92, 69–72.

30. Prata, J.C.; Reis, V.; Matos, J.T. V; da Costa, J.P.; Duarte, A.C.; Rocha-Santos, T. A New Approach for Routine Quantification of Microplastics Using Nile Red and Automated Software (MP-VAT). Sci. Total Environ. 2019, 690, 1277–1283.

31. Prata, J.C.; da Costa, J.P.; Duarte, A.C.; Rocha-Santos, T. Methods for Sampling and Detection of Microplastics in Water and Sediment: A Critical Review. TrAC Trends Anal. Chem. 2019, 110, 150–159.

32. Shruti, V.C.; Pérez-Guevara, F.; Roy, P.D.; Kutralam-Muniasamy, G. Analyzing Microplastics with Nile Red: Emerging Trends, Challenges, and Prospects. J. Hazard. Mater. 2022, 423, 127171.

33. Prata, J.C.; Alves, J.R.; da Costa, J.P.; Duarte, A.C.; Rocha-Santos, T. Major Factors Influencing the Quantification of Nile Red Stained Microplastics and Improved Automatic Quantification (MP-VAT 2.0). Sci. Total Environ. 2020, 719, 137498.

34. Eerkes-Medrano, D.; Leslie, H.A.; Quinn, B. Microplastics in Drinking Water: A Review and Assessment. Curr. Opin. Environ. Sci. Heal. 2019, 7, 69–75.

35. Lv, L.; Qu, J.; Yu, Z.; Chen, D.; Zhou, C.; Hong, P.; Sun, S.; Li, C. A Simple Method for Detecting and Quantifying Microplastics Utilizing Fluorescent Dyes-Safranine T, Fluorescein Isophosphate, Nile Red Based on Thermal Expansion and Contraction Property. Environ. Pollut. 2019, 255, 113283.

36. Li, J.; Liu, H.; Chen, J.P. Microplastics in Freshwater Systems: A Review on Occurrence, Environmental Effects, and Methods for Microplastics Detection. Water Res. 2018, 137, 362–374.

37. Sun, D.; Böhringer, K.F. Self-Cleaning: From Bio-Inspired Surface Modification to MEMS/Microfluidics System Integration. Micromachines 2019, 10, 101.

38. Verpoorte, E.; De Rooij, N.F. Microfluidics Meets MEMS. Proc. IEEE 2003, 91, 930–953.

39. Luke, C.S.; Selimkhanov, J.; Baumgart, L.; Cohen, S.E.; Golden, S.S.; Cookson, N.A.; Hasty, J. A Microfluidic Platform for Long-Term Monitoring of Algae in a Dynamic Environment. ACS Synth. Biol. 2016, 5, 8–14.

40. Grist, S.M.; Nasseri, S.S.; Laplatine, L.; Schmok, J.C.; Yao, D.; Hua, J.; Chrostowski, L.; Cheung, K.C. Long-Term Monitoring in a Microfluidic System to Study Tumour Spheroid Response to Chronic and Cycling Hypoxia. Sci. Rep. 2019, 9, 1–13.

41. Chen, C.K.; Zhang, J.; Bhingarde, A.; Matotek, T.; Barrett, J.; Hardesty, B.D.; Holl, M.M.B.; Khoo, B.L. A Portable Purification System for the

Rapid Removal of Microplastics from Environmental Samples. Chem. Eng. J. 2022, 428, 132614.

42. Elsayed, A.A.; Erfan, M.; Sabry, Y.M.; Dris, R.; Gaspéri, J.; Barbier, J.-S.; Marty, F.; Bouanis, F.; Luo, S.; Nguyen, B.T.T. A Microfluidic Chip Enables Fast Analysis of Water Microplastics by Optical Spectroscopy. Sci. Rep. 2021, 11, 1–11.

43. Lobnik, A.; Wolfbeis, O.S. Probing the Polarity of Sol-Gels and Ormosils via the Absorption of Nile Red. J. sol-gel Sci. Technol. 2001, 20, 303–311.

44. Sarvašová, N.; Ulbrich, P.; Tokárová, V.; Zadražil, A.; Štěpánek, F. Artificial Swarming: Towards Radiofrequency Control of Reversible Micro-Particle Aggregation and Deposition. Powder Technol. 2015, 278, 17–25.

45. Maes, T.; Jessop, R.; Wellner, N.; Haupt, K.; Mayes, A.G. A Rapid-Screening Approach to Detect and Quantify Microplastics Based on Fluorescent Tagging with Nile Red. Sci. Rep. 2017, 7, 1–10.

46. Nel, H.A.; Chetwynd, A.J.; Kelleher, L.; Lynch, I.; Mansfield, I.; Margenat, H.; Onoja, S.; Oppenheimer, P.G.; Smith, G.H.S.; Krause, S. Detection Limits Are Central to Improve Reporting Standards When Using Nile Red for Microplastic Quantification. Chemosphere 2021, 263, 127953.

47. Shim, W.J.; Song, Y.K.; Hong, S.H.; Jang, M. Identification and Quantification of Microplastics Using Nile Red Staining. Mar. Pollut. Bull. 2016, 113, 469–476.

48. Wang, C.; Jiang, L.; Liu, R.; He, M.; Cui, X.; Wang, C. Comprehensive Assessment of Factors Influencing Nile Red Staining: Eliciting Solutions for Efficient Microplastics Analysis. Mar. Pollut. Bull. 2021, 171, 112698.

49. Konde, S.; Ornik, J.; Prume, J.A.; Taiber, J.; Koch, M. Exploring the Potential of Photoluminescence Spectroscopy in Combination with Nile Red Staining for Microplastic Detection. Mar. Pollut. Bull. 2020, 159, 111475.

50. Chen, X.; Li, T.; Hu, Z. A Novel Research on Serpentine Microchannels of Passive Micromixers. Microsyst. Technol. 2017, 23, 2649–2656.

51. Hardt, S.; Drese, K.; Hessel, V.; Scho¨ nfeld, F. Passive Micro Mixers for Applications in the Micro Reactor and MTAS Field. In Proceedings of the International Conference on Nanochannels, Microchannels, and Minichannels; 2004; Vol. 41642, pp. 45–55.

52. Raza, W.; Hossain, S.; Kim, K.-Y. A Review of Passive Micromixers with a Comparative Analysis. Micromachines 2020, 11, 455.

53. Thiele, J.; Abate, A.R.; Shum, H.C.; Bachtler, S.; Förster, S.; Weitz, D.A. Fabrication of Polymersomes Using Double-emulsion Templates in Glass-coated Stamped Microfluidic Devices. Small 2010, 6, 1723–1727.

54. Kim, H.S.; Waqued, S.C.; Nodurft, D.T.; Devarenne, T.P.; Yakovlev, V. V; Han, A. Raman Spectroscopy Compatible PDMS Droplet Microfluidic Culture and Analysis Platform towards On-Chip Lipidomics. Analyst 2017, 142, 1054–1060.

55. Chen, X.; Liu, S.; Chen, Y.; Wang, S. A Review on Species Mixing in Droplets Using Passive and Active Micromixers. Int. J. Environ. Anal. Chem. 2021, 101, 422–432.

56. Cai, G.; Xue, L.; Zhang, H.; Lin, J. A Review on Micromixers. Micromachines 2017, 8, 274.

57. Bachman, H.; Chen, C.; Rufo, J.; Zhao, S.; Yang, S.; Tian, Z.; Nama, N.; Huang, P.-H.; Huang, T.J. An Acoustofluidic Device for Efficient Mixing over a Wide Range of Flow Rates. Lab Chip 2020, 20, 1238–1248.

58. Zhelev, T.; Strelow, O. Heat Integration in Micro-Fluidic Devices. In Computer Aided Chemical Engineering; Elsevier, 2006; Vol. 21, pp. 1863–1868 ISBN 1570-7946.

59. Meng, X.; Huang, H.; Yan, K.; Tian, X.; Yu, W.; Cui, H.; Kong, Y.; Xue, L.; Liu, C.; Wang, S. Smartphone Based Hand-Held Quantitative Phase Microscope Using the Transport of Intensity Equation Method. Lab Chip 2017, 17, 104–109.

60. Tan, W.; Powles, E.; Zhang, L.; Shen, W. Go with the Capillary Flow. Simple Thread-Based Microfluidics. Sensors Actuators B Chem. 2021, 334, 129670, doi:https://doi.org/10.1016/j.snb.2021.129670.

61. Li, B.; Li, L.; Guan, A.; Dong, Q.; Ruan, K.; Hu, R.; Li, Z. A Smartphone Controlled Handheld Microfluidic Liquid Handling System. Lab Chip 2014, 14, 4085–4092.

62. Desforges, J.-P.W.; Galbraith, M.; Dangerfield, N.; Ross, P.S. Widespread Distribution of Microplastics in Subsurface Seawater in the NE Pacific Ocean. Mar. Pollut. Bull. 2014, 79, 94–99, doi:https://doi.org/10.1016/j.marpolbul.2013.12.035.

63. Araujo, C.F.; Nolasco, M.M.; Ribeiro, A.M.P.; Ribeiro-Claro, P.J.A. Identification of Microplastics Using Raman Spectroscopy: Latest Developments and Future Prospects. Water Res. 2018, 142, 426–440.

64. Hengstmann, E.; Fischer, E.K. Nile Red Staining in Microplastic Analysis—Proposal for a Reliable and Fast Identification Approach for Large Microplastics. Environ. Monit. Assess. 2019, 191, 1–9.

CHAPTER 3. Separation of microplastics from blood samples using travelling surface acoustic waves

by

Pedro Mesquita, Liyuan Gong, Daniel Schwartz, Evan Vasquez, Jie Shen, and Yang Lin

Department of Mechanical, Industrial and Systems Engineering, University of Rhode Island, Kingston, Rhode Island, USA

In preparation for publication

ABSTRACT

Microplastic has emerged as a ubiquitous contaminant with increasing global attention. Recent evidence confirms the presence of microplastics in human blood, implying the ability of these particles to interact with cells. As blood is circulated around the body, these particles can potentially induce adverse physiological reactions in various organs. To quantify the distribution of microplastics and assess their potential effects on human health, effective separation of microplastics from blood is critical and essential. However, at present, there is a dearth of effective and simple separation methods in this regard. Here, we propose a microfluidic device that leverages the separation ability of traveling surface acoustic waves (TSAW) to separate microplastics from blood. Although TSAW has long been used to separate various particles, a systematic study on the separation of microplastics from blood samples has not been reported. To fill in the knowledge gap, we first studied the theoretical values of the acoustic radiation factor for various types of microplastics and blood cells. The notable difference between the resonant frequencies indicated that microplastics of different sizes and types can be separated from blood cells. The experiments were then conducted using a polydimethylsiloxane (PDMS) microfluidic device built on a piezoelectric lithium niobate substrate to validate the theoretical results using two common types of microplastics. Finally, the microfluidic device was used to demonstrate the separation of different sized (5 and 10 μm) polystyrene microplastics from blood samples. The effects of power and flow rate on the separation efficiency were also investigated.

1. Introduction

Since the advent of plastics, this lightweight but durable material has rapidly become an integral part of everyday life [1,2]. Considering the lack of alternative materials that provide similar properties and usefulness, the use of plastics is expected to continue for a long time [3]. The extensive and abusive use of plastic inevitably initiated the pollution in different ecosystems (contaminating water, soil, and air [4–8]), eventually posing negative impacts on public health [9,10]. In particular, microplastics with a size smaller than 5 mm have been found to be the most abundant plastic pollutants in oceans [11–13]. Owing to the small dimensions of these pollutants, microplastics can easily spread over the world [14]. As a result, the high levels of plastic pollution will considerably increase the exposure of humans to microplastics [10,15].

It is estimated that humans inhale and ingest more than 70,000 microplastics per year [16], as the presence of microplastics has been reported for food *(e.g.,* salt, seafood, *etc.*) [17–19], drinking water [20,21] and air [22,23]. Schwabl et. al. reported that human stool samples contained microplastics of an average of 20 particles (50-500 µm) per 10g of stool, with polypropylene and polyethylene being the most common types [24]. An average of 12 plastic particles were found in placenta samples with sizes ranging from 5-10 µm [25]. Microplastics (4 to 30 µm) were found in tissues of patients with cirrhotic liver injuries [26]. Human sputum samples were also examined and 21 types of plastic (44.67 to 210.64 µm) were identified [27].

The exposure to those particles has raised a global concern on public health with more evidence showing the adverse impacts given by these pollutants [28,29]. For example, polystyrene microbeads can lead to the undesired alteration of enzymatic activity [30,31]. Genotoxicity and DNA damage could also be caused by microplastics [32,33]. Spermatogenesis dysfunction induced by polystyrene particles was studied both in vivo (using mice) and in vitro with results suggesting that microplastics can lead to the disruption of blood-testis barrier (BTB) and imbalance of the mammalian target of rapamycin (mTOR) pathway [34].

More recently, the study from Leslie et. al. reported the presence of microplastics in the human blood [35]. Five widely used polymers, including poly(methyl methacrylate) (PMMA), polypropylene (PP), polystyrene (PS), polyethylene (PE) and polyethylene terephthalate (PET) were identified in the blood collected from 22 healthy donors with an average concentration of 1.6 µg/ml. As blood plays an important role connecting different organs, the presence of microplastics in blood speaks out its uptake within the human body [36]. However, it remains unclear how microplastics are transported and distributed in blood and human body, and whether these particles can potentially affect immune regulation and alter normal physiological activities. Therefore, the effective separation of microplastics from blood samples are expected to benefit the public risk assessment considering the high levels of microplastic pollution worldwide. The separation of microplastics from human blood is important as it enables further analyses of the collected microplastics (*e.g.,* type, size) [37,38]. However, sampling of microplastics in blood is not a simple task considering the typical size

of microplastics found in human samples (few micrometers, as aforementioned) [35]. In the works reported by Leslie *et. al.*, Ragusa *et. al.*, and Schwabl *et. al.* the approaches used for sampling require bulk filtering, which is time-consuming and laborious [24,25,35]. To provide a simpler and straightforward approach for the same purpose, in this paper, we propose an acoustofluidic device to separate microplastics from blood samples owing to its powerful particle manipulation capabilities and the non-contact, label-free nature of operation.

As an emerging and promising tool, acoustofluidics have been widely used in multiple separation applications: cancer cell, exosome and blood-plasma separation [39–42]. To the best of our knowledge, acoustofluidics has not yet been applied to the separation of microplastics from blood samples. Fundamentally, particles can be manipulated using different types of acoustic waves. Among them, surface acoustic waves (SAW) have been widely used in microfluidic applications [42–44]. SAW are generated by interdigitated transducers (IDTs), and by changing its geometry and layout, different acoustic fields can be generated to achieve various purposes (*e.g.,* particle focusing and separation) [43,45]. In particular, the layout of IDTs can give rise to two types of surface acoustic waves, namely the standing surface acoustic wave (SSAW) and travelling surface acoustic wave (TSAW) [43,46]. Here, the TSAW was used to separate microplastics from blood samples. Initially, we investigated the theoretical values for the acoustic radiation factor (ARF) of 10 types of common plastics with sizes of 1, 3, 5, and 10 μm and blood cells. Experiments were then conducted to validate the theoretical values of the ARF for two selected types of microplastics. Finally, to prove the hypothesis

that microplastics can be separated from the blood cells, 5 and 10 μm polystyrene particles were successfully separated from blood cells. The effects of power and flow rate in the separation efficiency were also investigated.

2. Results and discussion

2.1. Separation principle

The mechanism of microplastic separation from blood samples is depicted in Figure 1.3. The device consists of a piezoelectric lithium niobate ($LiNbO_3$) substrate and a polydimethylsiloxane (PDMS) microfluidic chip. Chirped IDTs were employed since they allow to test multiple frequencies [47,48]. The fabricated devices had IDTs with varying pitch from 6.8 to 22 μm, which allowed operation between 45 and 145 MHz. A sinusoidal alternating current (AC) signal created by a waveform generator was amplified and subsequently applied in the IDTs to generate the TSAW (Figure 1.3a). The leaky TSAW propagates in the direction perpendicular to the main microchannel and interacts with the fluid, generating a pressure gradient in the substrate surface, which propagates towards the fluid and induces particle displacement [48–50]. It is worth noting that the leaky wave will generate a dead pressure zone, in which particles are not subject to the acoustophoretic effects (upper left corner of the channel, as shown in Figure 1.3b) [42,51]. The size of the dead pressure zone can be estimated by the Rayleigh angle, $\theta = \sin^{-1}(c_f/c_{LiNbO3}) \approx 22.8°$, where c_f and c_{LiNbO3} are the speed of sound in the fluid and in the substrate, respectively. The actual device can be seen in Figure 1.3c, the microchannels were highlighted using food coloring.

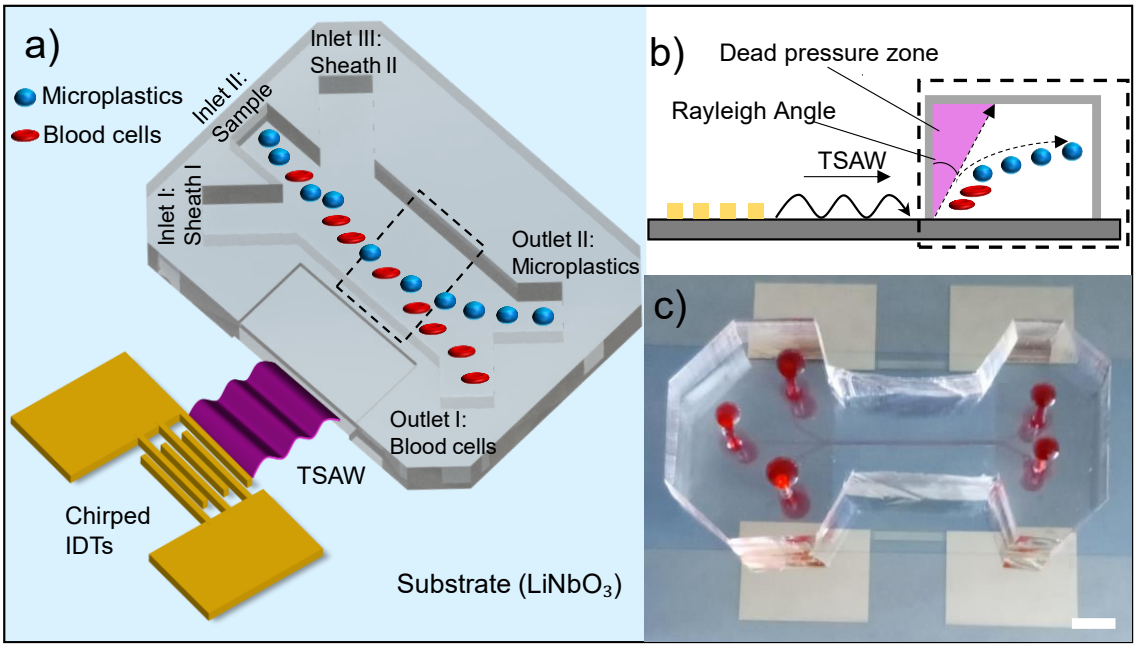

Figure 3.1. The microfluidic device used for blood microplastics separation. a) Schematic of the separation mechanism. Once the IDTs are actuated by electrical signals, the TSAW is established on the substrate surface and will displace the particles according to their physical properties (i.e., size, compressibility, *etc.*). The separation is achieved if the microplastics particles have higher ARF than blood cells with the same operational frequency (larger displacements of microplastic particles). b) Cross-sectional view of the separation process. The TSAW causes a pressure gradient that displaces the microplastics towards the separation region. Due to the Rayleigh angle, there is a dead pressure zone that traps particles and hinders their separation. This region is avoided with the use of Sheath flow I. c) Photo of the actual device. Scale bar is 5 mm.

The device consisted of three inlets, the central port was used for sample injection and the remaining inlets were used for the sheath flows. Both sheath flows were used to focus the sample at an appropriate distance from the walls. In addition, sheath flow I also prevented the particles from being trapped in the dead pressure zone [47,48]. The focused sample flows through the main microchannel, reaching the region where the TSAW was applied. Using a resonant frequency that induced higher acoustophoretic effects in microplastic particles than in blood cells caused the TSAW to deflect the microplastics transversely, while keeping

blood cells negligibly affected, directing the microplastics to the separation outlet. Two outlets were designed respectively for the collection of the separated blood cells and microplastics.

2.2. Microplastics separation aptitude

The separation principle is based on the fact that particles with different physical properties shall experience different F_{TSAW} (acoustophoretic force) at the same operational frequency [48,52,53]. From the theoretical description of the effects of TSAW in particles, it is possible to observe that the particle properties that influence the ARF are diameter, density, and compressibility (longitudinal and shear speed of sound) [54]. To induce substantial particle displacement, the applied frequency must match the particle resonance frequency, achieving significant ARF (therefore increasing the acoustophoretic force).

The acoustofluidic theory proposed by Hasegawa et. al. was used here to predict the force produced by the TSAW in particles within the microfluidic channel [54]. The average force (F_{TSAW}) induced by a TSAW on a spherical particle is expressed by equation 1; where a is the particle diameter, E is the mean energy density from the TSAW, and Y_P is the ARF.

$$F_{TSAW} = Y_P \pi a^2 \bar{E} \qquad (1)$$

The equation suggests that even though F_{TSAW} can be increased by increasing the applied power, the ARF still must be sufficiently high, otherwise the acoustophoretic force may become negligible. Equation 2 shows a numerical model to estimate Y_P, the details that lead to the derivation of this equation can be

found in the original article [54]. Since Y_P is a function of the Helmholtz number, choosing the proper operational frequency is fundamental for the effectiveness of the F_{TSAW}.

$$Y_P = \frac{4}{{x_0}^2}\sum_{n=0}^{\infty}\{(n+1)(V_n' U_{n+1}' - U_n' V_{n+1}'){x_0}^2 - n(n+1)(n+2)(V_n U_{n+1} - U_n V_{n+1}) + [n(n+1)(U_n V_{n+1}' - V_n U_{n+1}') - (n+1)(n+2)(U_n' V_{n+1} - V_n' U_{n+1})]x_0 + (n+1)(V_n U_{n+1} - U_n V_{n+1}){x_0}^2\} \quad (2)$$

The Helmholtz number (equation 3) is the dimensionless number that relates the applied frequency, particle diameter, and speed of sound with the ARF,

$$x_{0,1,2} = \frac{2\pi f a}{c_{f,l,s}} \quad (3)$$

where f is the frequency, c_f is the fluid speed of sound, c_l is the solid longitudinal speed of sound, and c_s is the solid shear speed of sound. The subindices 0, 1, and 2 refer to c_f, c_l, and c_s, respectively. The theoretical strength of a TSAW can be predicted given the particle and fluid properties.

Note that higher ARFs (or better separation performance) depends on the physical properties of the suspended particles and the media [48]. Thus, it is essential to determine the optimal operational frequency to achieve best separation performance for each type of particles. This section aimed at exploring the microplastics properties and their influence on the ARF. Given the properties shown in Table 1 and the particle size, we plotted the ARF as a function of the

applied frequency. Specifically, ten types of microplastics were studied, including: Acrylonitrile-butadiene-styrene (ABS), Poly-DGEBA/PDA (Epoxy), Poly-hexamethylene adipamide (Nylon), Polycarbonate (PC), Polyethylene (PE), Poly-methylmethacrylate (PMMA), Polypropylene (PP), Poly-vinyl chloride (PVC), Polystyrene (PS), Polytetrafluoroethylene (Teflon). Supplementary Information provides the algorithm used for the calculation of the theoretical ARF, along with further details about theoretical modelling.

Table 3.1 – Material properties used to calculate the theoretical ARF [55].

Acronym	**Poly-**	**Density (kg/m³)**	**C_L (m/s)**	**C_S (m/s)**
ABS	Acrylonitrile-butadiene-styrene	1,041	2,160	930
Epoxy	DGEBA/PDA	1,184	2,890	1,290
Nylon	Hexamethylene adipamide	1,147	2,710	1,120
PC	Carbonate	1,194	2,220	909
PE	Ethylene	957	2,430	950
PMMA	Methyl methacrylate	1,191	2,690	1,340
PP	Propylene	913	2,650	1,300
PS	Styrene	1,052	2,400	1,150
PVC	Vinyl chloride	1,386	2,330	1,070
Teflon	Tetrafluoroethylene	2,180	1,410	730

Moreover, as particle size is another important factor determining ARF, four different sizes were studied here, including 1, 3, 5, and 10 μm. As shown in Figure 2.3, all the particles have multiple resonant peaks. Owing to the potential overlapping between peak frequencies (not necessary the first resonance frequency), it is possible that particles of different types and sizes can be simultaneously separated. For instance, using an input frequency around 125 MHz would allow to separate 5 and 10 μm particles made of Epoxy and PMMA simultaneously (ARF ~ 10).

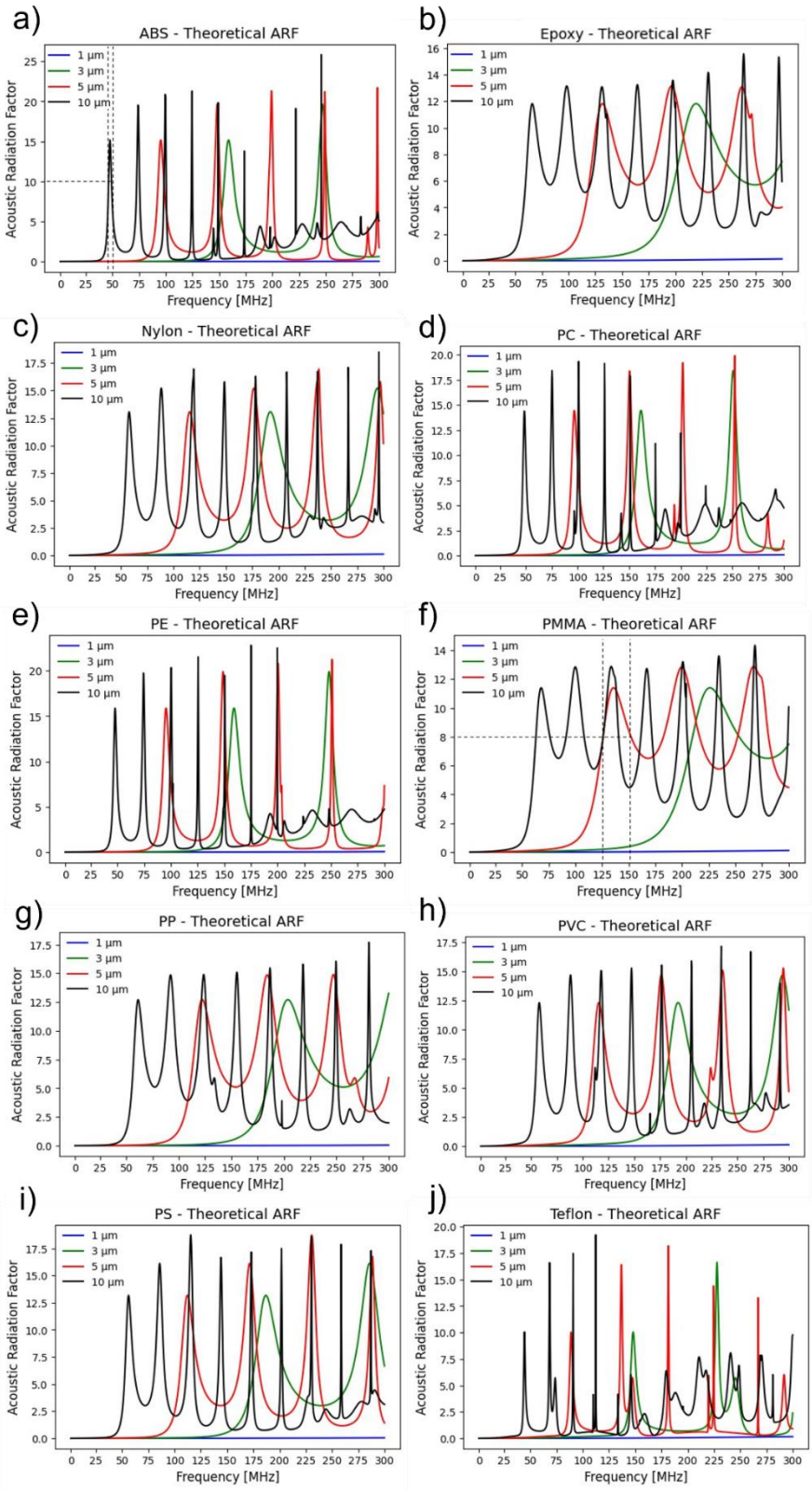

Figure 3.2. The theoretical ARFs of microplastics of different types and sizes as a function of the input frequency. The results suggested that the minimum

frequency required to produce significant ARF increases as the particle size decreases for all types of microplastics studied here. a) ABS. b) Epoxy. c) Nylon. d) PC. e) PE. f) PMMA. g) PP. h) PVC. i) PS. j) Teflon.

The bandgap of resonance frequencies is another important factor that should be considered here. Certain plastic types such as Epoxy, PMMA and PS have wide bandgaps. For example, 5 μm PMMA particles have high ARF from 125 MHz to 150 MHz, thus a wide spectrum of frequencies (25 MHz bandgap) could be applied for separating the PMMA particles. On the contrary, microplastics such as ABS, PE and Teflon have narrow bandgaps. For example, 10 μm ABS particles have high ARF within a small, confined frequency gap around 50 MHz, making the selection of operational frequencies a challenge. However, on the other hand, this downside can be turned to a benefit when only microplastics of certain type and size are desired to be separated.

Although a great amount of attention has been given to microplastics over the past years, Nanoplastics remain a potential issue for human health [56,57]. Therefore, it is also worth to theoretically explore of feasibility of using TSAW to separate these nanoparticles. Given the fact that the Helmholtz number is directly proportional to the particle radius [44,50], it is expected that as the particle size decreases to nanoscale, the minimum frequency required to produce sufficiently significant ARF will increase for all types of microplastics studied here. The Figure 3.3 shows the relationship between theoretical ARF and operational frequencies for several types of nanoplastics including ABS, PMMA, PS and Teflon.

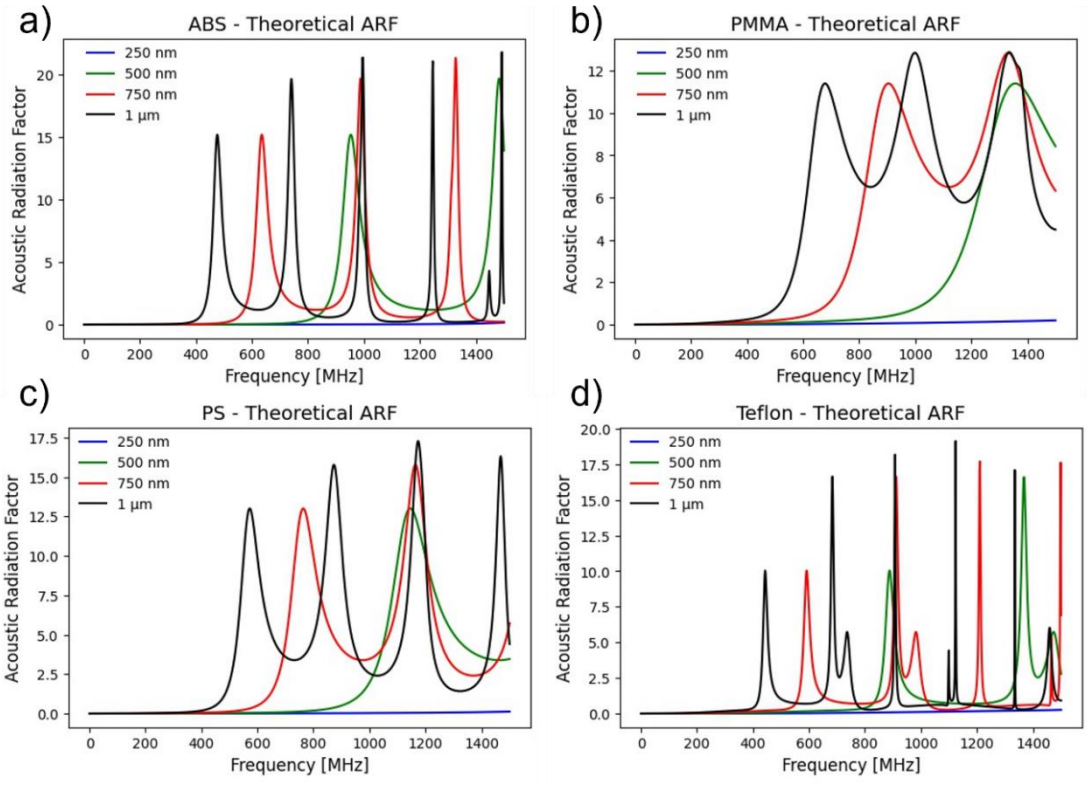

Figure 3.3. Theoretical calculations of the ARF as a function of the input frequency for nanoplastics. a) ABS. b) PMMA. c) PS. d) Teflon.

2.3. Experimental determination of ARF

As the ARF cannot be directly measured experimentally, the averaged transversal particle velocity was used to indirectly quantify the resonance peaks [48,50] since higher F_{TSAW} at resonant frequency cause larger particle displacement velocities [48,50]. Figure 4.3 shows the comparison between the theoretical prediction of ARF and the experimental measurement of particle velocity for different sized PS (selected models). In addition, we investigated the acoustophoretic behavior of blood cells, both theoretically and experimentally (also see the Supplementary Information). The longitudinal and shear speed of sound used for the theoretical calculation of the ARF in red blood cells were 1510 and

211 m/s, respectively [48,58–62]. For white blood cells the speed of sound values were 1506 and 210 m/s [60,62]. The density values used for the calculation of red blood cells and white blood cells were 1101 and 1054 kg/m³ [60].

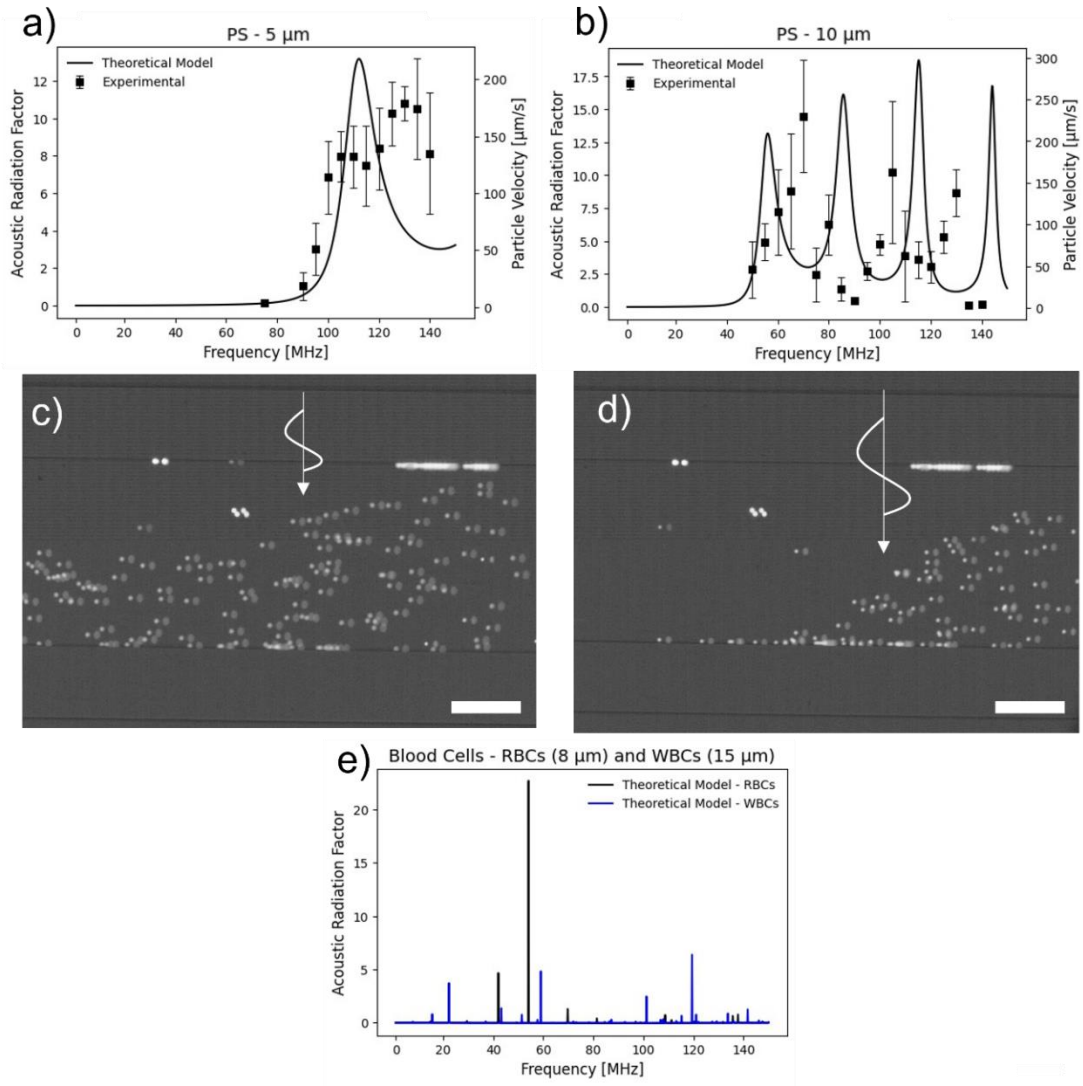

Figure 3.4. Comparison between the theoretical prediction of ARF and experimental particle velocity. a) Comparison between theoretical ARF and particle velocity for 5 µm polystyrene particles. b) Comparison between theoretical ARF and particle velocity for 10 µm PS particles. c) Displacement of 5 µm PS particles at 95 MHz. The scale bar is 100 µm. d) Displacement of 5 µm PS particles at 125 MHz. The higher ARF values at 125 MHz induce higher displacements in the particles than 95 MHz. The white arrow indicates the direction of the TSAW. The scale bar is 100 µm. e) Theoretical ARF for red and white blood cells. Blood cells were experimentally tested at resonant frequencies of microplastics such as 125 MHz, no significant displacement was observed.

As shown in Figure 4.3a and b, a frequency sweeping from 50 to 140 MHz with intervals of 5 MHz was conducted for both PS of 5 and 10 μm to determine frequency-dependent particle velocity. For 5 μm PS, the particle velocity became noticeable when the input frequency reached 80 MHz, and it continued increasing until the frequency reached 130 MHz. Note that even though the theoretical ARF started to decrease after 110 MHz, the increase of experimental particle velocity did not stop despite the low increasing rates. After the frequency reached 130 MHz, the particle velocity started to decrease, indicating the experimental resonant frequency. The difference between theoretical and experimental resonant frequencies may be attributed to the dissimilar particle and fluid properties used in theoretical derivation and experiments. The theoretical ARF was calculated assuming that the particles are immersed in an inviscid fluid [54,63], while in experiments, both water and blood were used. In addition, the theory did not account for the damping effect caused by the PDMS channels where the particles were confined. As in many other mechanical devices, the resonance peaks were also affected by the assembly and different part stiffness and defects in the fabrication (lift-off errors, contamination, *etc.*) [64,65].

Size is another important factor determining ARF, thus 10 μm PS particles were also used to examine the theoretical prediction of acoustophoretic behavior of different sized particles. In theoretical predictions (Figure 4.3b), there are four theoretical peaks within the studied frequency range (50 – 140 MHz). However, similar to the frequency delay suggested in studies of 5 μm PS particles, only three experimental peaks were identified at 70, 105, and 130 MHz. It is expected that

the fourth experimental peak was also delayed at a higher frequency beyond our test range. The displacement of PS microplastic particles subjected to TSAW at both 95 and 125 MHz were also recorded under a microscope, as respectively shown in Figure 4.3e and 4.3f. As ARF at 95 MHz was smaller than that at 125 MHz, particle displacement was larger at 125 MHz.

2.4. Separation of microplastics from blood samples

Compiling the theoretical and experimental knowledge from the previous sections, we were able to demonstrate the continuous separation of microplastics from blood samples using the microfluidic device. As a demonstration we have separated 5 and 10 µm PS microplastics from blood. From the theoretical graphs it was possible to observe that using frequencies around 125 MHz would result in relevant values for the ARF for both 5 and 10 µm PS particles, while having low ARF values for the blood cells, which would benefit the separation. With that information, we have experimentally tested the resonant frequencies, by sweeping the input frequency and observing the acoustophoretic effect on the particles. From this experiment we noticed that the acoustophoretic effect was highest on both the 5 and 10 µm PS microplastics but weak to the blood cells at 128 MHz (available in Supplementary Information). Thus, we have chosen the operational frequency to be 128 MHz.

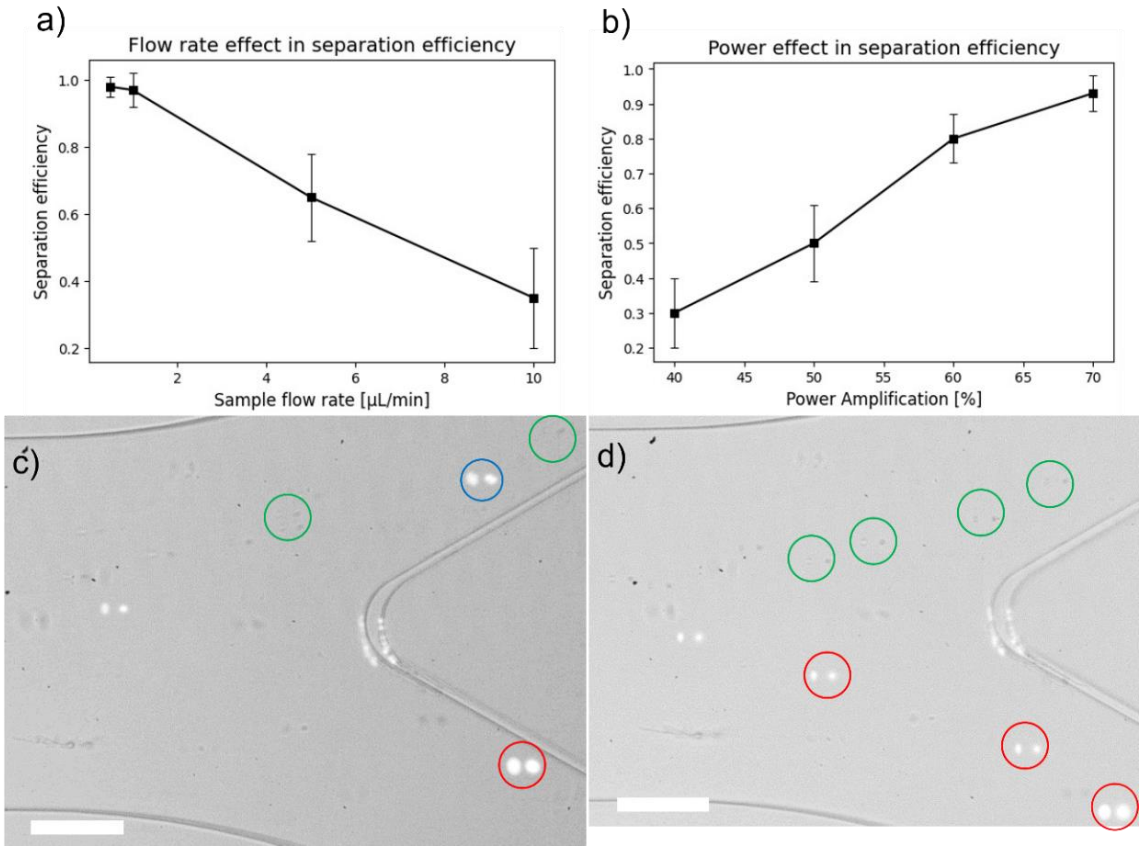

Figure 3.5. Separation of 5 and 10 µm PS microplastics from blood samples using 128 MHz. a) Flow rate effect in separation efficiency. Power was fixed at 50% to investigate the flow rate effect. b) Power effect in the separation efficiency. Flow rate was fixed at 5 µL/min. c) Blood PS separation using 128 MHz, 50% power, and 10 µL/min. Using this operation setup, the separation could not overcome performances of 60%. The image shows a 5 µm PS particle (circled in blue) being deflected towards the wrong outlet, while the 10 µm particle (circled in red) was deflected towards the correct microplastics outlet. The particles circled in green were blood cells. Scale bar is 100 µm. d) Blood PS separation using 128 MHz, 50% power, and 1 µL/min. Reducing the flow rate considerably increased the separation efficiency, achieving values close to 100%. The image shows that both 5 and 10 µm PS particles (circled in red) were displaced towards the microplastic collection outlet. The particles circled in green were blood cells. Supplementary Information contains videos demonstrating the separation process. Scale bar is 100 µm.

The sample to sheath flow ratio was selected as 1:1:3 (sheath:sample:sheath), which was a suitable option to other SAW devices according to the literature [44,48,50]. The effects of flow rate and power in the separation efficiency were

studied by performing the separation using 0.5, 1.0, 5.0, and 10 µL/min (sample flow rate). The lowest flow rates and highest power resulted in the best separation performances (Figures 5.3a and b). The separation performance is equivalent to the recovery rate of microplastics from the sample (percentage of microplastics deflected from the sample stream towards the correct collection outlet). The separation performance approached 100% when using flow rates of 1.0 µL/min, whereas when using 10 µL/min the performance could not overcome 60%. All the flow rate experiments used the same power amplification (50%), and the flow rate was fixed at 5 µL/min when studying the effect of power in the separation efficiency. The separation performance increased from 40% to almost 100% by increasing the power amplification from 40% to 70%. Reducing the flow rate increases the time in which particles are exposed to the acoustophoretic effects, thus increasing the particle displacement and the separation efficiency. The reduced exposure time caused by high flow rates can be compensated by using increased power values. The videos available at the Supplementary Information demonstrate the separation process.

3. Conclusion

The ability to separate microplastic particles from blood samples in a continuous manner was demonstrated using a TSAW microfluidic device. We have estimated theoretical values of the ARF for 10 common types of microplastics of four different sizes, elaborating on their advantages and limitations. We also discussed on the theoretical feasibility of nanoplastics separation using GHz

waves. The ARF was experimentally determined to compare the theoretical predictions with the actual acoustophoretic strength; microplastics and blood cells were observed under different frequencies to establish the adequate operational setup. The separation of 5 and 10 μm PS microplastics from blood samples using the same frequency (128 MHz) was demonstrated. The effects of flow rate and power were analyzed, and the trends followed the expectations, with lower flow rates and higher power providing higher separation efficiency. Even though all the plastic types and sizes cannot be separated at once due to the necessity of using multiple frequencies, it is possible to add more than one pair of IDTs and apply multiple frequencies in the same device, thus separating multiple microplastics simultaneously. It is also possible to run the samples repeatedly using different frequencies. In fact, using acoustic pumps and continuously alternating the frequency could be a future application. Considering the growing concerns over microplastics and its recent findings in human samples, having a device to separate microplastics from blood is of immediate need. The device demonstrated its usefulness by separating microplastics from blood samples.

4. Experimental Section

4.1. Microfluidic device fabrication

The substrate used for SAW transducer was a Y + 128 X-propagation LiNbO3 wafer (University Wafer Inc., Boston, MA, USA). The IDTs design was patterned on the LiNbO3 wafer using a photolithography process (AZ nLOF 2035, Integrated Micro Materials Inc., Argyle, TX, USA) performed in a Maskless Aligner (MLA 150,

Heidelberg Instruments Mikrotechnik GmbH, Heidelberg, Germany). After that, we performed a double metal layer (Cr/Au, 50 A˚/800 A˚) deposition (e-beam evaporator, Lesker Lab 18, Kurt J. Lesker Company, Jefferson Hills, PA, USA), and a lift-off process to obtain the desired IDTs for SAW generation. Similar IDT patterning process can be found in different references [48,50,66]. To enhance the bonding between the PDMS device and the LiNbO3 substrate, a 100 nm SiO2 layer was deposited on top of the final IDTs [67–69].

The standard soft-lithography method was used to fabricate the PDMS device [70]. The main PDMS channel is 400 µm in width and 40 µm in depth, while the inlets are 133 µm x 40 µm, and outlets are 200 µm x 40 µm. The PDMS device was permanently bonded with the LiNbO3 substrate via oxygen plasma treatment (50 sccm, 100 mTorr, 100 W, 2 min). The devices were placed in an oven at 80 °C for 30 minutes to complete bonding. To test the largest number of frequencies possible, the devices had chirped IDTs fingers (variable width and pitch). Two devices were fabricated, both for low- and high-frequency testing. The width and pitch were progressively increased by 0.5 µm according to the guidelines of other references [59,71,72]. The low-frequency device operated from 45-85 MHz (22-11.5 µm pitch and width), while the high-frequency device operated from 90-145 MHz (11-6.8 µm pitch and width).

4.2. Microplastics and blood preparation

Microplastics solutions were prepared by diluting synthetic microspheres in deionized water. Particles consisted of PS with sizes of 5 and 10 µm (Thermo Fisher Scientific, Hanover Park, IL, USA).

Porcine whole blood (Innovative Grade US Origin Porcine Whole Blood K2 EDTA 100ml, Innovative Research Inc., Novi, MI, USA) was diluted in phosphate buffered saline (Thermo Fisher Scientific, Hanover Park, IL, USA) following the guidelines of [73]. The highest dilution (20% blood 80% PBS) was used to avoid clogging in the microfluidic channels. Diluted blood was mixed (gently stirred in a sterile conical Eppendorf tube) with microplastics in order to obtain the samples used for separation.

4.3. Separation quantification and data analysis

An inverted microscope (Zeiss Axio Vert.A1) with a camera (VEO E310L, Phantom, Wayne, NJ, USA) was used to observe the flow and record images and videos. For the fluorescent particles, a fluorescence illuminator (X-Cite mini+ 365 nm, Excelitas, Waltham, MA) was used. Syringe pumps (Fusion 200, Chemyx Inc., Stafford, TX, USA) were used to inject the fluids. The signal from a waveform generator (RIGOL DG4162 Arbitrary Waveform Generator - 160 MHz, RIGOL Technologies Inc., Portland, OR, USA) was amplified by an amplifier (AR Microwave Instrumentation, Model 100A250A amplifier, Souderton, PA, USA) and then applied to the IDTs. The solution of particles and DI water was injected in the device middle inlet. DI water was used as sheath flow and injected in inlets I and III (Figure 1.3).

Separation was quantified by counting the collected particles from samples acquired from the outlets. In addition to that, images and videos were recorded and analyzed using Phantom camera software (Phantom Camera Control and Phantom Video Player version 3.7, Phantom, Wayne, NJ, USA). Videos

demonstrating the separation of blood and microplastics are available in the Supplementary Information.

5. References

1. Prata, J.C.; da Costa, J.P.; Lopes, I.; Duarte, A.C.; Rocha-Santos, T. Environmental Exposure to Microplastics: An Overview on Possible Human Health Effects. Sci. Total Environ. 2020, 702, 134455, doi:https://doi.org/10.1016/j.scitotenv.2019.134455.

2. Dick, V.A.; Juliette, L. Microplastics and Human Health. Science (80-.). 2021, 371, 672–674, doi:10.1126/science.abe5041.

3. Adyel, T.M. Accumulation of Plastic Waste during COVID-19. Science (80-.). 2020, 369, 1314–1315.

4. MacLeod, M.; Arp, H.P.H.; Tekman, M.B.; Jahnke, A. The Global Threat from Plastic Pollution. Science (80-.). 2021, 373, 61–65.

5. Gasperi, J.; Wright, S.L.; Dris, R.; Collard, F.; Mandin, C.; Guerrouache, M.; Langlois, V.; Kelly, F.J.; Tassin, B. Microplastics in Air: Are We Breathing It In? Curr. Opin. Environ. Sci. Heal. 2018, 1, 1–5.

6. Law, K.L.; Thompson, R.C. Microplastics in the Seas. Science (80-.). 2014, 345, 144–145.

7. de Souza Machado, A.A.; Lau, C.W.; Till, J.; Kloas, W.; Lehmann, A.; Becker, R.; Rillig, M.C. Impacts of Microplastics on the Soil Biophysical Environment. Environ. Sci. Technol. 2018, 52, 9656–9665.

8. Colmer, J.; Hardman, I.; Shimshack, J.; Voorheis, J. Disparities in PM2. 5 Air Pollution in the United States. Science (80-.). 2020, 369, 575–578.

9. Silva, A.L.P.; Prata, J.C.; Walker, T.R.; Duarte, A.C.; Ouyang, W.; Barcelò, D.; Rocha-Santos, T. Increased Plastic Pollution Due to COVID-19 Pandemic: Challenges and Recommendations. Chem. Eng. J. 2021, 405, 126683.

10. Rochman, C.M.; Hoellein, T. The Global Odyssey of Plastic Pollution. Science (80-.). 2020, 368, 1184–1185.

11. Cózar, A.; Echevarría, F.; González-Gordillo, J.I.; Irigoien, X.; Úbeda, B.; Hernández-León, S.; Palma, Á.T.; Navarro, S.; García-de-Lomas, J.; Ruiz, A. Plastic Debris in the Open Ocean. Proc. Natl. Acad. Sci. 2014, 111, 10239–10244.

12. Fok, L.; Cheung, P.K.; Tang, G.; Li, W.C. Size Distribution of Stranded Small Plastic Debris on the Coast of Guangdong, South China. Environ. Pollut. 2017, 220, 407–412, doi:https://doi.org/10.1016/j.envpol.2016.09.079.

13. Pedrotti, M.L.; Petit, S.; Elineau, A.; Bruzaud, S.; Crebassa, J.-C.; Dumontet, B.; Martí, E.; Gorsky, G.; Cózar, A. Changes in the Floating Plastic Pollution of the Mediterranean Sea in Relation to the Distance to Land. PLoS One 2016, 11, e0161581.

14. Rahman, A.; Sarkar, A.; Yadav, O.P.; Achari, G.; Slobodnik, J. Potential Human Health Risks Due to Environmental Exposure to Nano- and Microplastics and Knowledge Gaps: A Scoping Review. Sci. Total Environ. 2021, 757, 143872, doi:https://doi.org/10.1016/j.scitotenv.2020.143872.

15. Rillig, M.C.; Lehmann, A. Microplastic in Terrestrial Ecosystems. Science (80-.). 2020, 368, 1430–1431.

16. Cox, K.D.; Covernton, G.A.; Davies, H.L.; Dower, J.F.; Juanes, F.; Dudas, S.E. Human Consumption of Microplastics. Environ. Sci. Technol. 2019, 53, 7068–7074, doi:10.1021/acs.est.9b01517.

17. Liebezeit, G.; Liebezeit, E. Non-Pollen Particulates in Honey and Sugar. Food Addit. Contam. Part A 2013, 30, 2136–2140, doi:10.1080/19440049.2013.843025.

18. Neves, D.; Sobral, P.; Ferreira, J.L.; Pereira, T. Ingestion of Microplastics by Commercial Fish off the Portuguese Coast. Mar. Pollut. Bull. 2015, 101, 119–126, doi:https://doi.org/10.1016/j.marpolbul.2015.11.008.

19. Karami, A.; Golieskardi, A.; Keong Choo, C.; Larat, V.; Galloway, T.S.; Salamatinia, B. The Presence of Microplastics in Commercial Salts from Different Countries. Sci. Rep. 2017, 7, 46173, doi:10.1038/srep46173.

20. Schwabl, P. Microplastics in Hot Water. Nat. Food 2020, 1, 671–672, doi:10.1038/s43016-020-00174-9.

21. Oßmann, B.E.; Sarau, G.; Holtmannspötter, H.; Pischetsrieder, M.; Christiansen, S.H.; Dicke, W. Small-Sized Microplastics and Pigmented Particles in Bottled Mineral Water. Water Res. 2018, 141, 307–316, doi:https://doi.org/10.1016/j.watres.2018.05.027.

22. Prata, J.C. Airborne Microplastics: Consequences to Human Health? Environ. Pollut. 2018, 234, 115–126, doi:https://doi.org/10.1016/j.envpol.2017.11.043.

23. Vianello, A.; Jensen, R.L.; Liu, L.; Vollertsen, J. Simulating Human Exposure to Indoor Airborne Microplastics Using a Breathing Thermal Manikin. Sci. Rep. 2019, 9, 8670, doi:10.1038/s41598-019-45054-w.

24. Schwabl, P.; Köppel, S.; Königshofer, P.; Bucsics, T.; Trauner, M.; Reiberger, T.; Liebmann, B. Detection of Various Microplastics in Human Stool. Ann. Intern. Med. 2019, 171, 453–457, doi:10.7326/M19-0618.

25. Ragusa, A.; Svelato, A.; Santacroce, C.; Catalano, P.; Notarstefano, V.; Carnevali, O.; Papa, F.; Rongioletti, M.C.A.; Baiocco, F.; Draghi, S.; et al. Plasticenta: First Evidence of Microplastics in Human Placenta. Environ. Int. 2021, 146, 106274, doi:https://doi.org/10.1016/j.envint.2020.106274.

26. Horvatits, T.; Tamminga, M.; Liu, B.; Sebode, M.; Carambia, A.; Fischer, L.; Püschel, K.; Huber, S.; Fischer, E.K. Microplastics Detected in Cirrhotic Liver Tissue. eBioMedicine 2022, 82, 104147, doi:https://doi.org/10.1016/j.ebiom.2022.104147.

27. Huang, S.; Huang, X.; Bi, R.; Guo, Q.; Yu, X.; Zeng, Q.; Huang, Z.; Liu, T.; Wu, H.; Chen, Y. Detection and Analysis of Microplastics in Human Sputum. Environ. Sci. Technol. 2022, 56, 2476–2486.

28. Schirinzi, G.F.; Pérez-Pomeda, I.; Sanchís, J.; Rossini, C.; Farré, M.; Barceló, D. Cytotoxic Effects of Commonly Used Nanomaterials and Microplastics on Cerebral and Epithelial Human Cells. Environ. Res. 2017, 159, 579–587.

29. Wu, B.; Wu, X.; Liu, S.; Wang, Z.; Chen, L. Size-Dependent Effects of Polystyrene Microplastics on Cytotoxicity and Efflux Pump Inhibition in Human Caco-2 Cells. Chemosphere 2019, 221, 333–341.

30. Prüst, M.; Meijer, J.; Westerink, R.H.S. The Plastic Brain: Neurotoxicity of Micro- and Nanoplastics. Part. Fibre Toxicol. 2020, 17, 24, doi:10.1186/s12989-020-00358-y.

31. Ribeiro, F.; Garcia, A.R.; Pereira, B.P.; Fonseca, M.; Mestre, N.C.; Fonseca, T.G.; Ilharco, L.M.; Bebianno, M.J. Microplastics Effects in Scrobicularia Plana. Mar. Pollut. Bull. 2017, 122, 379–391.

32. Rubio, L.; Barguilla, I.; Domenech, J.; Marcos, R.; Hernández, A. Biological Effects, Including Oxidative Stress and Genotoxic Damage, of Polystyrene Nanoparticles in Different Human Hematopoietic Cell Lines. J. Hazard. Mater. 2020, 398, 122900, doi:https://doi.org/10.1016/j.jhazmat.2020.122900.

33. Sun, T.; Zhan, J.; Li, F.; Ji, C.; Wu, H. Evidence-Based Meta-Analysis of the Genotoxicity Induced by Microplastics in Aquatic Organisms at Environmentally Relevant Concentrations. Sci. Total Environ. 2021, 783, 147076.

34. Wei, Y.; Zhou, Y.; Long, C.; Wu, H.; Hong, Y.; Fu, Y.; Wang, J.; Wu, Y.; Shen, L.; Wei, G. Polystyrene Microplastics Disrupt the Blood-Testis Barrier Integrity through ROS-Mediated Imbalance of MTORC1 and MTORC2. Environ. Pollut. 2021, 289, 117904, doi:https://doi.org/10.1016/j.envpol.2021.117904.

35. Leslie, H.A.; van Velzen, M.J.M.; Brandsma, S.H.; Vethaak, A.D.; Garcia-Vallejo, J.J.; Lamoree, M.H. Discovery and Quantification of Plastic Particle Pollution in Human Blood. Environ. Int. 2022, 163, 107199, doi:https://doi.org/10.1016/j.envint.2022.107199.

36. Vethaak, A.D.; Leslie, H.A. Plastic Debris Is a Human Health Issue. Environ. Sci. Technol. 2016, 50, 6825–6826, doi:10.1021/acs.est.6b02569.

37. Kutralam-Muniasamy, G.; Shruti, V.C.; Pérez-Guevara, F.; Roy, P.D. Microplastic Diagnostics in Humans:“The 3Ps” Progress, Problems, and Prospects. Sci. Total Environ. 2022, 159164.

38. Fu, W.; Min, J.; Jiang, W.; Li, Y.; Zhang, W. Separation, Characterization and Identification of Microplastics and Nanoplastics in the Environment. Sci. Total Environ. 2020, 721, 137561.

39. Li, S.; Ma, F.; Bachman, H.; Cameron, C.E.; Zeng, X.; Huang, T.J. Acoustofluidic Bacteria Separation. J. Micromechanics Microengineering 2016, 27, 15031.

40. Antfolk, M.; Magnusson, C.; Augustsson, P.; Lilja, H.; Laurell, T. Acoustofluidic, Label-Free Separation and Simultaneous Concentration of Rare Tumor Cells from White Blood Cells. Anal. Chem. 2015, 87, 9322–9328.

41. Fan, Y.; Wang, X.; Ren, J.; Lin, F.; Wu, J. Recent Advances in Acoustofluidic Separation Technology in Biology. Microsystems Nanoeng. 2022, 8, 1–16.

42. Wu, M.; Ozcelik, A.; Rufo, J.; Wang, Z.; Fang, R.; Jun Huang, T. Acoustofluidic Separation of Cells and Particles. Microsystems Nanoeng. 2019, 5, 1–18.

43. Gao, Y.; Wu, M.; Lin, Y.; Xu, J. Acoustic Microfluidic Separation Techniques and Bioapplications: A Review. Micromachines 2020, 11, 921.

44. Destgeer, G.; Lee, K.H.; Jung, J.H.; Alazzam, A.; Sung, H.J. Continuous Separation of Particles in a PDMS Microfluidic Channel via Travelling Surface Acoustic Waves (TSAW). Lab Chip 2013, 13, 4210–4216.

45. Zhao, S.; Wu, M.; Yang, S.; Wu, Y.; Gu, Y.; Chen, C.; Ye, J.; Xie, Z.; Tian, Z.; Bachman, H. A Disposable Acoustofluidic Chip for Nano/Microparticle Separation Using Unidirectional Acoustic Transducers. Lab Chip 2020, 20, 1298–1308.

46. Devendran, C.; Gunasekara, N.R.; Collins, D.J.; Neild, A. Batch Process Particle Separation Using Surface Acoustic Waves (SAW): Integration of Travelling and Standing SAW. RSC Adv. 2016, 6, 5856–5864.

47. Ma, Z.; Collins, D.J.; Ai, Y. Detachable Acoustofluidic System for Particle Separation via a Traveling Surface Acoustic Wave. Anal. Chem. 2016, 88, 5316–5323, doi:10.1021/acs.analchem.6b00605.

48. Ma, Z.; Collins, D.J.; Guo, J.; Ai, Y. Mechanical Properties Based Particle Separation via Traveling Surface Acoustic Wave. Anal. Chem. 2016, 88, 11844–11851.

49. Ding, X.; Li, P.; Lin, S.-C.S.; Stratton, Z.S.; Nama, N.; Guo, F.; Slotcavage, D.; Mao, X.; Shi, J.; Costanzo, F. Surface Acoustic Wave Microfluidics. Lab Chip 2013, 13, 3626–3649.

50. Destgeer, G.; Ha, B.H.; Jung, J.H.; Sung, H.J. Submicron Separation of Microspheres via Travelling Surface Acoustic Waves. Lab Chip 2014, 14, 4665–4672.

51. Fakhfouri, A.; Devendran, C.; Ahmed, A.; Soria, J.; Neild, A. The Size Dependant Behaviour of Particles Driven by a Travelling Surface Acoustic Wave (TSAW). Lab Chip 2018, 18, 3926–3938.

52. Qian, J.; Begum, H.; Lee, J.E.-Y. Acoustofluidic Localization of Sparse Particles on a Piezoelectric Resonant Sensor for Nanogram-Scale Mass Measurements. Microsystems Nanoeng. 2021, 7, 61, doi:10.1038/s41378-021-00288-5.

53. Wang, K.; Zhou, W.; Lin, Z.; Cai, F.; Li, F.; Wu, J.; Meng, L.; Niu, L.; Zheng, H. Sorting of Tumour Cells in a Microfluidic Device by Multi-Stage Surface Acoustic Waves. Sensors Actuators B Chem. 2018, 258, 1174–1183, doi:https://doi.org/10.1016/j.snb.2017.12.013.

54. Hasegawa, T.; Yosioka, K. Acoustic-radiation Force on a Solid Elastic Sphere. J. Acoust. Soc. Am. 1969, 46, 1139–1143.

55. Sinha, M.; Buckley, D.J. Acoustic Properties of Polymers. In Physical properties of polymers handbook; Springer, 2007; pp. 1021–1031.

56. Yee, M.S.-L.; Hii, L.-W.; Looi, C.K.; Lim, W.-M.; Wong, S.-F.; Kok, Y.-Y.; Tan, B.-K.; Wong, C.-Y.; Leong, C.-O. Impact of Microplastics and Nanoplastics on Human Health. Nanomaterials 2021, 11, 496.

57. Chang, X.; Xue, Y.; Li, J.; Zou, L.; Tang, M. Potential Health Impact of Environmental Micro-and Nanoplastics Pollution. J. Appl. Toxicol. 2020, 40, 4–15.

58. Carvalho, M.R.; Barata, D.; Teixeira, L.M.; Giselbrecht, S.; Reis, R.L.; Oliveira, J.M.; Truckenmüller, R.; Habibovic, P. Colorectal Tumor-on-a-Chip System: A 3D Tool for Precision Onco-Nanomedicine. Sci. Adv. 2019, 5, eaaw1317, doi:10.1126/sciadv.aaw1317.

59. Amin, R.; Knowlton, S.; Hart, A.; Yenilmez, B.; Ghaderinezhad, F.; Katebifar, S.; Messina, M.; Khademhosseini, A.; Tasoglu, S. 3D-Printed Microfluidic Devices. Biofabrication 2016, 8, 22001.

60. Cushing, K.W.; Garofalo, F.; Magnusson, C.; Ekblad, L.; Bruus, H.; Laurell, T. Ultrasound Characterization of Microbead and Cell Suspensions by Speed of Sound Measurements of Neutrally Buoyant Samples. Anal. Chem. 2017, 89, 8917–8923.

61. Sun, C.; Pye, S.D.; Browne, J.E.; Janeczko, A.; Ellis, B.; Butler, M.B.; Sboros, V.; Thomson, A.J.W.; Brewin, M.P.; Earnshaw, C.H. The Speed of Sound and Attenuation of an IEC Agar-Based Tissue-Mimicking Material for High Frequency Ultrasound Applications. Ultrasound Med. Biol. 2012, 38, 1262–1270.

62. Fung, Y.-C.; Fung, Y.-C. Bioviscoelastic Solids. Biomech. Mech. Prop. living tissues 1993, 242–320.

63. King, L.V. On the Acoustic Radiation Pressure on Spheres. Proc. R. Soc. London. Ser. A-Mathematical Phys. Sci. 1934, 147, 212–240.

64. Leung, E.; Lee, C.P.; Jacobi, N.; Wang, T.G. Resonance Frequency Shift of an Acoustic Chamber Containing a Rigid Sphere. J. Acoust. Soc. Am. 1982, 72, 615–620.

65. Chanaud, R.C. Effects of Geometry on the Resonance Frequency of Helmholtz Resonators. J. Sound Vib. 1994, 178, 337–348.

66. Shi, J.; Huang, H.; Stratton, Z.; Huang, Y.; Huang, T.J. Continuous Particle Separation in a Microfluidic Channel via Standing Surface Acoustic Waves (SSAW). Lab Chip 2009, 9, 3354–3359.

67. Weng, H.; Duan, F.L.; Xie, Z.; Liu, S.; Ji, Z.; Zhang, Y. LiNbO 3-Based SAW Sensors Capable to Measure up to 1100° C High Temperature. IEEE Sens. J. 2020, 20, 12679–12683.

68. Duan, F.L.; Xie, Z.; Ji, Z. Breakthrough of Upper Limit of Temperature Measurement of SAW Sensors for Wireless Passive Sensing inside Propulsion System. In Proceedings of the AIAA Propulsion and Energy 2020 Forum; 2020; p. 3512.

69. Freudenberg, J.; Von Schickfus, M.; Hunklinger, S. A SAW Immunosensor for Operation in Liquid Using a SiO2 Protective Layer. Sensors Actuators B Chem. 2001, 76, 147–151.

70. Xia, Y.; Whitesides, G.M. Soft Lithography. Annu. Rev. Mater. Sci. 1998, 28, 153–184.

71. Bourquin, Y.; Reboud, J.; Wilson, R.; Cooper, J.M. Tuneable Surface Acoustic Waves for Fluid and Particle Manipulations on Disposable Chips. Lab Chip 2010, 10, 1898–1901.

72. Reboud, J.; Bourquin, Y.; Wilson, R.; Pall, G.S.; Jiwaji, M.; Pitt, A.R.; Graham, A.; Waters, A.P.; Cooper, J.M. Shaping Acoustic Fields as a Toolset for Microfluidic Manipulations in Diagnostic Technologies. Proc. Natl. Acad. Sci. 2012, 109, 15162–15167.

73. Xu, X.; Wang, R.K.; Elder, J.B.; Tuchin, V. V Effect of Dextran-Induced Changes in Refractive Index and Aggregation on Optical Properties of Whole Blood. Phys. Med. Biol. 2003, 48, 1205.

APPENDICES

Appendix A – Theoretical model for the calculation of average force (F_{TSAW}) applied by a TSAW in a spherical particle

The acoustofluidic theory proposed by Hasegawa *et. al.* was used here to predict the force produced by a travelling surface acoustic wave (TSAW) in elastic spheres submerged in inviscid fluids [54]. The average force (F_{TSAW}) applied by a TSAW in a sphere is expressed by equation 1; where *a* is the particle diameter, *E* is the mean energy density from the TSAW, and Y_P is the acoustic radiation factor.

$$F_{TSAW} = Y_P \pi a^2 \bar{E} \qquad (1)$$

Even though F_{TSAW} is increased by tuning the applied energy (*i.e.*, increasing the applied power), the acoustic radiation factor has to be sufficiently high, otherwise the force may become negligible. Equation 2 shows a numerical model to estimate Y_P, the details that lead to the derivation of this equation can be found in the original article [1]. Since Y_P is a function of the Helmholtz number, choosing the proper operational frequency is fundamental for the effectiveness of the F_{TSAW}.

$$\begin{aligned} Y_P = \frac{4}{{x_0}^2} \sum_{n=0}^{\infty} \{ & (n+1)(V_n' U_{n+1}' - U_n' V_{n+1}') {x_0}^2 - n(n+1)(n+2)(V_n U_{n+1} - U_n V_{n+1}) \\ & + [n(n+1)(U_n V_{n+1}' - V_n U_{n+1}') \\ & - (n+1)(n+2)(U_n' V_{n+1} - V_n' U_{n+1})] x_0 \\ & + (n+1)(V_n U_{n+1} - U_n V_{n+1}) {x_0}^2 \} \end{aligned} \qquad (2)$$

The Helmholtz number (equation 3) is the dimensionless number that relates the applied frequency, particle diameter, and speed of sound with the acoustic radiation factor.

$$x_{0,1,2} = \frac{2\pi f a}{c_{f,l,s}} \qquad (3)$$

Where f is the frequency, c_f is the fluid speed of sound, c_l is the solid longitudinal speed of sound, and c_s is the solid shear speed of sound. The subindices 0, 1, and 2 refer to c_f, c_l, and c_s. The parameters U_n, V_n, α_n, β_n, and F_n are defined in equations 4-8.

$$U_n = (1 + \alpha_n) j_n(x_0) + \beta_n n_n(x_0) \qquad (4)$$

$$V_n = \beta_n j_n(x_0) - \alpha_n n_n(x_0) \qquad (5)$$

$$\alpha_n = -\frac{[F_n j_n(x_0) - x_0 j_n'(x_0)]^2}{[F_n j_n(x_0) - x_0 j_n'(x_0)]^2 + [F_n n_n(x_0) - x_0 n_n'(x_0)]^2} \qquad (6)$$

$$\beta_n = -\frac{[F_n j_n(x_0) - x j_n'(x_0)][F_n n_n(x_0) - x n_n'(x_0)]}{[F_n j_n(x_0) - x j_n'(x_0)]^2 + [F_n n_n(x_0) - x n_n'(x_0)]^2} \qquad (7)$$

$$F_n = \frac{1}{2}\frac{\rho_F}{\rho_P} x_2^2 \frac{\dfrac{x_1 j_n'(x_1)}{x_1 j_n'(x_1) - j_n(x_1)} - \dfrac{2n(n+1) j_n(x_2)}{(n+2)(n-1) j_n(x_2) + x_2^2 j_n''(x_2)}}{\dfrac{x_1^2 \left[\dfrac{\sigma}{1-2\sigma} j_n(x_1) - j_n''(x_1)\right]}{x_1 j_n'(x_1) - j_n(x_1)} - \dfrac{2n(n+1)[j_n(x_2) - x_2 j_n'(x_2)]}{(n+2)(n-1) j_n(x_2) + x_2^2 j_n''(x_2)}} \qquad (8)$$

F_n is a function of the fluid density (ρ_F), particle density (ρ_p), Poisson number (σ), c_l, and c_s. Bessel functions of the first (j_n) and second order (n_n) are used to model

the vibrational behavior of the particles. The prime denotes the order of the derivative with respect to the assigned Helmholtz number. With this background it is possible to predict the theoretical strength of a TSAW given the particle and fluid properties (Table 3.1).

Appendix B – Algorithm used for the calculation of average force (F_{TSAW}) applied by a TSAW in a spherical particle

The algorithm used for the calculation of the theoretical acoustic radiation factor can be found in the link below:

https://github.com/pedrommesquita/acousticradiationfactor.git